NUREG/CR–6467

Impact of Ground Motion Characterization on Conservatism and Variability in Seismic Risk Estimates

R. T. Sewell, G. R. Toro, R. K. McGuire

Risk Engineering, Inc.

Prepared for
U.S. Nuclear Regulatory Commission

AVAILABILITY NOTICE

Availability of Reference Materials Cited in NRC Publications

Most documents cited in NRC publications will be available from one of the following sources:

1. The NRC Public Document Room, 2120 L Street, NW., Lower Level, Washington, DC 20555-0001

2. The Superintendent of Documents, U.S. Government Printing Office, P. O. Box 37082, Washington, DC 20402-9328

3. The National Technical Information Service, Springfield, VA 22161-0002

Although the listing that follows represents the majority of documents cited in NRC publications, it is not intended to be exhaustive.

Referenced documents available for inspection and copying for a fee from the NRC Public Document Room include NRC correspondence and internal NRC memoranda; NRC bulletins, circulars, information notices, inspection and investigation notices; licensee event reports; vendor reports and correspondence; Commission papers; and applicant and licensee documents and correspondence.

The following documents in the NUREG series are available for purchase from the Government Printing Office: formal NRC staff and contractor reports, NRC-sponsored conference proceedings, international agreement reports, grantee reports, and NRC booklets and brochures. Also available are regulatory guides, NRC regulations in the *Code of Federal Regulations*, and *Nuclear Regulatory Commission Issuances*.

Documents available from the National Technical Information Service include NUREG-series reports and technical reports prepared by other Federal agencies and reports prepared by the Atomic Energy Commission, forerunner agency to the Nuclear Regulatory Commission.

Documents available from public and special technical libraries include all open literature items, such as books, journal articles, and transactions. *Federal Register* notices, Federal and State legislation, and congressional reports can usually be obtained from these libraries.

Documents such as theses, dissertations, foreign reports and translations, and non-NRC conference proceedings are available for purchase from the organization sponsoring the publication cited.

Single copies of NRC draft reports are available free, to the extent of supply, upon written request to the Office of Administration, Distribution and Mail Services Section, U.S. Nuclear Regulatory Commission, Washington, DC 20555-0001.

Copies of industry codes and standards used in a substantive manner in the NRC regulatory process are maintained at the NRC Library, Two White Flint North, 11545 Rockville Pike, Rockville, MD 20852-2738, for use by the public. Codes and standards are usually copyrighted and may be purchased from the originating organization or, if they are American National Standards, from the American National Standards Institute, 1430 Broadway, New York, NY 10018-3308.

NUREG/CR-6467

Impact of Ground Motion Characterization on Conservatism and Variability in Seismic Risk Estimates

Manuscript Completed: April 1996
Date Published: July 1996

Prepared by
R. T. Sewell, G. R. Toro, R. K. McGuire

Risk Engineering, Inc.
4155 Darley Avenue, Suite A
Boulder, CO 80303

N. Chokshi, NRC Project Manager

Prepared for
Division of Engineering Technology
Office of Nuclear Regulatory Research
U.S. Nuclear Regulatory Commission
Washington, DC 20555-0001
NRC Job Code L1279

ABSTRACT

This study evaluates the impact, on estimates of seismic risk and its uncertainty, of alternative methods in treatment and characterization of earthquake ground motions. The objective of this study is to delineate specific procedures and characterizations that may lead to less biased and more precise seismic risk results. This report focuses on sources of conservatism and variability in risk that may be introduced through the analytical processes and ground-motion descriptions which are commonly implemented at the interface of seismic hazard and fragility assessments. In particular, implication of the common practice of using a single, composite spectral shape to characterize motions of different magnitudes is investigated. Also, the impact of parameterization of ground motion on fragility and hazard assessments is shown.

Examination of these results demonstrates the following. (1) There exists significant conservatism in the review spectra (usually, spectra characteristic of western U.S. earthquakes) that have been used in conducting past seismic risk assessments and seismic margin assessments for eastern U.S. nuclear power plants. (2) There is a strong dependence of seismic fragility on earthquake magnitude when PGA is used as the ground-motion characterization. When, however, magnitude-dependent spectra are anchored to a common measure of elastic spectral acceleration averaged over the appropriate frequency range, seismic fragility shows no important nor consistent dependence on either magnitude or strong-motion duration. Use of inelastic spectral acceleration (at the proper frequency) as the ground spectrum anchor demonstrates a very similar result.

This study concludes that a single, composite-magnitude spectrum can generally be used to characterize ground motion for fragility assessment without introducing significant bias or uncertainty in seismic risk estimates. Use of PGA, vis-à-vis inelastic or elastic spectral acceleration, is observed to introduce a slight conservatism in the estimate of mean seismic risk; this conservatism is due to a decreased precision in predicting failure using PGA. Uncertainty in overall seismic risk, being dominated by the large uncertainty in hazard, is somewhat insensitive to reductions in fragility uncertainty. For cases where a legitimate reduction in hazard uncertainty can be acheived, however, a significant additional reduction in uncertainty may be obtained by using a ground-motion characterization based on appropriate measures of inelastic or elastic spectral acceleration.

CONTENTS

LIST OF FIGURES

LIST OF TABLES

ACKNOWLEDGMENTS

This report was prepared by Risk Engineering, Inc., and documents research work performed under Contract No. NRC–04–89–098 with the U.S. Nuclear Regulatory Commission (NRC). The authors are grateful to the NRC for sponsoring this study, and to Dr. Nilesh Chokshi, NRC project officer, for providing expert technical guidance and advice on the direction and scope of the work.

Drs. Robert P. Kennedy and C. Allin Cornell performed as expert consultants for this project, and as reviewers for the final report. Northeast Utilities (Walt Briggs, Dave Dakers, and Cal Chunglo), EQE Inc. (Wen Tong and Dr. M. K. Ravindra), and Impell (Don Wesley) assisted in providing design, safety analysis, and fragility analysis data for the Millstone Unit 3 nuclear power reactor. The authors are grateful for the help of these individuals.

Section 1

INTRODUCTION

This study evaluates the impact, on estimates of seismic risk and risk uncertainty, of alternate treatments and characterizations of earthquake ground motion. Three aspects are given particular emphasis: (1) the effect of using a conservative spectral shape (representative of western U.S. earthquakes) to characterize eastern U.S. motions, (2) the effect of disaggregating seismic hazard and fragility estimates by magnitude, and (3) the effect on fragility and risk assessments of alternate parameterizations of ground motion. This report documents the investigation and results of Phase 1 research, aimed at developing preliminary conclusions and recommendations based on a limited scope study that considers a representative failure mode for a single nuclear power plant. Phase 2 of this study will test the validity of Phase 1 conclusions for a larger set of plants (and their failure modes), and will address a broader category of issues, including effects on various types of nuclear plant systems, that pertain to conservatism and uncertainty in seismic risk analysis.

1.1 BACKGROUND

1.1.1 Effects of Conservatism and Uncertainty in Seismic Risk Assessment

Due to variabilities in structural behavior and even larger variabilities in seismic threat, seismic design procedures for nuclear power plant structures and equipment appropriately introduce substantial conservatism. Existing design procedures for nuclear power plants (1) do not, however, explicitly account for seismic load and resistance uncertainties, but rather, are based upon deterministic earthquake characterization and general (building code) load factors. As a result of this design approach, uniform seismic safety among plants has not been achieved, and measures of general safety are vague. In addition, occurrence of an earthquake that exceeds a plant's deterministic design basis may unnecessarily precipitate further review of the plant, with possible adjustment to the design basis, because the actual level of conservatism or margin is unknown. In part to verify the adequacy of past regulatory design practice in assuring plant seismic margin, and in part to desensitize the industry from new ground-motion data, seismic margin assessments and probabilistic risk assessments have been undertaken. Also, the U.S. Nuclear Regulatory Commission (NRC) is implementing its Severe Accident Policy Integration Plan (2), requiring individual plant examinations (IPEs);

for seismic events, seismic margin assessment (SMA) or seismic probabilistic risk assessment (SPRA) methodologies will be undertaken for the IPE for many U.S. nuclear power plants.

As opposed to design practice, in seismic risk, margin, or safety analysis it is important that all known conservatisms be eliminated, and that the analysis be as close as possible to reality. The purpose of margin or safety assessment is to aid in determining appropriate action, if any, required to effectively enhance plant safety. The introduction of conservative assumptions and procedures in seismic safety analyses creates the potential for implementing an ineffective safety solution or for not implementing an effective one. This potential is particularly significant when the conservatisms have an inconsistent effect in identifying dominant contributors among plant components.

In SPRA, uncertainties are also a key result of the analysis, and are essential in decision-making. For example, mean seismic risk estimates are typically significant in comparison to mean risk estimates from other initiators; for some plants, mean seismic risk may dominate the mean total risk. Uncertainties in seismic risk, however, are often large; in general, even though the mean seismic risk may be dominant, a large fraction of seismic risk estimates comprising the seismic risk distribution may be substantially lower than even the lowest estimates of risk from other events. In such a case, therefore, the fact that the mean risk from seismic events dominates does not preclude the potential for effective safety action for the other initiators. That is, the significant probability that the seismic risk is relatively low directly suggests that other contributors (or combination of contributors) will dominate the risk for several cases (i.e., plant-model and initiating-event-rate interpretations). Stated differently, if a small fraction of interpretations that led to the highest seismic risk estimates were eliminated, then seismic risk would no longer be perceived as dominant; effective safety action for other initiators, therefore, may be erroneously precluded on the basis of just a few interpretations.

Ignoring important aspects of risk uncertainty by considering only the mean risk may lead to an undesirable decision process. In basing decisions on mean risk, a small fraction of interpretations may dominate the decision; if these few interpretations are removed, the resulting decision may change drastically. Stable decisionmaking requires a more complicated examination of the uncertainty, and in some cases, evaluation of all decisions (and their weights) obtained by examining each of the variety of individual interpretations (that led to the uncertainty distribution) considered (or combined) separately. In such a case, the final decision is less sensitive to extreme interpretations; hence, the decision process can become more stable.

It is, therefore, essential that uncertainty in seismic risk be represented as accurately as possible; unnecessary sources of uncertainty should be eliminated to sharpen focus on effective safety decisions.

1.1.2 Technical Issues Pertaining to Elements of Seismic Risk Methodology

Procedures conventionally employed in seismic risk assessment are significantly different from methods used in assessing risk due to other events that might initiate accident sequences in nuclear power plants [this fact may be verified, for instance, by examination of the *PRA Procedures Guide* (3)]. Derivation of a plant-level fragility curve from component fragilities, and derivation of a site hazard curve — both fragility and hazard curves being applicable to a continuum of complex events that are described by values of a single parameter — and the procedure used to combine fragility and hazard curves to obtain an estimate of failure rate, are elements of a process largely unique to determination of seismic risk. This uniqueness, combined with the very large uncertainties that accompany (and have seemingly typified) seismic risk results has led a number of experts outside the field of earthquake risk assessment to informally question[1] the validity of seismic risk results and their usefulness in both comparing risks among classes of initiating event and in establishing risk-dominance among seismic contributors (i.e., among components).

Even among seismic risk experts, there have been raised a number of technical issues that question the accuracy and validity of techniques employed in conventional seismic risk methodology. For instance, significant discussions at a January 1987 workshop on engineering characterization of small-magnitude earthquakes revealed a need to investigate the effect of magnitude-disaggregation on seismic hazard, fragility and risk. A paper by Cornell and Sewell (4) revealed that spectral-shape characteristics of small-magnitude ground motions are varied and that, given the same level of spectral acceleration at the structural frequency of interest, small-magnitude motions, despite being of shorter duration, can be just as severe as large-magnitude motions. At a given distance, however, the likelihood of experiencing a damaging intensity of ground motion (e.g., spectral acceleration) would be less given a small-magnitude earthquake than given a large-magnitude earthquake; yet the occurrence rate of small-magnitude ground-motions affecting a given site would be greater. From extensive discussions pertaining to the impact of varied spectral characteristics on damage and of damage likelihoods for events of different magnitudes, the workshop proceedings summarize (5):

[1]Recent, realistic assessments in source-term and offsite-consequence modeling, however, have produced uncertainties that exceed those produced by seismic risk modeling, suggesting that the large uncertainties in seismic risk may be becoming viewed as less questionable.

"...the point was raised that it is important that the seismic hazard results transfer adequate information to the structural engineer who must assess the response and damage to structures. Engineers pointed out that a [composite] uniform hazard spectrum is not an adequate engineering characterization of ground motion. Since it is a synthesized estimate of hazard, it is not representative of ground motions that would be experienced at a site. In general, engineers require information on the duration of shaking, the breadth of frequency content and a measure of the amplitude of the motion.

Kennedy discussed the engineering characterization of small-magnitude earthquakes. Based on studies of ground motion for a range of earthquake magnitudes, he concludes that spectral acceleration is a preferred measure of damage capability (i.e., ductility reached) for a wide variety of earthquake magnitudes (M_L 4.7 to 7.2). Furthermore, he concluded that aggregating in a seismic hazard analysis the ground motion from earthquakes with very different characteristics is inappropriate since it is not possible to realistically correlate the ground motion hazard to the expected damage. He suggests that seismic hazard estimates be deaggregated for ground motions with very different frequency content."

This discussion reveals the desirability of structural engineers to have seismic hazard information that distinguishes among the various types of spectral (and duration) characteristics that may be experienced at a site; that is, hazard disaggregation into groups associated with common earthquake characteristics is viewed as being important. The structural engineer is capable of using this refined ground-motion information to develop refined fragility estimates, thus leading to improved seismic risk assessment. Inasmuch as a large-magnitude earthquake motion generally has broader frequency content and longer duration that a small-magnitude motion (at a given site), one obvious and useful basis for disaggregating hazard spectra would be by earthquake magnitude (i.e., magnitude range).

In the above discussion, Kennedy recommends that spectral acceleration would be an improved basis for damage prediction (vis-à-vis the conventional use of peak ground acceleration as the motion parameter in hazard and fragility assessments). Specifically, based on earlier work by Kennedy (6), the spectral acceleration averaged over a frequency range of interest has been identified as an improved ground-motion characterization. This averaged (linear) spectral acceleration parameter has been recommended because it well approximates the inelastic spectral acceleration at a specific structural frequency of interest, where constant ductility is

used as the inelastic (damage) measure. By definition (for a single-degree-of-freedom structure, at least), inelastic spectral acceleration (based on relevant damage models) directly quantifies the damage effectiveness of ground motion. Based on discussion by Cornell, a recent workshop on seismic hazard mapping (7) recommended exploring the use of inelastic spectral acceleration for parameterizing ground motion in hazard mapping. Research by Sewell (8) has developed ground-motion functions and methodology for performing seismic hazard analyses directly on inelastic spectral acceleration (based on a variety of damage models); that work also suggests that appropriate measures of average spectral acceleration can be used to adequately describe earthquake damage potential, regardless of how one chooses to model damage. Examination of the current earthquake engineering literature clearly reveals that there is keen interest among structural engineers as to the effect of the use of alternate characterizations (e.g., PGA, spectral acceleration, inelastic spectral acceleration) of ground motion on estimates of seismic hazard, fragility, and risk.

In addition to technical questions pertaining to the effects on seismic risk of magnitude disaggregation and of ground-motion characterization, it is commonly known that the spectral shapes (typical of ground motions in the western U.S., albeit from small-magnitude earthquakes) used in past SPRAs and those recommended in conducting SMAs are conservative with respect to motions expected in the eastern U.S. Recent research (9,10) on ground motions in the eastern U.S. has enabled the hazard quantification (11,12) of realistic earthquake spectra specific to eastern U.S. sites. A recent NRC study on severe-accident risks to five eastern U.S. nuclear power plants [NUREG–1150 (13)], made use of PGA hazard curves consistent with these eastern U.S. spectra in quantifying seismic core-damage risk at two nuclear plants. No study hitherto (including NUREG 1150), however, has either used these realistic eastern U.S. spectral shapes in quantifying seismic fragilities and risks, or compared the results of such quantification with what results from the use of conventional, conservative spectral shapes.

1.2 OBJECTIVE OF STUDY

As alluded to in the above discussion, concern by various experts has been expressed related to a number of potential sources of bias (largely conservative) and reducible uncertainty in seismic risk evaluation. This study addresses these concerns, which are largely related to protocol in analysis and information passage between seismic hazard and seismic fragility assessments; specifically, we consider the following issues:

- Use of a conservative response spectrum shape.

- Use of a single, composite spectrum to characterize the ground motion threat for earthquakes of all magnitudes.
- Use of peak ground acceleration (PGA) as the common basis (parameterization) of ground motion intensity.

The objective of this study is to quantify the impact of these issues on seismic risk estimates, including estimates of uncertainty, for a selected nuclear power plant SPRA.

1.3 STUDY APPROACH

This study is organized into five separate tasks:

1. Selection of a case-study nuclear power plant and description of its SPRA data and results.
2. Generation of magnitude-dependent ground motions.
3. Assessment of magnitude-dependent fragilities for alternate ground motion characterizations.
4. Assessment of magnitude-dependent seismic hazard for alternate ground motion characterizations.
5. Risk quantification from magnitude-dependent hazard and fragility assessments.

The major emphasis of the study is on development of magnitude-dependent ground motions and fragilities. The methods used to generate ground motions incorporate realistic peak-to-valley variabilities (14) and are derived from ground motion spectra developed from state-of-the-art random-vibrations techniques in ground motion modeling (15).

The methods used to derive fragility curves are based on detailed, nonlinear dynamic modeling and analysis, also implementing state-of-the-art procedures (16). In addition to the modern use of elastic spectral acceleration (averaged over an appropriate frequency range) and the past use of PGA as fragility parameters in SPRA, this study also explores the use of inelastic spectral acceleration as a ground-motion characterization basis for fragility assessment.

1.4 REPORT OUTLINE

Section 2 provides a description of the nuclear power plant selected for investigation. The case study plant is located in the eastern United States. Specific details of the SPRA for this plant, as they pertain to this study, are described. A representative failure mode for this plant is selected and discussed. Replicating exactly certain minute details of this failure mode proved to be both impractical and unnecessary; consequently, a hypothetical, yet realistic model was developed. This hypothetical failure-mode model represents a general situation that may exist at a number of U.S. nuclear power plants.

For comparative purposes, the SPRA methods and results are used as a base case; that is, the SPRA hazard, fragility, and risk assessment procedures are replicated for subsequent reference and comparison with results of other cases.

Section 3 provides a general description of the methods developed and implemented for generating ground motions that are used subsequently in fragility determinations (a more detailed description of the methods is given in Appendix A). Motions are generated to match each of the following target spectra:

- The SPRA (base case) spectrum. This spectrum is considered to be conservative for the site because its shape is based on motions characteristic of the western United States, and it has considerably more energy at frequencies below 10 Hz (i.e., the frequency range of interest for most nuclear power plant structures) than is characteristic of eastern U.S. locations.
- A composite-magnitude ($4.5 \leq m_b \leq 7.0$) site spectrum. This spectrum is representative of motions produced by eastern U.S. earthquakes.
- A suite of magnitude-dependent site spectra, one spectrum for each of the following five magnitude ranges: $4.5 \leq m_b < 5.0$ ($m_b = 4.75$), $5.0 \leq m_b < 5.5$ ($m_b = 5.25$), $5.5 \leq m_b < 6.0$ ($m_b = 5.75$), $6.0 \leq m_b < 6.5$ ($m_b = 6.25$), and $6.5 \leq m_b \leq 7.0$ ($m_b = 6.75$). These spectra are representative of different magnitude motions in the eastern U.S. and, if aggregated, will produce a spectrum similar to the composite-magnitude spectrum.

Motions generated for the above cases are used to develop seismic fragilities corresponding to each target spectrum. Section 4 documents the methods used in the fragility assessments,

and their results. Details of the simulation procedure used in the uncertainty analysis are described. Discussion on damage-effectiveness characterizations of ground motion is presented, as related to determinant effects on fragility parameters.

Section 5 discusses the procedures for replicating the SPRA hazard curves and performing the composite-magnitude and magnitude-dependent seismic hazard analyses.

Section 6 presents and compares the risk (failure rate) results obtained from integrations of appropriate hazard/fragility combinations. Fragility and hazard curves derived for corresponding composite-magnitude and magnitude-dependent motions are used in these integrations.

Section 7 summarizes results of Phase 1 research, draws conclusions, and makes recommendations pertaining to the applicability of the results and direction of future study.

1.5 REFERENCES

1. Atomic Energy Commission. "Reactor Site Criteria: Seismic and Geologic Siting Criteria." *Federal Register* – 10 CFR Part 100, Vol. 38, No. 218. November 13, 1973.

2. USNRC. *Policy Issue (Information): Integration Plan for Closure of Severe Accident Issues.* SECY–88–147, May 25, 1988. USNRC Memorandum from Victor Stello, Jr. to Commissioners.

3. American Nuclear Society and Institute of Electrical and Electronic Engineers. *PRA Procedures Guide.* Technical Report NUREG/CR–2300, U.S. Nuclear Regulatory Commission, January 1983.

4. C. A. Cornell and R. T. Sewell. Equipment response in linear and non-linear nuclear power plant structures: small magnitude versus design-type motions. In *Proceedings: Engineering Characterization of Small-Magnitude Earthquakes*, M. W. McCann and J. W. Reed, editors. Report No. NP–6389, Electric Power Research Institute, June 1989.

5. EPRI. Session Summary: Characterization of ground motion associated with small-magnitude earthquakes. In *Proceedings: Engineering Characterization of Small-Magnitude Earthquakes*, M. W. McCann and J. W. Reed, editors. Report No. NP–6389, Electric Power Research Institute, June 1989.

6. R. P. Kennedy, S. A. Short, K. L. Merz, F. J. Tokarz, I. M. Idriss, M. S. Power, and K. Sadigh. *Engineering Characterization of Ground Motion – Task I: Effects of characteristics of free-field motion on structural response.* Technical Report NUREG/CR–3805, U.S. Nuclear Regulatory Commission, February 1984. Vol. 1.

7. National Center for Earthquake Engineering Research. *Workshop on Ground Motion Parameters for Seismic Hazard Mapping.* R. V. Whitman, editor, 1989. 68 pp.

8. R. T. Sewell. Damage-Effectiveness of Earthquake Ground Motion: Characterizations based on the performance of structures and equipment. *Ph.D. Thesis*, Stanford University. Stanford, CA, 1989.

9. EPRI. *Proceedings: Earthquake Ground-Motion Estimation in Eastern North America.* Electric Power Research Institute, August 1988.

10. D. L. Bernreuter, J. B. Savy, R. W. Mensing, and D. H. Chung. *Development of Eastern United States Ground Motion Models.* Technical Report NUREG/CR-3756, U. S. Nuclear Regulatory Commission, 1987. Appendix C in Seismic Hazard Characterization of the Eastern United States: Methodology and Interim Results for Ten Sites.

11. R. K. McGuire, G. R. Toro, J. P. Jacobson, T. F. O'Hara, and W. J. Silva. *Probabilistic Seismic Hazard Evaluations in the Central and Eastern United States: Resolution of the Charleston Earthquake Issue.* Special Report NP-6395-D, Electric Power Research Institute, April 1989.

12. D. L. Bernreuter, J. B. Savy, R. W. Mensing, and J. C. Chen. *Seismic Hazard Characterization of 69 Plant Sites East of the Rocky Mountains.* Technical Report NUREG/CR5250, UCID-21517, U. S. Nuclear Regulatory Commission, 1988.

13. USNRC Office of Nuclear Regulatory Research. *Severe Accident Risks: An Assessment for Five U.S. Nuclear Power Plants.* Technical Report NUREG–1150, U.S. Nuclear Regulatory Commission, 1989. Summary Report — Second Draft for Peer Review.

14. T. Inoue. Ground Motion Damage Effectiveness for MDOF Structures. Engineer's Thesis, Department of Civil Engineering, Stanford University, 1990.

15. G. R. Toro and R. K. McGuire. "An Investigation into Earthquake Ground Motion Characteristics in Eastern North America". *Bulletin of the Seismological Society of America*, 77(2):468–489, April 1987.

16. R. P. Kennedy, D. A. Wesley, and W. H. Tong. *Probabilistic Evaluation of the Diablo Canyon Turbine Building Seismic Capacity Using Nonlinear Time History Analysis.* Technical Report 1643.01, Pacific Gas and Electric, 1989.

Section 2

CASE STUDY NUCLEAR POWER PLANT AND FAILURE MODE

This section describes the nuclear power plant and plant failure mode selected for examination in this study. The objective of Phase 1 research is to explore potential sources of conservatism and uncertainty in seismic probabilistic risk estimates previously undertaken for a particular plant (i.e., plant failure mode). Millstone Unit 3 was chosen as the base-case study plant.

The Millstone 3 SPRA is generally recognized as a well developed study. It is also considered to reflect reasonably modern procedure, and is judged to be of high quality, representative of the more-detailed SPRAs performed to date for eastern U.S. nuclear power plants.

2.1 PLANT AND PRA DESCRIPTION

Millstone 3 is located in southern Connecticut. The plant is a pressurized water reactor (PWR) with a 4-loop steam supply. The containment structure is built of heavily reinforced concrete with a steel liner.

Millstone 3 was designed in the early 1970's. The safe-shutdown earthquake (SSE), seismic design-basis acceleration for this plant is 0.17g, and the operating basis earthquake (OBE) is 0.09g.

The probabilistic risk assessment for Millstone 3 was published in 1983 (1). The seismic fragility analysis was performed by Structural Mechanics Associates and the seismic hazard analysis was conducted by Dames & Moore.

2.2 SEISMIC FRAGILITY RESULTS

The SPRA evaluation of seismic fragilities for Millstone 3 structures and equipment was based on the standard, well-established analytical approach (2). In this method, component fragility parameters $\breve{A}$, β_R, and β_U (defined later) are obtained through analysis and judgment of safety factors. An overall (random-variable) safety factor F is defined simply as an ultimate failure (or non-operability) capacity divided by a reference (e.g., design-basis or

working) load. Under this definition, the median acceleration failure capacity $\breve{A}$ is obtained as:

$$\breve{A} = \breve{F} \cdot A_{SSE} \qquad (2-1)$$

where $\breve{F}$ is the median overall safety factor and A_{SSE} is the SSE design acceleration.

The overall median safety factor $\breve{F}$ consists of the product of various elemental safety factors. Consistent with the assumption of lognormal fragilities, elemental safety factors are assumed lognormal, and Eq. 2-1 can be expanded in the following form:

$$\breve{A} = \breve{F}_S \cdot \breve{F}_\mu \cdot \breve{F}_{ED} \cdot \breve{F}_{SS} \cdot \breve{F}_\xi \cdot \breve{F}_M \cdot \breve{F}_{MC} \cdot \breve{F}_{SRSS} \cdot \breve{F}_{SSI} \cdot A_{SSE} \qquad (2-2)$$

where the elemental safety factors are defined in Table 2-1.

The parameters β_R and β_U denote, respectively, the logarithmic standard deviation in capacity given knowledge of a median capacity, and the logarithmic standard deviation in the median capacity itself; hence, β_R describes variability in capacity due to randomness, and β_U describes variability in capacity due to modeling uncertainty. The component values of β_R and β_U can be constructed from elemental values; again assuming lognormality, these variability parameters can be expressed as:

$$\beta_R = \sqrt{(\beta_S)_R^2 + (\beta_\mu)_R^2 + (\beta_{ED})_R^2 + \ldots} \qquad (2-3)$$

and

$$\beta_U = \sqrt{(\beta_S)_U^2 + (\beta_\mu)_U^2 + (\beta_{ED})_U^2 + \ldots} \qquad (2-4)$$

Given values of $\breve{A}$, β_R and β_U, a component HCLPF (high-confidence of low-probability of failure) capacity may be found as

$$\text{HCLPF} = \breve{A} e^{-1.65(\beta_R + \beta_U)} \qquad (2-5)$$

In words, the HCLPF capacity is the ground motion at which one is 95% confident that the probability of failure does not exceed 5%.

Results of the SPRA fragility analysis for key structures and equipment at Millstone 3 are summarized in Table 2-2. These results are based on a single, composite-magnitude ground motion spectrum used in determining component responses. This base-case ground motion spectrum is shown in Figure 2-1, and is associated with a magnitude of 5.8 (i.e., the magnitude that was determined to dominate the seismic hazard). The base-case spectral shape is characteristic of magnitude 5.8 ground motions experienced in the western U.S.,

Table 2-1

Definitions of Elemental Factors of Safety Used in Standard Seismic Fragility Analysis

Elemental Safety Factor	Description
F_S	Elastic Strength Reserve
F_μ	Inelastic Capacity Reserve
F_{ED}	Earthquake Duration/Response-Cycles Safety Factor
F_{SS}	Spectral Shape Safety Factor
F_ξ	Damping Safety Factor
F_M	Structural Model Safety Factor
F_{MC}	Modal Combination Safety Factor
F_{SRSS}	Combination of Earthquake Components Safety Factor
F_{SSI}	Soil Structure Interaction Safety Factor

Table 2-2

Fragility Parameters of Millstone 3 Structures and Equipment that Are Important in Plant-Damage-State Logic. [Source: (1)].

Component Number	Component Description	$\breve{A}$ (g)	β_R	β_U	HCLPF (g)	Plant Damage Impacts
		Structures				
3	Emergency Generator Enclosure Building	0.88	0.20	0.46	0.30	TE, AE, SE
4	Refueling Water Storage Tank (Buckling)	0.88	0.30	0.36	0.30	AE, SE
7	Control Building (Diaphragm Failure)	1.00	0.24	0.43	0.33	TE, AE, SE
12	Service Water Pumphouse (Sliding)	1.30	0.24	0.49	0.39	TE, AE, SE
20	Engineered Safeguard Features Bldg (Basemat/ Shear Wall Failure)	1.70	0.23	0.43	0.57	TE, AE, SE
27	Containment Crane Wall (Shear Wall Failure)	2.20	0.39	0.38	0.62	V3
		Equipment				
1	Loss of Offsite Power (Ceramic Insulator Breakage)	0.20	0.20	0.25	0.10	TE
5	Emergency Diesel Generator (Oil Cooler Anchor Bolt Fails)	0.91	0.24	0.43	0.30	TE, AE, SE
6	Reactor Vessel Core Geometry Distortion	0.99	0.21	0.33	0.41	SE
9	Control Rod Drive System (Failure to SCRAM)	1.00	0.30	0.38	0.33	SE
15	Reactor Coolant System Piping (Large LOCA)	1.59	0.48	0.51	0.31	AE

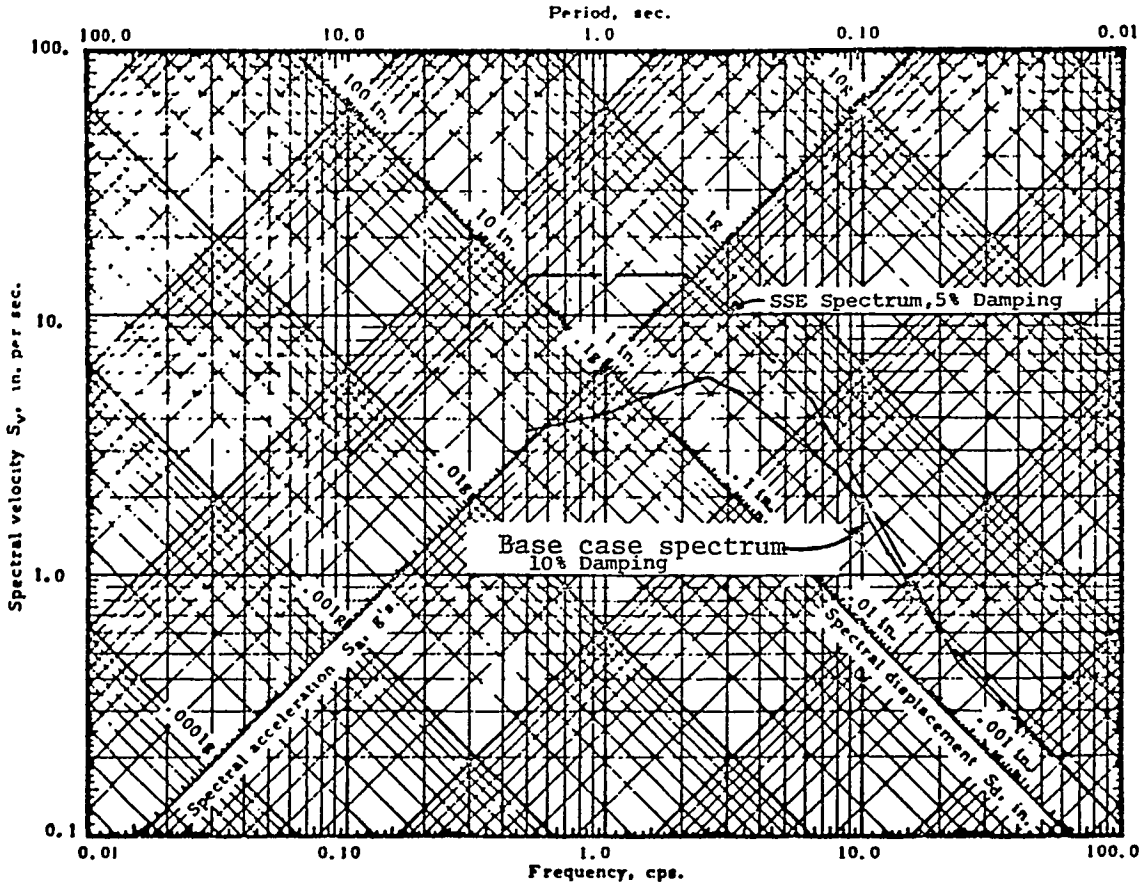

Figure 2-1. SPRA Base Case spectrum, anchored to a peak ground acceleration of 0.17g (Damping= 10%). This spectrum characterizes the median input motion for the SPRA fragility analyses. [Source: (1)].

and as shown later in Section 4, is very conservative (for response of most components) in comparison to eastern U.S. ground motion spectra (for similar magnitudes) derived from modern interpretations and motion databases.

It is also important to note that fragility assessments within the usual SPRA format are obtained by comparison with linear response calculations and design models, as opposed to direct nonlinear time-history-response failure analysis. This approach involves the use of significant judgment which may introduce a conservative bias in the fragility result. The procedure for fragility analysis discussed in Section 4, and based on detailed nonlinear dynamic analysis, eliminates the need to determine elemental safety factors, and hence, eliminates a significant potential for conservative judgment to effect fragility results.

2.3 SEISMIC HAZARD RESULTS

The base-case seismic hazard results obtained from the Millstone 3 SPRA analysis are shown in Figure 2-2. Ten curves are used to represent the uncertainty in seismic hazard for the site.

2.4 SEISMIC PLANT-DAMAGE-STATE LOGIC

Evaluation of the results of the Millstone 3 SPRA indicates that the following four plant damage states dominate both the core-damage risk and the risk of offsite consequences (3):

Plant Damage State	Description
TE	Transient (caused by loss of offsite power) with failure of onsite emergency power or RCS heat removal
AE	Large Loss of Coolant Accident (LOCA) with failure of safety injection system and containment quench sprays
SE	Small LOCA or Anticipated Transient Without SCRAM (ATWS) with failure of safety injection system and containment quench sprays
V3	LOCA with containment bypass

The impact on each of these plant damage states of the important plant structures and equipment is shown in Table 2-2. Boolean logic for these major plant-damage-state groups

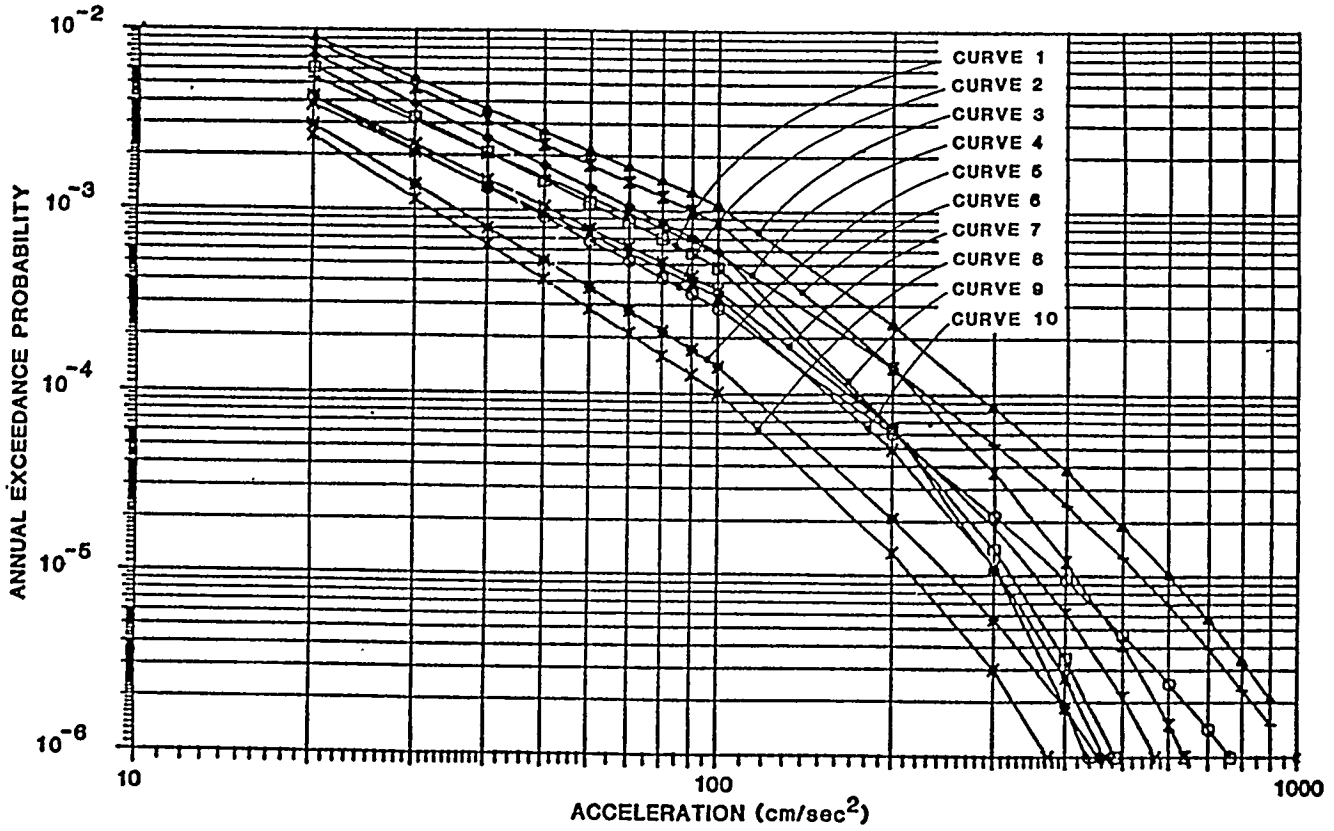

Figure 2-2. SPRA Base Case seismic hazard curves for peak ground acceleration. [Source: (1)].

is presented in the Millstone 3 SPRA (1) and seismic margin report (3). This Boolean logic can be simplified to the following equations:

$$\mathrm{TE} \approx 1 \cap (3 \cup 5 \cup 7 \cup 12 \cup 20 \cup R19) \qquad (2-6)$$

$$\mathrm{AE} \approx (3 \cup 4 \cup 5 \cup 7 \cup 12 \cup 20 \cup R19) \cap 15 \qquad (2-7)$$

$$\mathrm{SE} \approx (3 \cup 4 \cup 5 \cup 7 \cup 12 \cup 20 \cup R19) \cap (6 \cup 9) \qquad (2-8)$$

$$\mathrm{V3} \approx 27 \qquad (2-9)$$

$$\mathrm{CD} \approx [(3 \cup 5 \cup 7 \cup 12 \cup 20 \cup R19) \cap (1 \cup 6 \cup 9 \cup 15)] \cup \left[\overline{3} \cap 4 \cap \overline{5} \cap \overline{7} \cap \overline{12} \cap \overline{20} \cap \overline{R19} \cap (6 \cup 9 \cup 15)\right] \cup 27 \qquad (2-10)$$

where $R19$ denotes random failure of the emergency AC system (median failure rate of 2×10^{-4} per demand), CD denotes core damage, and $\overline{(\cdot)}$ denotes non-failure of the specified component.

2.5 SELECTION OF FAILURE MODE

Of the above plant damage states, TE and V3 are of particular importance because TE dominates the contribution to seismic core-damage risk and V3 is nearly the sole contributor to offsite-consequence acute-fatality risk from seismic events. Examination of the Boolean expressions for these two plant damage states, and of Table 2-2, demonstrates that shear-wall failure or floor-diaphragm failure [1] is the most frequently encountered failure mode that has important implications to seismic core-damage and offsite-consequence risks. The conclusion that shear-wall failure is the most frequently occurring mode of failure remains true even if the less-important plant damage states AE and SE are included.

Shear-wall failure is a characteristic mode of the stiff, massive concrete structures used to house and/or support critical nuclear power plant components; for this reason, shear-wall failure has been a consideration in every SPRA performed to date. Consequently, shear-wall failure has been extensively studied, and little professional contention exists over established understanding of its mechanism and methods of analysis. For these reasons, shear-wall failure is selected as the principal failure mode for case study in this report.

[1] The mechanisms of shear-wall and floor-diaphragm failures are nearly identical; that is, shear stiffness, shear strength, and relative shear deformations (drift) dominate the dynamic response and failure in both cases. A floor diaphragm failure can be idealized as a shear-wall failure in the horizontal plane, excluding the (typically negligible) effects of gravity (axial, in-plane) loads that exist in shear walls. As a result, in this study, floor-diaphragm and shear-wall failures are considered to be synonymous modes.

To illustrate the impacts of magnitude-dependent spectra and alternate characterizations of ground motion on risk estimates, a hypothetical (yet highly realistic) idealization of the Millstone 3 control building is used. The shear-wall failure mode for this structure is failure of the floor diaphragm at the third-floor level, in the vicinity of numerous cut-outs. In addition to the effects of the cut-outs, the capacity/demand ratio for this diaphragm element is relatively low due to discontinuity in shear path from the story above (discussed in Section 4). This type of shear-path discontinuity is typical of some nuclear power plant structures.

Diaphragm failure in the control building was the most critical (i.e., lowest median capacity) case of shear-wall failure discovered in the SPRA analysis of the Millstone 3 reactor, which was a major motivation for its selection in this study. From a review of the Millstone 3 SPRA fragility notes for the control building, however, it was anticipated that this failure mode might, in fact, not be probable. In performing the detailed nonlinear time-history-based fragility analyses of Section 4, this anticipation was verified; i.e., the analyses clearly showed that diaphragm failure was extremely unlikely to occur due to concurrent nonlinear behavior of the bottom-floor shear walls. Although the capacity/demand ratio of the bottom-floor shear walls is greater than that of the third-floor diaphragm, once the bottom element goes nonlinear (typically, when the ductility ratio in the floor diaphragm is less than $\mu = 3.0$), the diaphragm becomes isolated from the input motion, and the failure of the shear wall becomes critical. In other words, the SPRA fragility study indirectly and conservatively assumed no nonlinearity in other than the floor-diaphragm element of the structure.

This example serves (purposefully) to illustrate a potential source of conservatism that results from application of one's judgment in the standard fragility (i.e., safety factor) approach. Of course, such application of judgement can also potentially lead to unconservative results; in general, however, when making judgements, engineers have been trained to approach problems conservatively. The introduction of such conservatism may likely have occurred frequently in past seismic fragility analyses. The effects of such conservatism are not quantified in this report, but they are likely to be significant. *The use of nonlinear time-history analysis in fragility assessment reduces significantly the potential for the introduction of these and several other modeling conservatisms.*

Despite the finding here that diaphragm response does not in fact govern failure of the control building, the floor-diaphragm failure mechanism is nevertheless of relevant interest and is representative of shear-wall/diaphragm failure problems. Consequently, (and to facilitate comparison with the SPRA base-case analysis) this study examines failure of the floor diaphragm under the same conditions assumed in the SPRA analysis, and constrains the bottom element of the control building to linear behavior.

2.6 REFERENCES

1. Northeast Utilities. *Millstone Unit 3 Probabilistic Safety Study.* 1983.

2. American Nuclear Society and Institute of Electrical and Electronic Engineers. *PRA Procedures Guide.* Technical Report NUREG/CR–2300, U.S. Nuclear Regulatory Commission, January 1983.

3. M. Ravindra, R. Sues, R. Kennedy, and D. Wesley. *A Program to Determine the Capability of the Millstone 3 Nuclear Power Plant to Withstand Seismic Excitation Above the Design SSE.* 1984. Report No. 20601.01-R2 prepared by Structural Mechanics Associates for Northeast Utilities.

Section 3
GENERATION OF ARTIFICIAL GROUND MOTIONS

3.1 INTRODUCTION

This section describes the method used to generate artificial ground motions for the calculation of fragilities of the hypothetical control building shear-wall/floor-diaphragm model. This section also presents graphical summaries of the generated time histories.

We generate multiple artificial ground motions (typically 25) for each of the seven types of seismic-hazard results in Section 5. Therefore, we consider seven types of ground motions as follows: (1) ground motions typical of the SPRA hazard analysis; (2) ground motions typical of a seismic hazard analysis that uses the current understanding of seismicity and ground motions in the eastern United States [we will call this the composite seismic-hazard analysis]; and (3–7) ground motions typical of a seismic-hazard analysis disaggregated by magnitude [we call these magnitude-dependent analyses].

The artificial ground motions must meet the following requirements:

- On average, they must have the frequency content, duration, and time-domain appearance of the type of ground motions being simulated.
- They must have record-to-record variability and jagged spectral shapes typical of actual ground motions.

The standard methods for the generation of artificial ground motions [see, for example, References (1,2,3)] do not convey a realistic representation of variability. These methods include only the variability introduced by random phasing, and they under-estimate the record-to-record variability exhibited by real earthquakes.

3.2 CHARACTERIZATION OF GROUND-MOTION TYPES

A ground-motion type is characterized here by its geometric-average[1] response spectrum shape and its average duration. Duration is defined as the time between 5% and 75% of the energy in a cumulative energy plot, as proposed by Kennedy *et al.* (4).

The selection of response spectrum and duration for each ground-motion type are described below. Table 3-1 contains a summary of these characteristics.

Table 3-1

Events Used to Generate the Spectral Shapes for Magnitude-Dependent Hazard Analysis

Magnitude Range (m_b)	$M_o^\dagger$ (dyne-cm)	f_o (Hz)	Hypocentral Distance (km)	Durations (sec) T_s	T_p	T
4.5 – 5.0	3.04×10^{22}	2.522	10	0.39	0.5	0.49
5.0 – 5.5	1.50×10^{23}	1.499	20	0.67	1.0	0.77
5.5 – 6.0	9.95×10^{23}	0.798	30	1.25	1.5	1.75
6.0 – 6.5	1.01×10^{25}	0.368	30	2.71	1.5	4.21
6.5 – 7.0	1.88×10^{26}	0.139	30	7.20	1.5	8.70

†Calculated for the magnitude at the center of the magnitude range.

3.2.1 Ground Motions Corresponding to the SPRA Hazard Analysis

The seismic hazard study performed in the PRA (5) characterizes the event that dominates the hazard as an earthquake with m_b 5.8 at 30 to 50 km. Its geometric-average spectral shape is given by the response spectrum in Figure 3-1. This spectral shape is similar to the spectral shapes obtained in Reference (4) for California earthquakes in the same magnitude range.

We assigned a duration of 2.5 sec to this event. This duration is consistent with the average durations obtained in Reference (4) for earthquakes in this magnitude range; it is also

[1]The geometric average is the same as the anti-logarithm of the average of the logarithms of a quantity. It is typically used to characterize the central tendency of random quantities that exhibit lognormal-like distributions.

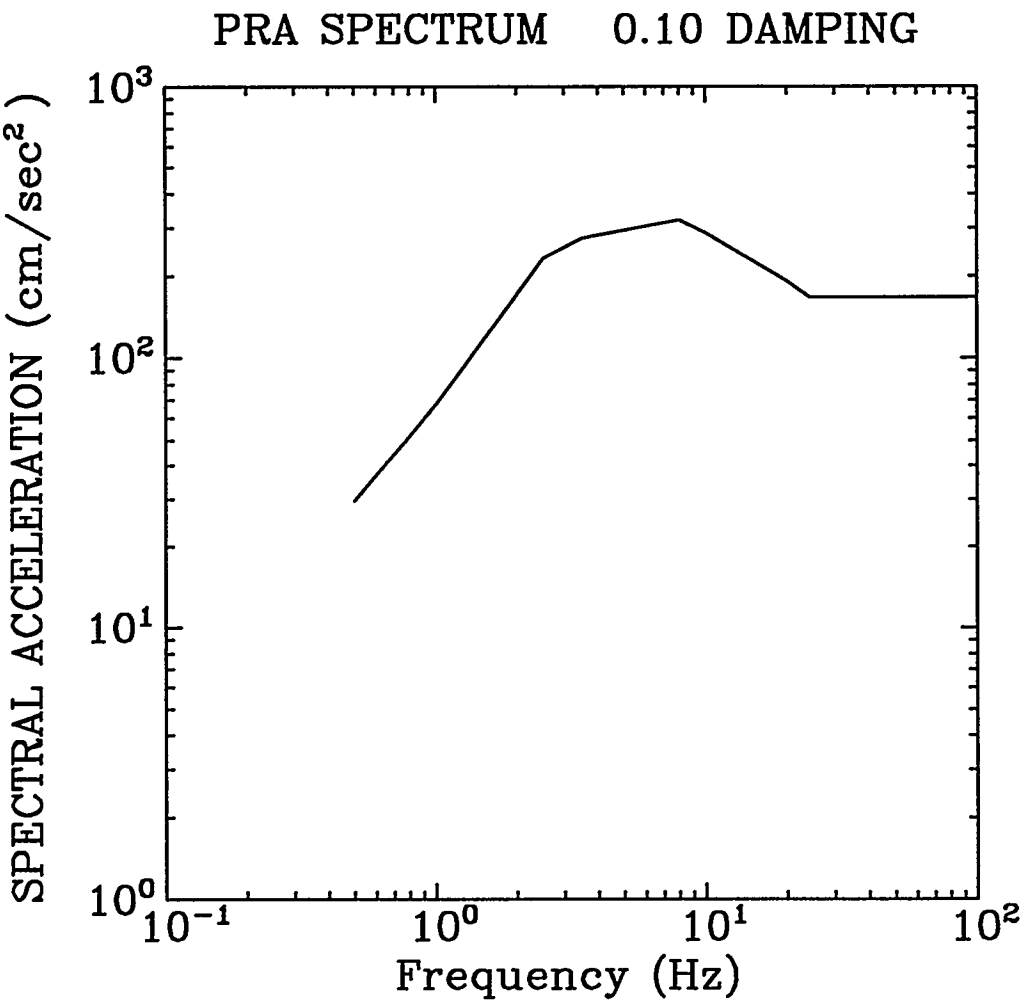

Figure 3-1. Geometric-Average response spectral shape for ground motions corresponding to the PRA seismic hazard analysis. Damping ratio: 10%.

consistent with the durations obtained from Equation 3-3.

3.2.2 Ground Motions Corresponding to the Composite Seismic Hazard Analysis

The geometric-average spectral shape for these motions is given by the (5%-damped) uniform-hazard spectrum corresponding to an exceedance probability of 10^{-6}. This spectrum is shown in Figure 3-2, where it appears as the dashed line. This spectral shape roughly corresponds to m_b 5.75 at high frequencies (> 2 Hz) and to a higher m_b 6.0 at lower frequencies. This record is assigned an average duration of 2.8 sec. This value is appropriate for an event with m_b 5.8 to 6.0, based on the methods to be presented in Sections 3.2.3 and 3.3.

Strong-motion records obtained in the eastern United States and southeastern Canada during the last ten years have consistently shown more high-frequency energy than records from California. Current models of ground motions for the eastern United States (6,7,8,9) predict ground motions with significant energy up to 50 Hz. Models of this type are given significant weight in current seismic-hazard analyses (10,11) and dominate the shape of the uniform-hazard spectrum. This is the reason for the large difference between the spectral shapes from the SPRA and composite hazard analyses.

3.2.3 Ground Motions Typical of the Magnitude-Dependent Hazard Analyses

The geometric-average spectral shapes and durations for the magnitude-dependent hazard analyses are obtained using the ground-motion model by Toro and McGuire (7,8) with minor variations. The following is a brief description of this model.

The frequency-content of ground motions at the site is given by the Fourier amplitude of acceleration, which is assumed to be of the form:

$$|\tilde{a}(\omega)| = \frac{0.85 M_o}{4\pi\rho\beta^3 R} \frac{\omega^2}{1+(\frac{\omega}{\omega_o})^2} e^{-\frac{\omega R}{2Q\beta}} e^{-\frac{\kappa\omega}{2}} \qquad (3-1)$$

The first term in the above equation represents the static displacement at the site. M_0 is the seismic moment (a measure of earthquake size, with units of dyne-cm), ρ is the crustal density (2.7 g/cm^3), β is the shear-wave velocity (3.5 $\times$ 10^5 cm/sec), and R is hypocentral distance (cm).

The second term represents the shape of the Fourier spectrum, which is controlled by the corner frequency. We assume that corner frequency is related to seismic moment through

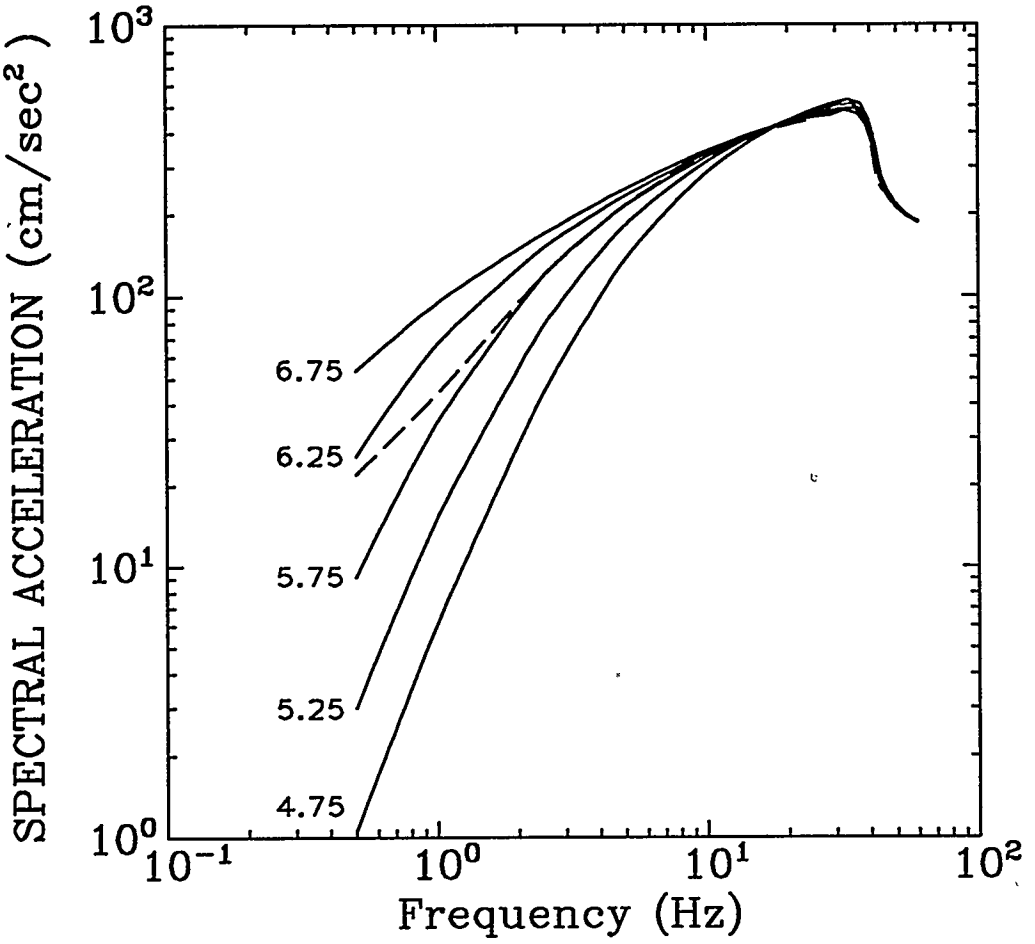

Figure 3-2. Geometric-Average response spectral shapes (5% damping) for ground motions corresponding to the composite (dashes) and magnitude-dependent (solid) seismic hazard analyses.

the expression $f_o = \omega_o/2\pi = 7.973 \times 10^7 M_o^{-1/3}$, which applies to earthquakes with stress drops of 100 bars (8).

The relationship between seismic moment and magnitude m_b (or, more precisely, m_{bLg}) is given by the curve in Figure 5-2 of Reference (8), which is well approximated by the equation

$$M_o = \exp[35.783 + 4.3714 m_b - 0.054438 m_b^2 - 0.093901 m_b^3 + 0.0127984 m_b^4] \qquad (3-2)$$

The third term in Equation 3-1 represents anelastic attenuation (e.g., damping) and is of little importance for the calculation of spectral shapes at distances shorter than 100 km.

The fourth term represents near-site anelastic attenuation and it controls the shape of the acceleration spectrum at high frequencies. Parameter κ is given a value of 4×10^{-3} sec (8).

Based on the work of Herrmann (12), the strong-motion duration T is expressed as the sum of the source duration, $T_s = 1/f_o$, and the propagation duration, $T_p = 0.05R$ (T_p has units of seconds, R has units of km), i.e.,[2]

$$T = \frac{1}{f_o} + 0.05R \qquad (3-3)$$

The power-spectral density function (PSDF) of ground acceleration is evaluated from the quantities above as

$$S_a(\omega) = \frac{|\tilde{a}(\omega)|^2}{2\pi T} \qquad (3-4)$$

These PSDFs are used to calculate expected values of peak oscillator response and peak ground acceleration [details are provided in Appendix A and in References (7,8)], which are then converted to response spectra.

Table 3-1 lists the parameters used to generate the spectral shapes for the five magnitude ranges considered in the hazard analysis in Section 5. The choice of distances is judgmental; it is intended to approximate the expected distance given magnitude and given that a ground-motion amplitude of engineering interest is felt at the site.

[2]We assume here that Equation 3-3 applies to Kennedy *et al.'s* (4) definition of duration as the time interval between 5 and 75% of the energy. Ou (13) has calculated the 5-75% duration for records from small earthquakes in eastern Canada and for synthesized ground motions using an eastern-US crustal model. He finds that Equation 3-3 over-predicts durations. The extent of this over-prediction is small for distances of 50 km or less.

3.3 TIME VARIATION OF AMPLITUDE

The variation of amplitudes as a function of time is introduced in the records by means of an envelope function of the form

$$A(t) = 4(e^{-1.13t/T} - e^{-2.26t/T}) \qquad (3-5)$$

This general functional form was proposed by Shinozuka (1) and has been used by several other investigators.

The parameterization used here has two convenient properties: (1) the time window between 5% and 75% of $\int A^2(t)dt$ is equal to T [see Figure 3-3], which makes it consistent with our definition of duration; and (2) the peak value of $A(t)$ is 1.

3.4 MODELING OF GROUND MOTION VARIABILITY

Because we wish to capture the variability in structural capacities, it is important to model the observed variability in ground motions. This variability is observed even when one is considering a given magnitude and distance. We consider two sources of variability, as follows: variability in spectral shape and variability in duration.

3.4.1 Variability in Spectral Shape

This is the variability that exists between the spectra of ground motions from earthquakes of the same magnitude recorded at the same distance.

This variability is routinely characterized in a marginal sense (i.e., one frequency at a time) in the development of attenuation equations for spectral velocity. Results are typically presented in the form

$$\ln[PSV(f)] = \overline{\ln[PSV(f)]} + \varepsilon \qquad (3-6)$$

where $PSV(f)$ is the pseudo-velocity spectrum and ε is a lognormal random variable that represents variability. The standard deviation of ε is on the order of 0.37 to 0.65 for frequencies above 1 Hz (14).

Inoue (15) has investigated the correlation structure of ε as a function of frequency. He performed regression analyses of the type performed by Joyner and Boore (16) for frequencies of 0.25 to 10 Hz, using the same data set. He examined the residuals [or values of $\varepsilon(f)$] from

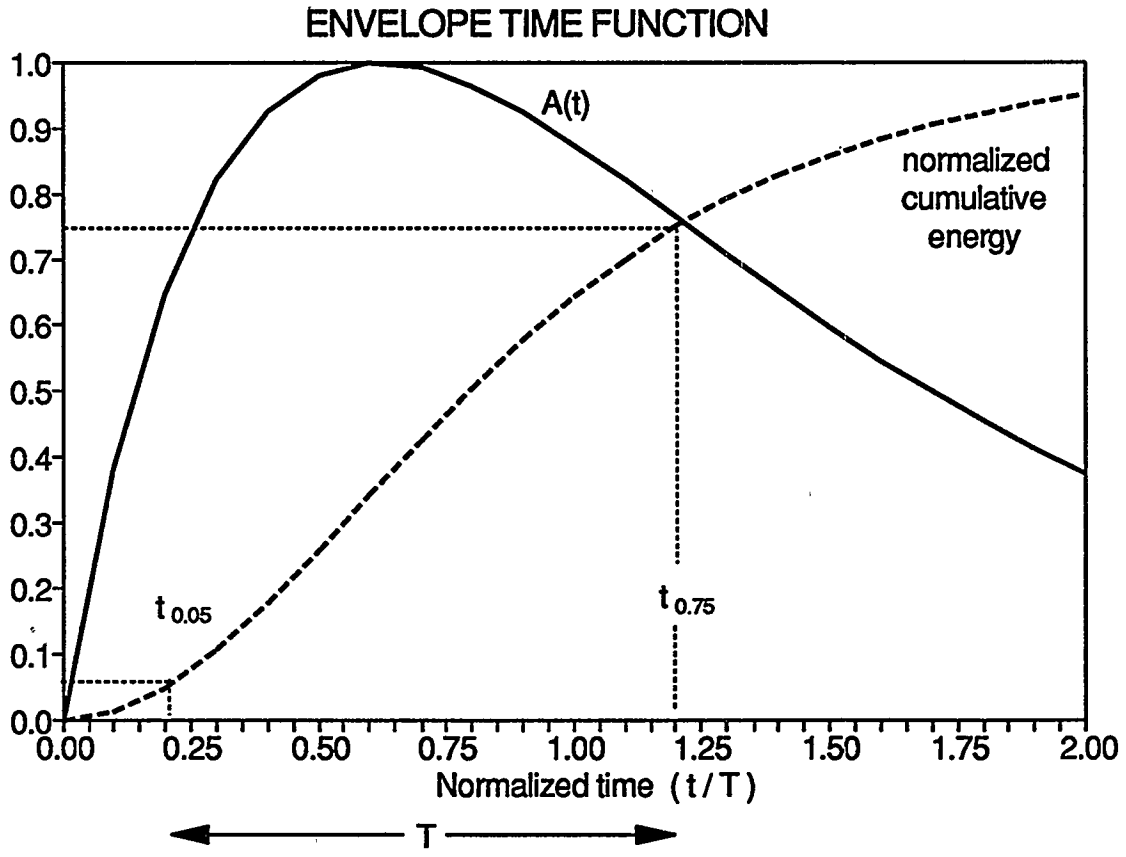

Figure 3-3. Envelope time function $A(t)$ and associated cumulative energy curve. Duration is defined as the time between 5 and 75% in the cumulative energy curve.

each record, and calculated their covariance as a function of frequency. He concluded that the correlation coefficient between residuals from the same record at frequencies f_1 and f_2 may be characterized by the expression (see Figure 3-4)

$$\text{Corr}[\varepsilon(f_1), \varepsilon(f_2)] \approx \begin{cases} 1 - \frac{1}{3}|\ln(f_1/f_2)|; & |\ln(f_1/f_2)| \leq 3 \\ 0; & |\ln(f_1/f_2)| > 3 \end{cases} \qquad (3-7)$$

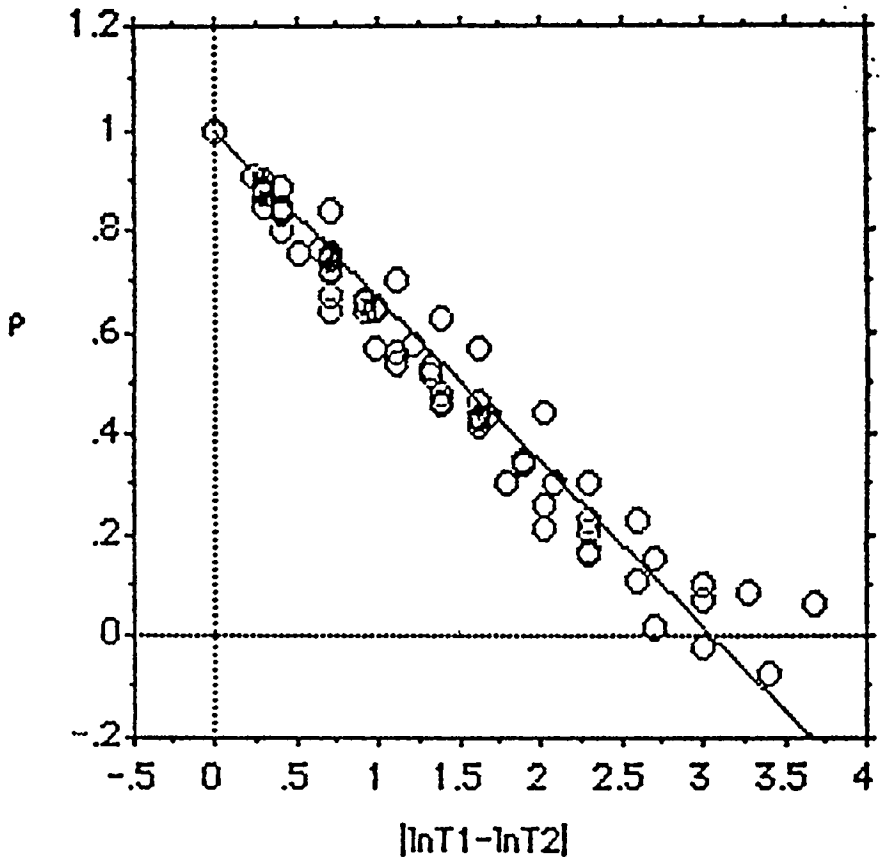

Figure 3-4. Correlation between spectral-velocity residuals from the same record plotted as a function of period separation ($|\ln(T_1/T_2)|$; or, equivalently, $|\ln(f_1/f_2)|$). Source: Inoue (15).

For this study, we assume that $\varepsilon(f)$ has a standard deviation of 0.5 (for all frequencies) and has a correlation structure given by the above equation[3]. These two assumptions imply that ε may be viewed as a stationary random process with parameter $\ln(f)$.

To generate each ground motion time history, we multiply the corresponding geometric-mean spectrum by a realization of the random function $\exp[\varepsilon(f)]$ and use the result as the target

[3]Because the technique to generate ground motions (given a power spectrum) introduces some small variability, we actually use a standard deviation of 0.43 to generate realizations of ε.

spectrum to be generated. The steps in the generation of the artificial ground motions are summarized in Section 3.5 and described in Appendix A.

The correlation model in Equation 3-7 does not apply to frequencies such that the oscillator response is mostly static (i.e., f > 10 Hz for California ground motions; f > 50 Hz for eastern U.S. ground motions). The procedure used in this study to calculate the power spectrum given the response spectrum (see Appendix A) avoids potential problems at high frequencies and generates realistic motions (see Appendix A and Figures 3-5 through 3-18).

We introduce variability through $\varepsilon(f)$ because random phasing alone introduces only a small amount of variability in peak amplitudes and very little variability in response spectral shapes.

3.4.2 Variability in Duration

As stated in Section 3.2.3, we decompose duration into two parts: source duration T_s and propagation duration T_p. T_s is a function of earthquake size, T_p is a function of distance.

T_s is assumed to be lognormal, with mean duration $1/f_o$ and a coefficient of variation of 0.1. T_p is assumed to be exponential, with a mean of $0.05R$ (for R in km and T_p in sec). As a result of these assumptions, the durations of small earthquakes have much larger coefficients of variation than those of large earthquakes.

3.5 PROCEDURE TO GENERATE THE GROUND MOTIONS

The steps in the generation of each artificial ground-motion are summarized below.

1. Simulate one realization of the response-spectrum residuals [$\varepsilon(f)$].
2. Calculate a target response spectrum by multiplying the geometric-average spectrum by exp[$\varepsilon(f)$].
3. Simulate the duration T for this artificial ground motion.
4. Using the target response spectrum and the duration, calculate the required power spectrum.
5. Generate white noise in the time domain (with unit power); multiply by time-envelope function $A(t)$ using the value of T from step 3; transform to frequency domain; multiply by square root of power spectrum from step 4; transform back to time domain.

Appendix A contains a detailed description of the algorithms used in steps 1, 4, and 5.

Figures 3-12 through 3-18 show the pseudo-acceleration response spectra for the various ground-motion types.

3.6 DISCUSSION

The spectral shape used for SPRA hazard analysis is considerably different from the shapes used for the composite and magnitude-dependent hazard analyses (compare Figures 3-1 and 3-2). These differences arise because the former spectral shape, like most spectral shapes used in earthquake-engineering practice, was constructed from ground motions recorded in California. In contrast, the latter spectral shapes are constructed from ground-motion models calibrated to recordings from the eastern United States and southeastern Canada, which have consistently shown considerable energy at frequencies as high as 50 Hz.

On the other hand, these spectral shapes are not so different if each shape is considered in relation to its associated peak acceleration. If the shape from the SPRA hazard analysis is anchored to a peak acceleration that is lower by a factor of 2 to 3, it coincides with the spectral shape for the 5.5–6.0 magnitude range, over most frequencies of engineering interest. It is not unreasonable to associate lower accelerations to the SPRA spectral shape, because the high-frequency energy in the other spectra tends to enhance peak accelerations. Also, if all spectral shapes are normalized in terms of a ground-motion measure of more relevance to structural response — such as the average spectral acceleration between 2 and 10 Hz — the SPRA spectral shape coincides with the spectral shape for the 5.5–6.0 magnitude range.

The time histories and spectra of the artificial ground motions (Figures 3-5 through 3-18) show that these motions are realistic and show realistic variability, both in frequency content and in duration. The correlation model used to characterize variability in spectral shape produces the desired effects: the spectral shapes are not smooth, they show the peaks and valleys typical of real earthquake records, and the location of these peaks and valleys varies from record to record.

For some ground-motion types, one or two of the generated spectra show considerable energy at 100 Hz. This effect is likely related to the application of the correlation model for $\varepsilon(f)$ to these high frequencies. Because this effect occurs in a small fraction of the simulated ground motions, and because typical structures are not sensitive to these very high frequencies, this effect is not a source of concern.

3.7 REFERENCES

1. M. Shinozuka. "Digital Simulation of Ground Accelerations". In *Proceedings, 5th World Conference of Earthquake Engineering*, Rome, 1973.

2. A. M. Reinhorn, M. J. Seidel, S. K. Kunnath, and Y. J. Park. *Damage Assessment of Reinforced Concrete Structures in Eastern United States.* Technical Report NCEER-88-0016, National Center for Earthquake Engineering Research, June 1988.

3. J. Jaw and H. H. M. Hwang. *Seismic Fragility Analysis of Shear Wall Structures.* Technical Report NCEER-88-0090, National Center for Earthquake Engineering Research, April 1988.

4. R. P. Kennedy, S. A. Short, K. L. Merz, F. J. Tokarz, I. M. Idriss, M. S. Power, and K. Sadigh. *Engineering Characterization of Ground Motion, Task I: effects of Caracteristics of Free Field Motions on Structural Response.* Technical Report NUREG/CR-3805, U. S. Nuclear Regulatory Commission, 1984.

5. Dames and Moore. *Seismic Hazard and Design Spectra at Millstone Nuclear Power Plant, Unit 3.* Technical Report, Dames and Moore, Inc., 1984. Amendment 2.

6. D. M. Boore and G. M. Atkinson. "Stochastic Prediction of Ground Motion and Spectral Response Parameters at Hard-Rock Sites in Eastern North America". *Bulletin of the Seismological Society of America*, 77(2):440–467, 1987.

7. G. R. Toro and R. K. McGuire. "An Investigation into Earthquake Ground Motion Characteristics in Eastern North America". *Bulletin of the Seismological Society of America*, 77(2):468–489, April 1987.

8. R. K. McGuire, G. R. Toro, and W. J. Silva. *Engineering Model of Earthquake Ground Motion for Eastern North America.* Technical Report NP-6074, Electric Power Research Institute, 1988.

9. W. J. Silva and R. K. Green. "Magnitude and Distance Scaling of Response Spectral Shapes for Rock sites with Application to North American Tectonic Environments". *Earthquake Spectra*, 5(4):591–624, 1989.

10. R. K. McGuire, G. R. Toro, J. P. Jacobson, T. F. O'Hara, and W. J. Silva. *Probabilistic Seismic Hazard Evaluations in the Central and Eastern United States: Resolution of the Charleston Earthquake Issue.* Special Report NP-6395-D, Electric Power Research Institute, April 1989.

11. D. L. Bernreuter, J. B. Savy, R. W. Mensing, and J. C. Chen. *Seismic Hazard Characterization of 69 Plant Sites East of the Rocky Mountains.* Technical Report NUREG/CR5250, UCID-21517, U. S. Nuclear Regulatory Commission, 1988.

12. R. B. Herrmann. "An Extension of Random Vibration Theory Estimates of Strong Ground Motion to Large Distances". *Bulletin of the Seismological Society of America*, 75:1447–1453, 1985.

13. G. Ou. *A Study of the Use of Estimation Theory in Strong Ground Motion Seismology.* PhD thesis, St. Louis University, 1990.

14. W. B. Joyner and D. M. Boore. "Measurement, Characterization, and Prediction of Strong Ground Motion". In J. L. Von Thun, editor, *Earthquake Engineering and Soil Dynamics II – Recent Advances in Ground-Motion Evaluation*, American Society of Civil Engineers, 1988. Publication No. 20.

15. T. Inoue. Ground Motion Damage Effectiveness for MDOF Structures. Engineer's Thesis, Department of Civil Engineering, Stanford University, 1990.

16. W. B. Joyner and D. M. Boore. *Prediction of Earthquake Response Spectra.* Open-File Report 82-977, U. S. Geological Survey, 1982.

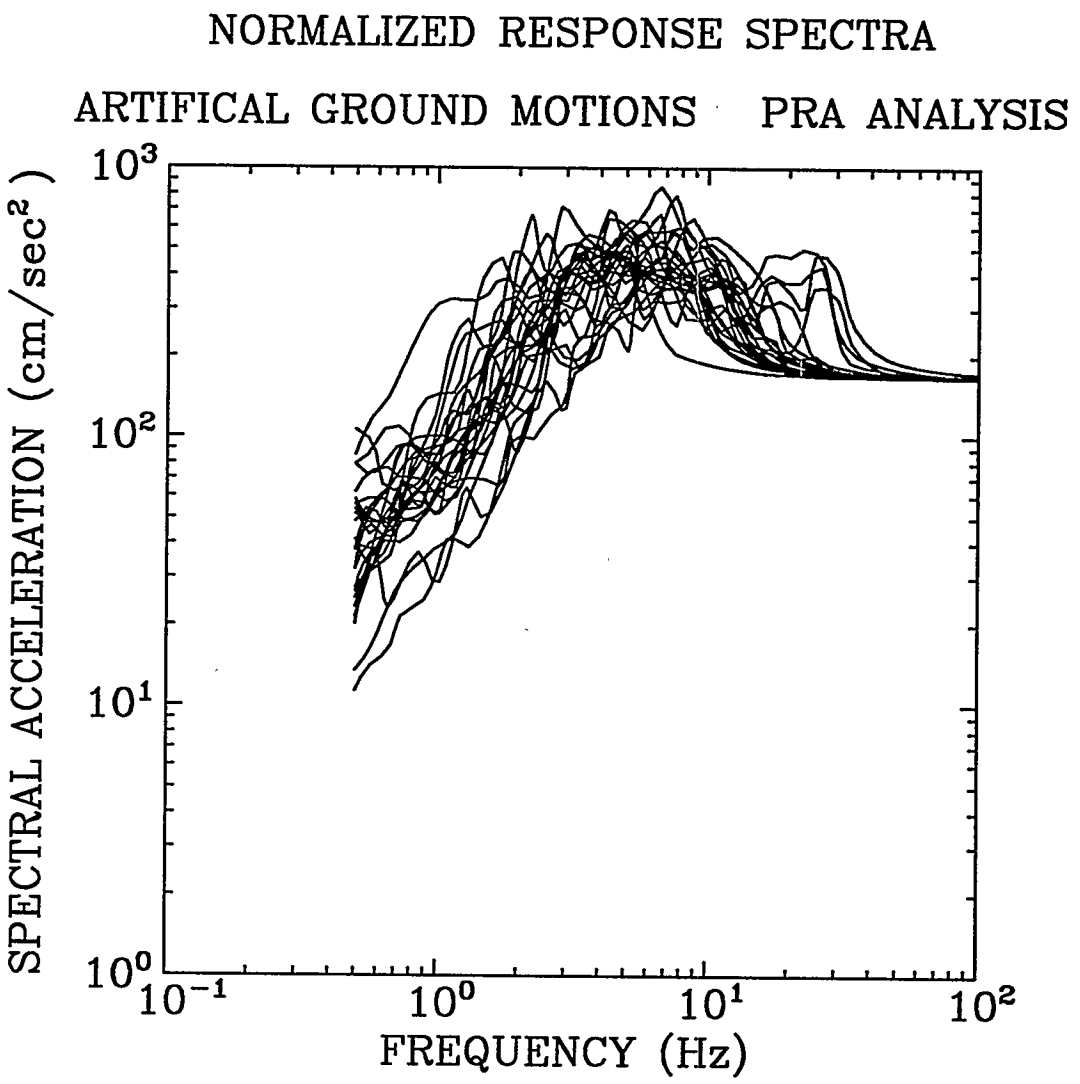

Figure 3-5. Spectral shapes (5% damping) calculated from 25 artificial ground motions corresponding to the PRA seismic hazard analysis.

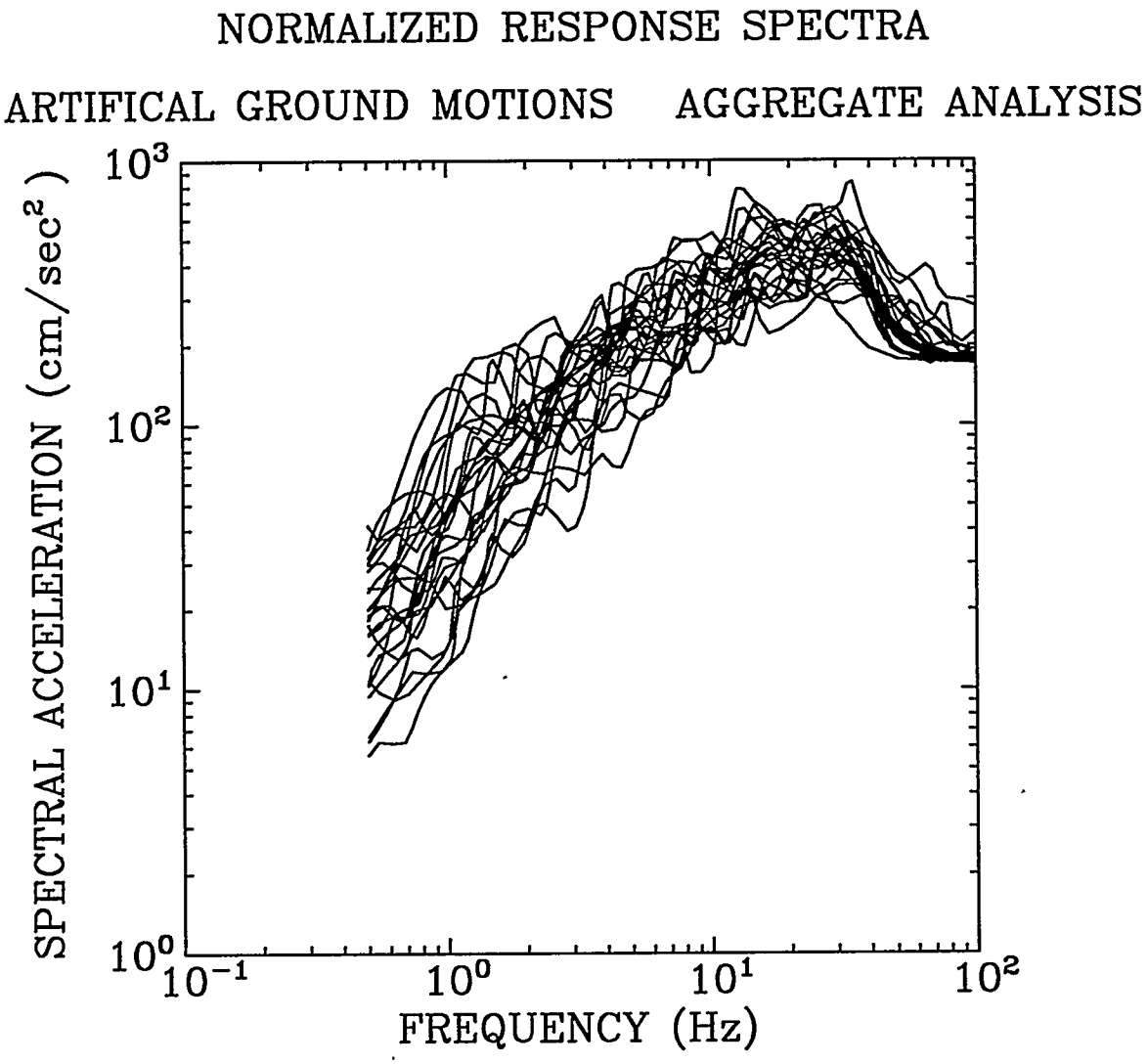

Figure 3-6. Spectral shapes (5% damping) calculated from 25 artificial ground motions corresponding to the composite seismic hazard analysis.

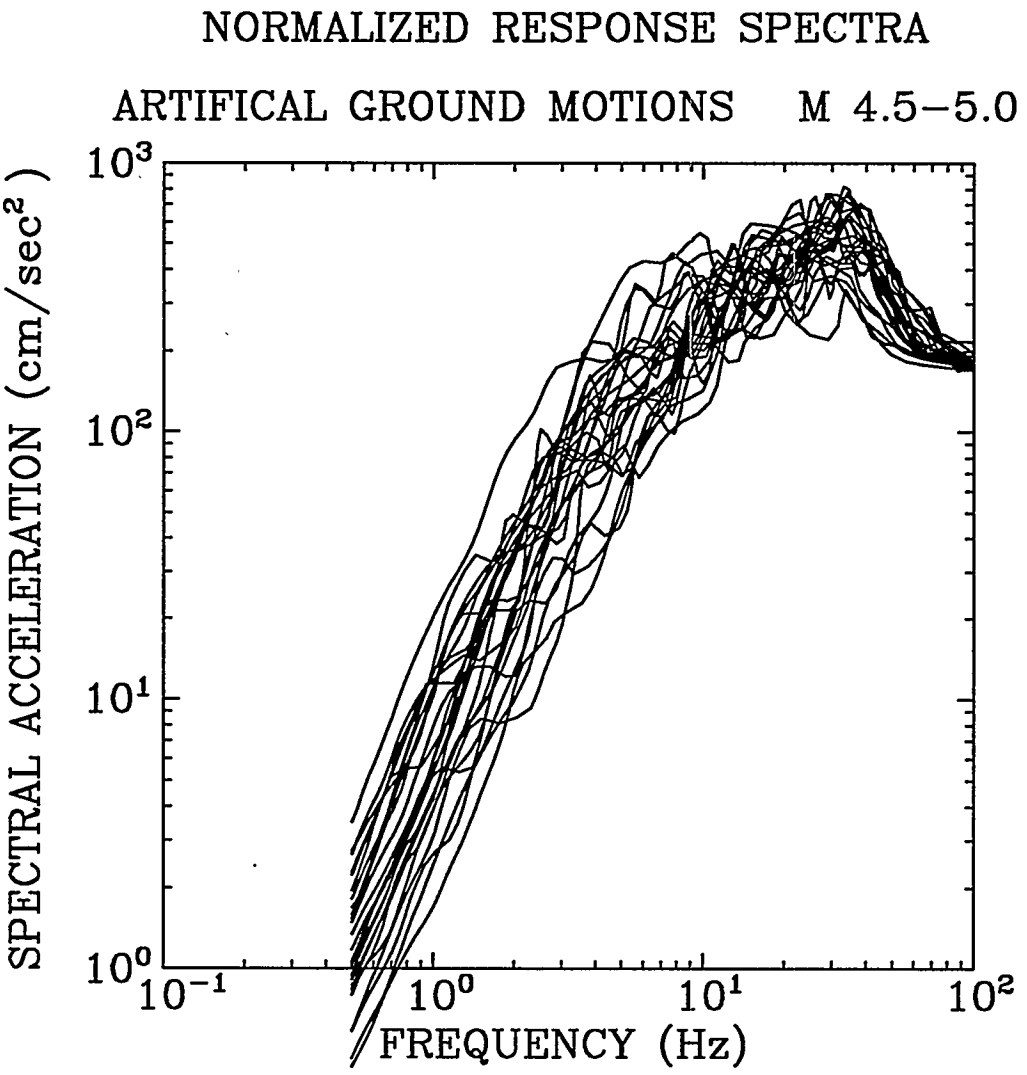

Figure 3-7. Spectral shapes (5% damping) calculated from 25 artificial ground motions corresponding to the magnitude-dependent seismic hazard analysis (m_b 4.5–5.0).

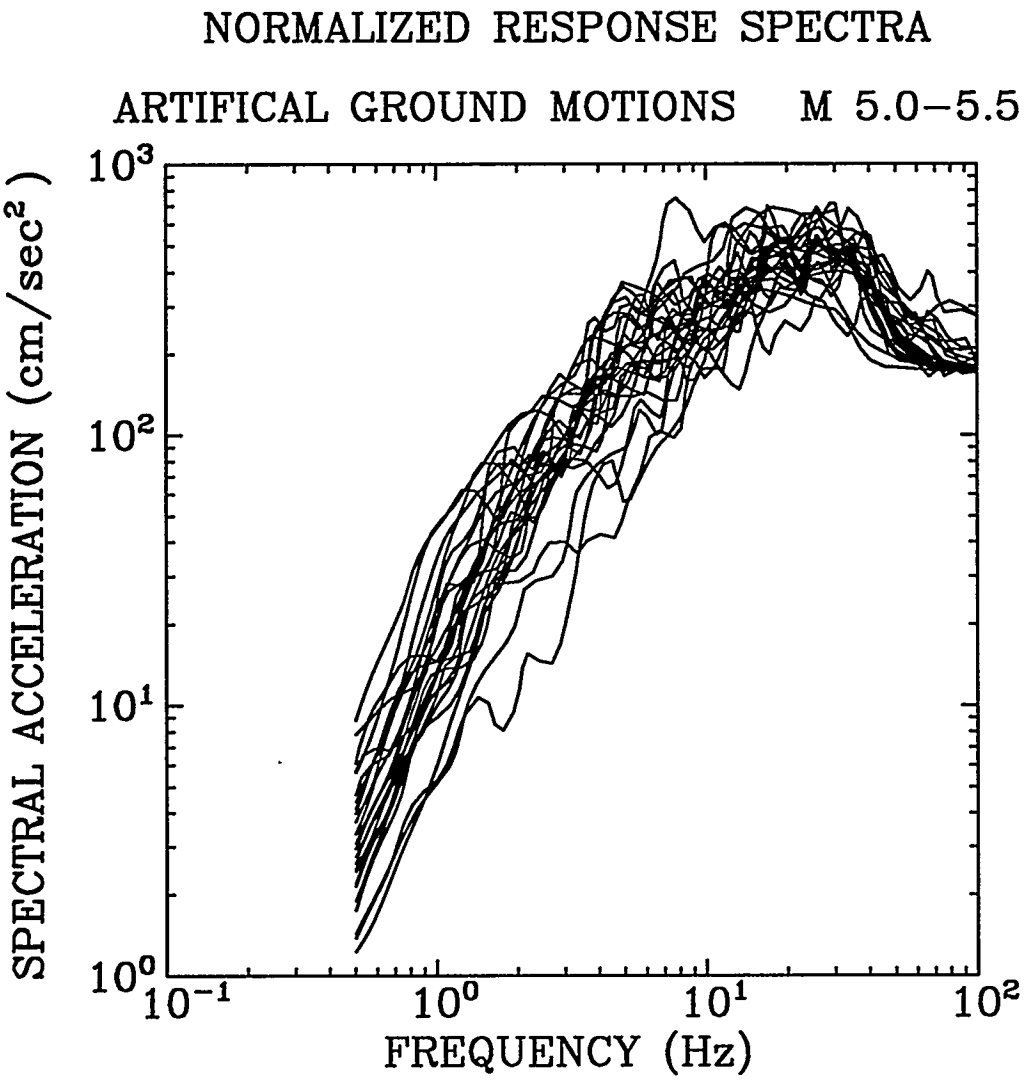

Figure 3-8. Spectral shapes (5% damping) calculated from 25 artificial ground motions corresponding to the magnitude-dependent seismic hazard analysis (m_b 5.0–5.5).

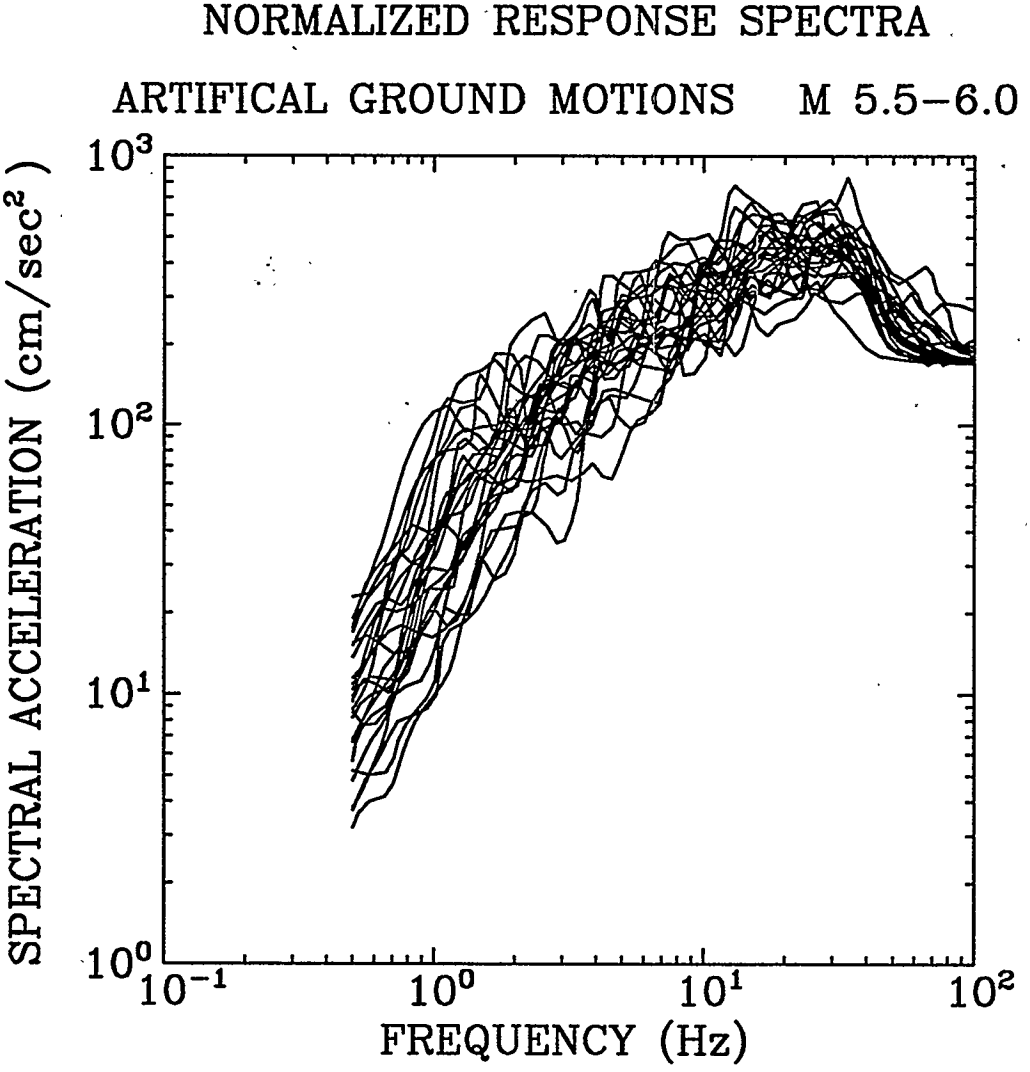

Figure 3-9. Spectral shapes (5% damping) calculated from 25 artificial ground motions corresponding to the magnitude-dependent seismic hazard analysis (m_b 5.5–6.0).

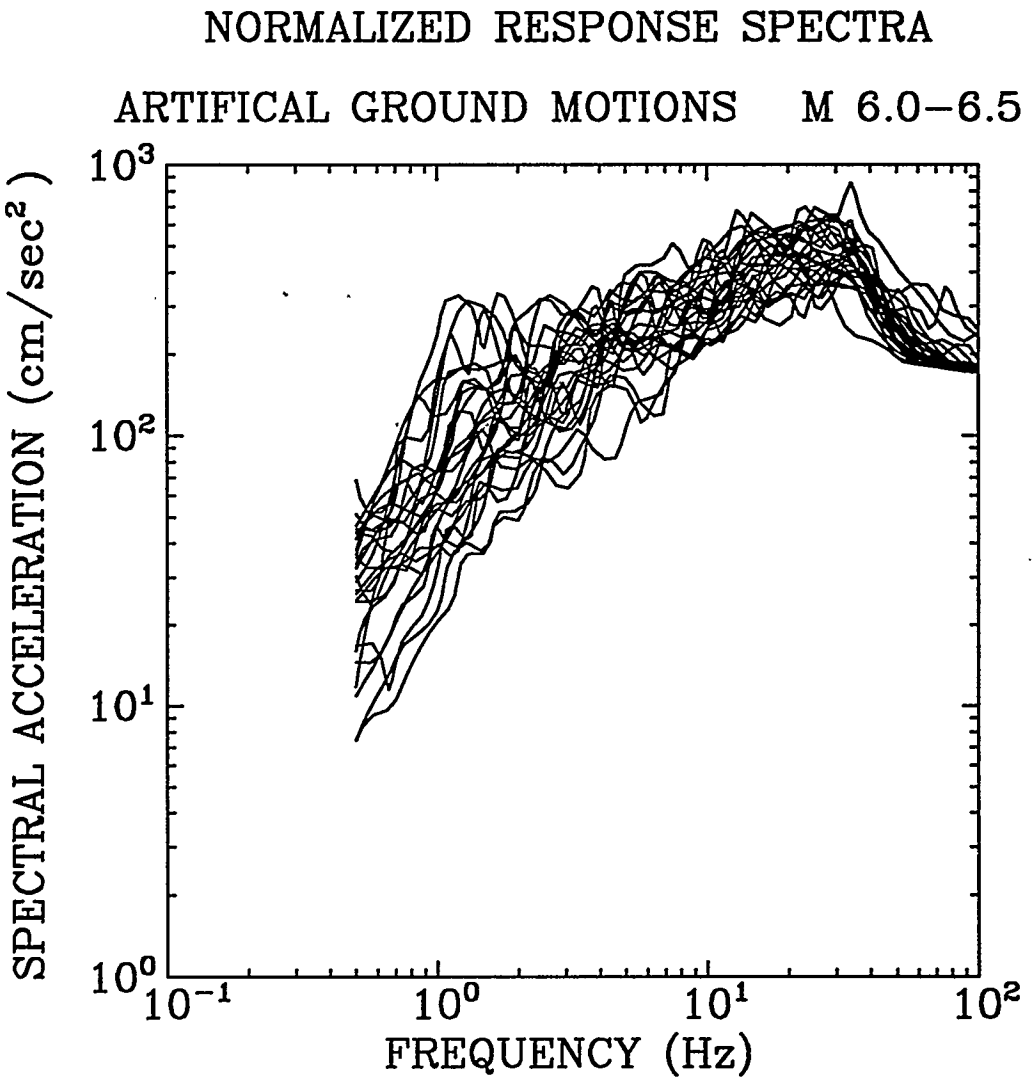

Figure 3-10. Spectral shapes (5% damping) calculated from 25 artificial ground motions corresponding to the magnitude-dependent seismic hazard analysis (m_b 6.0–6.5).

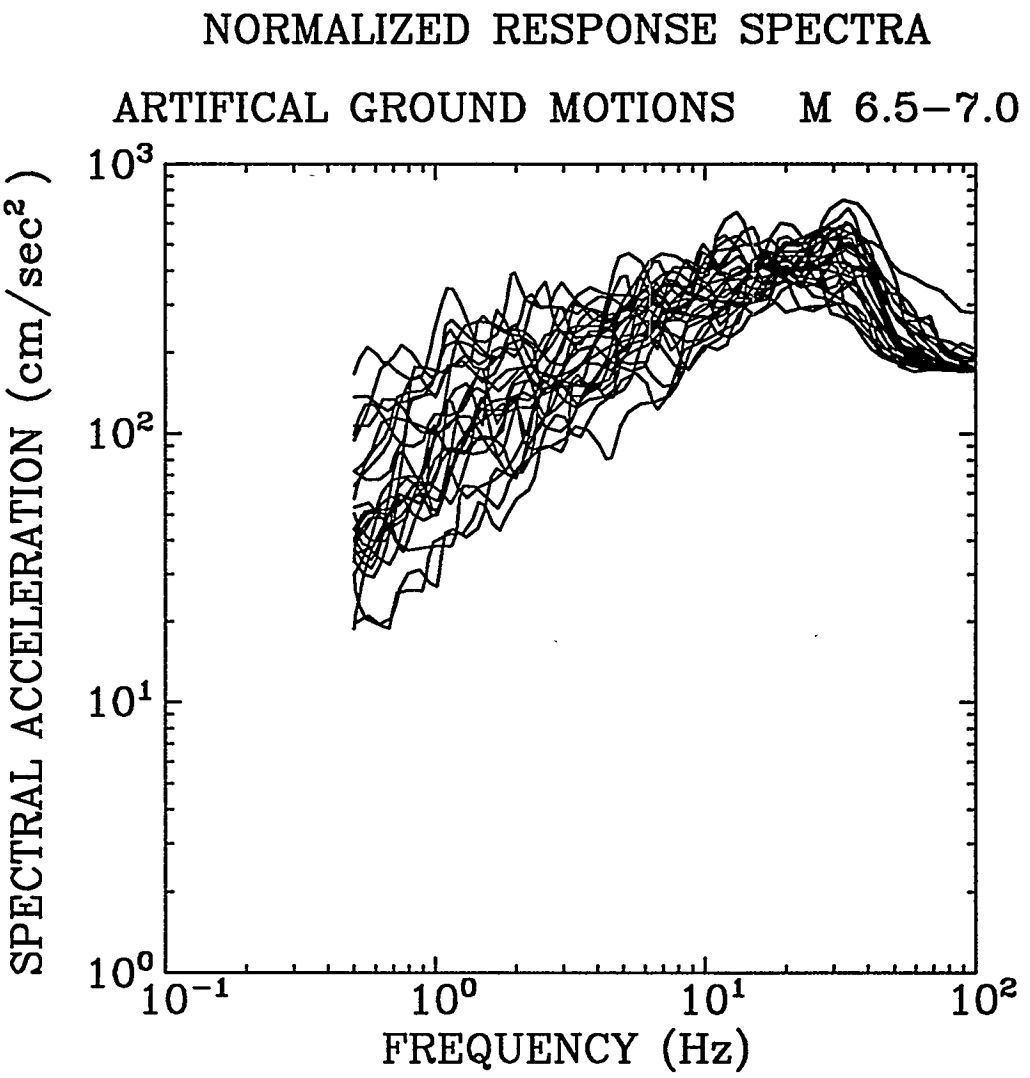

Figure 3-11. Spectral shapes (5% damping) calculated from 25 artificial ground motions corresponding to the magnitude-dependent seismic hazard analysis (m_b 6.5–7.0).

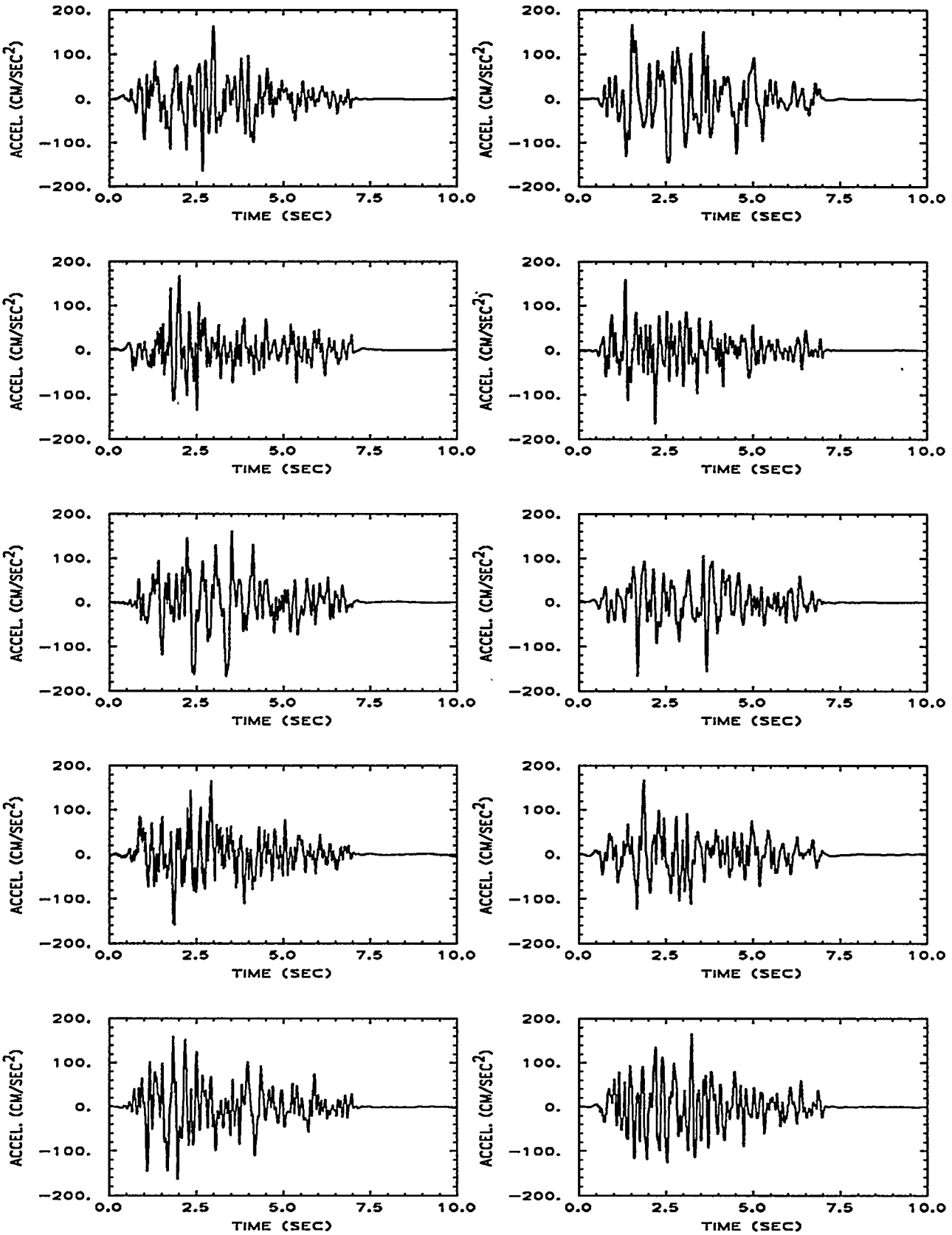

Figure 3-12. Time histories from 25 artificial ground motions generated for the PRA seismic hazard analysis.

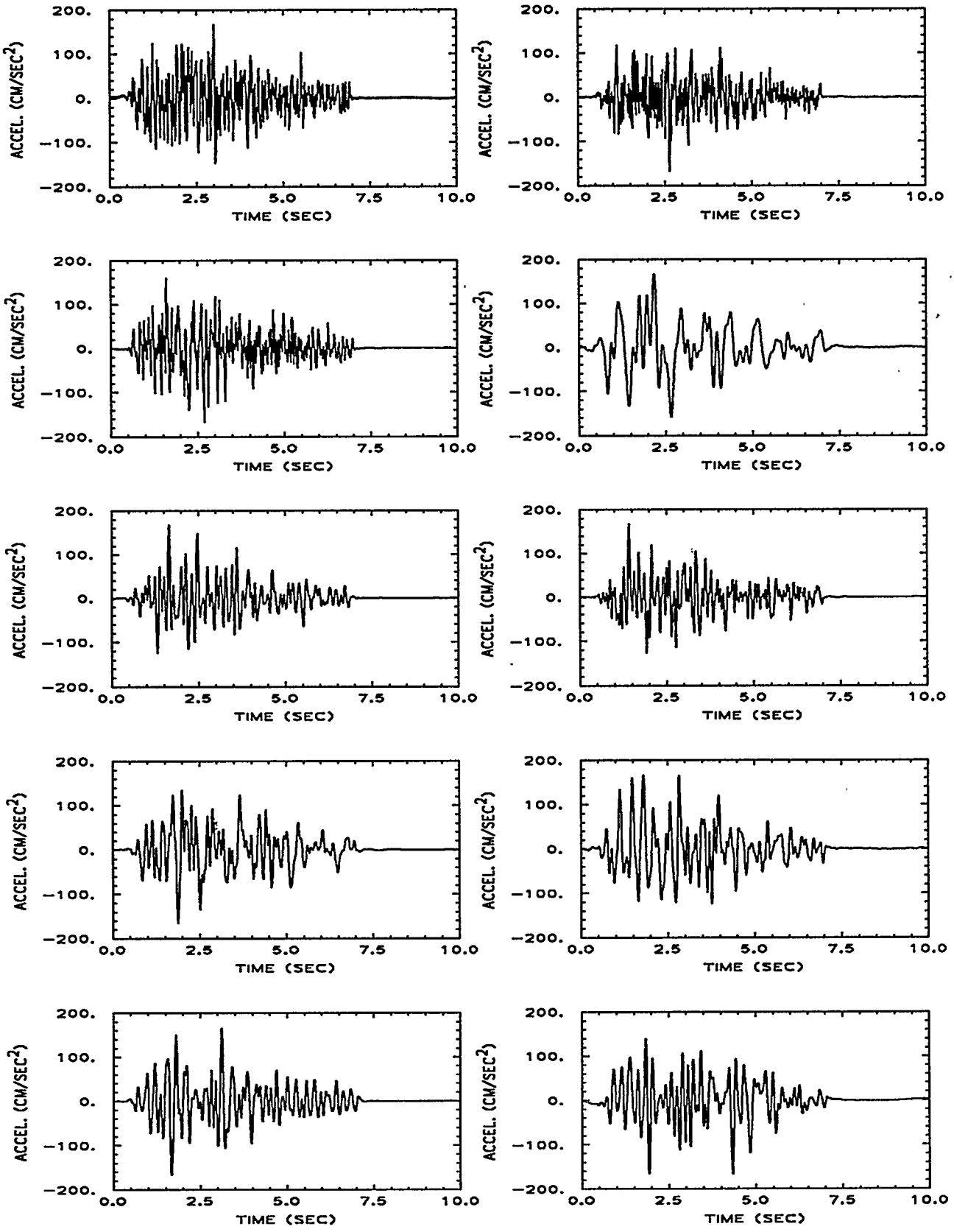

Figure 3-12 (continued)

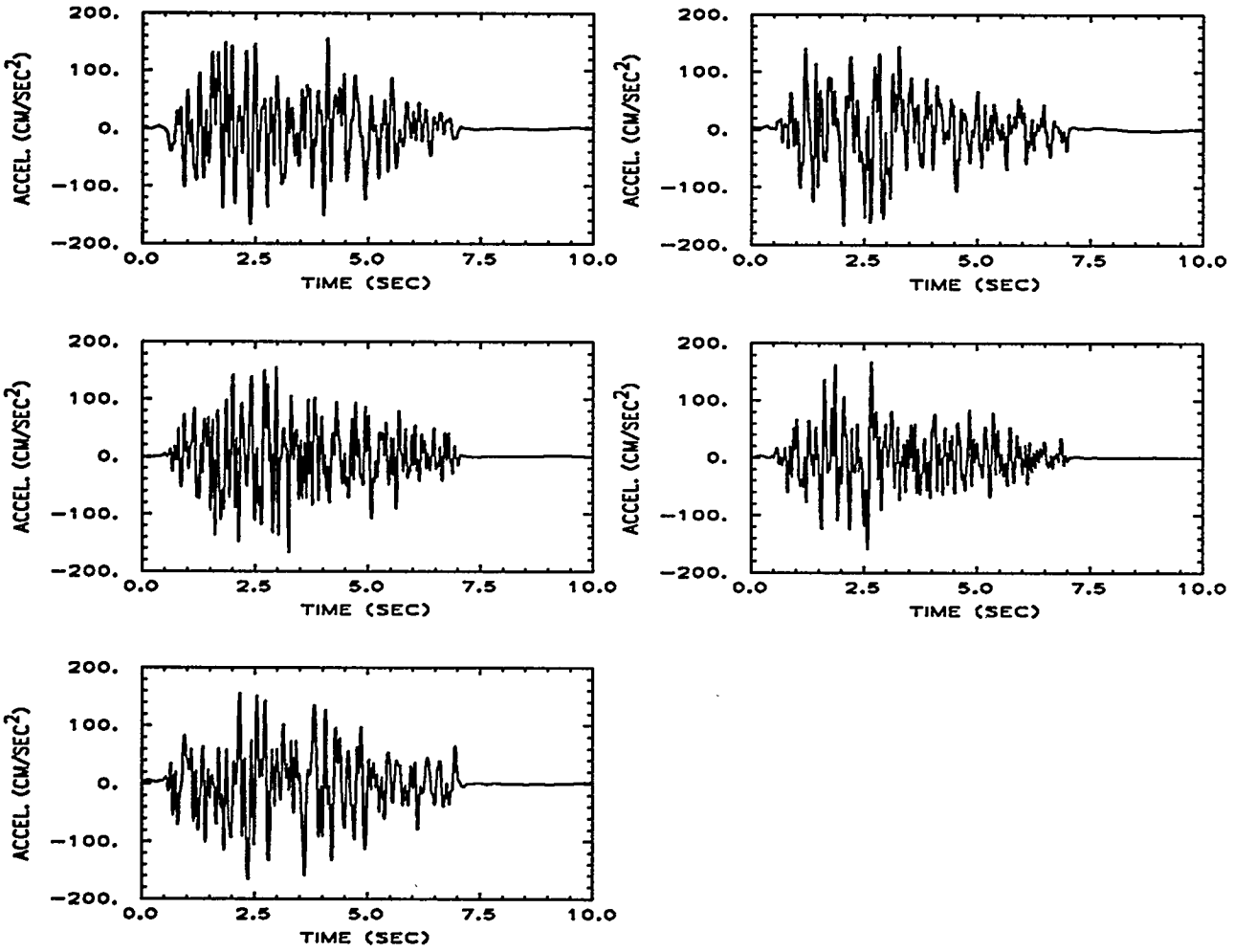

Figure 3-12 (continued)

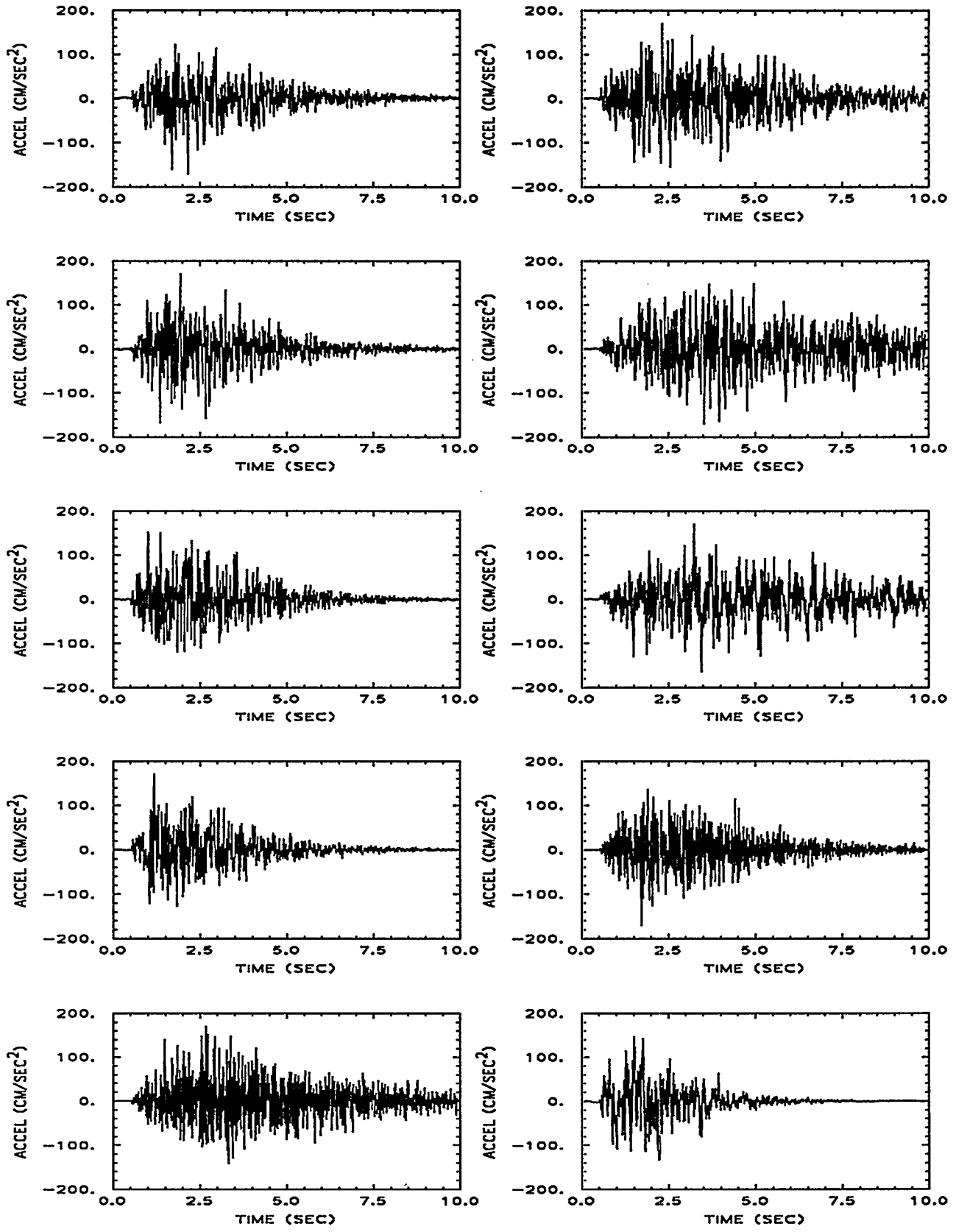

Figure 3-13. Time histories from 25 artificial ground motions generated for the composite seismic hazard analysis.

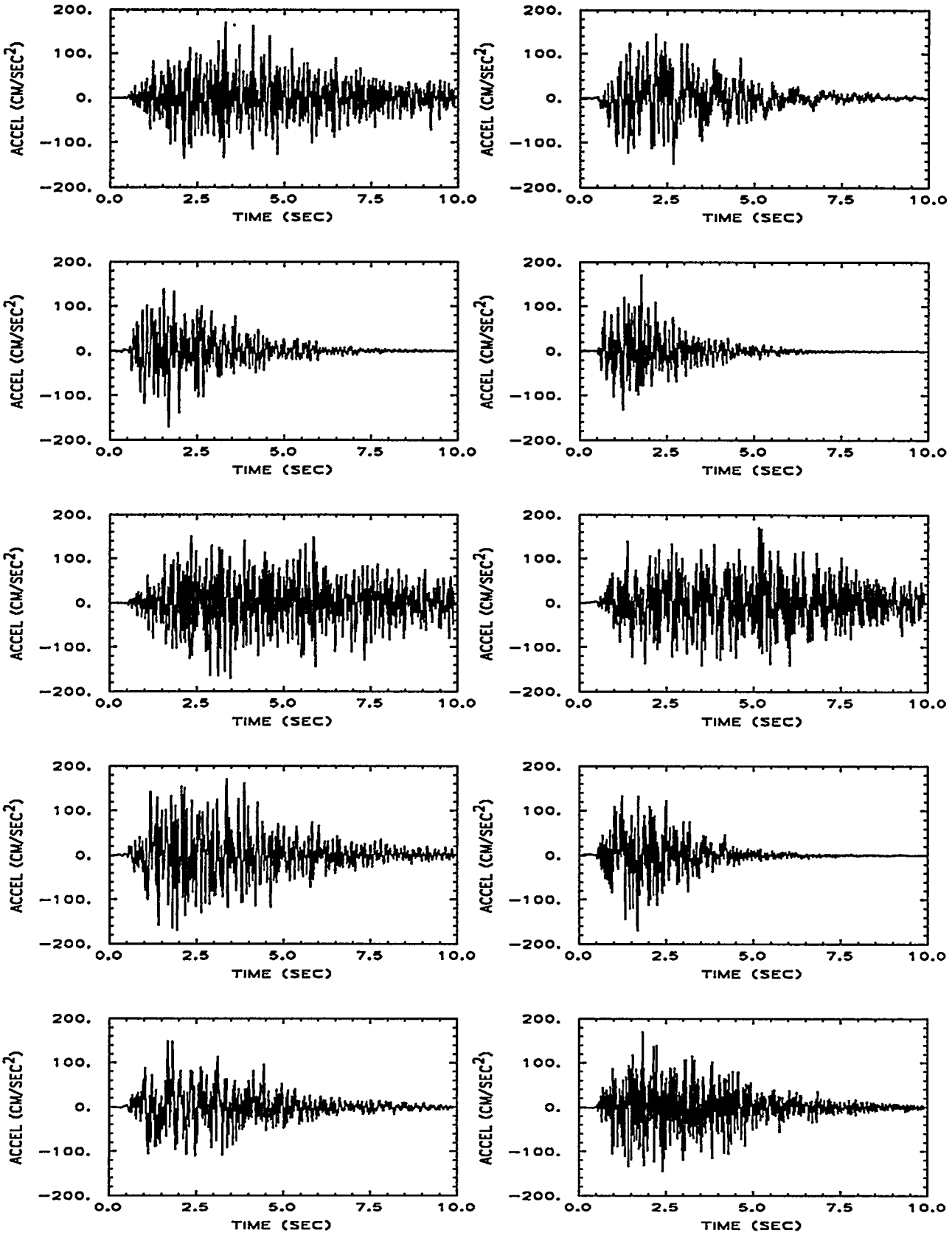

Figure 3-13 (continued)

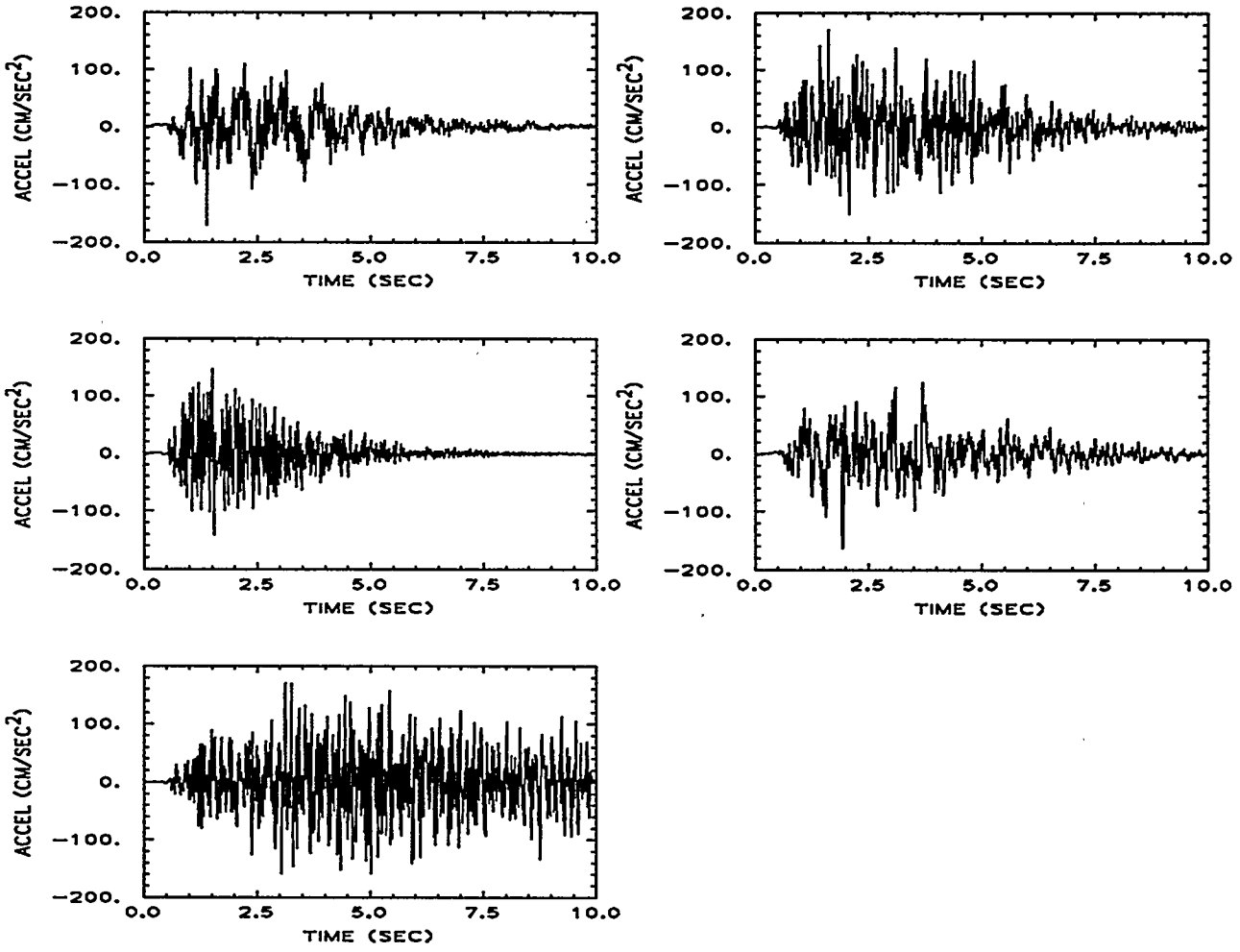

Figure 3-13 (continued)

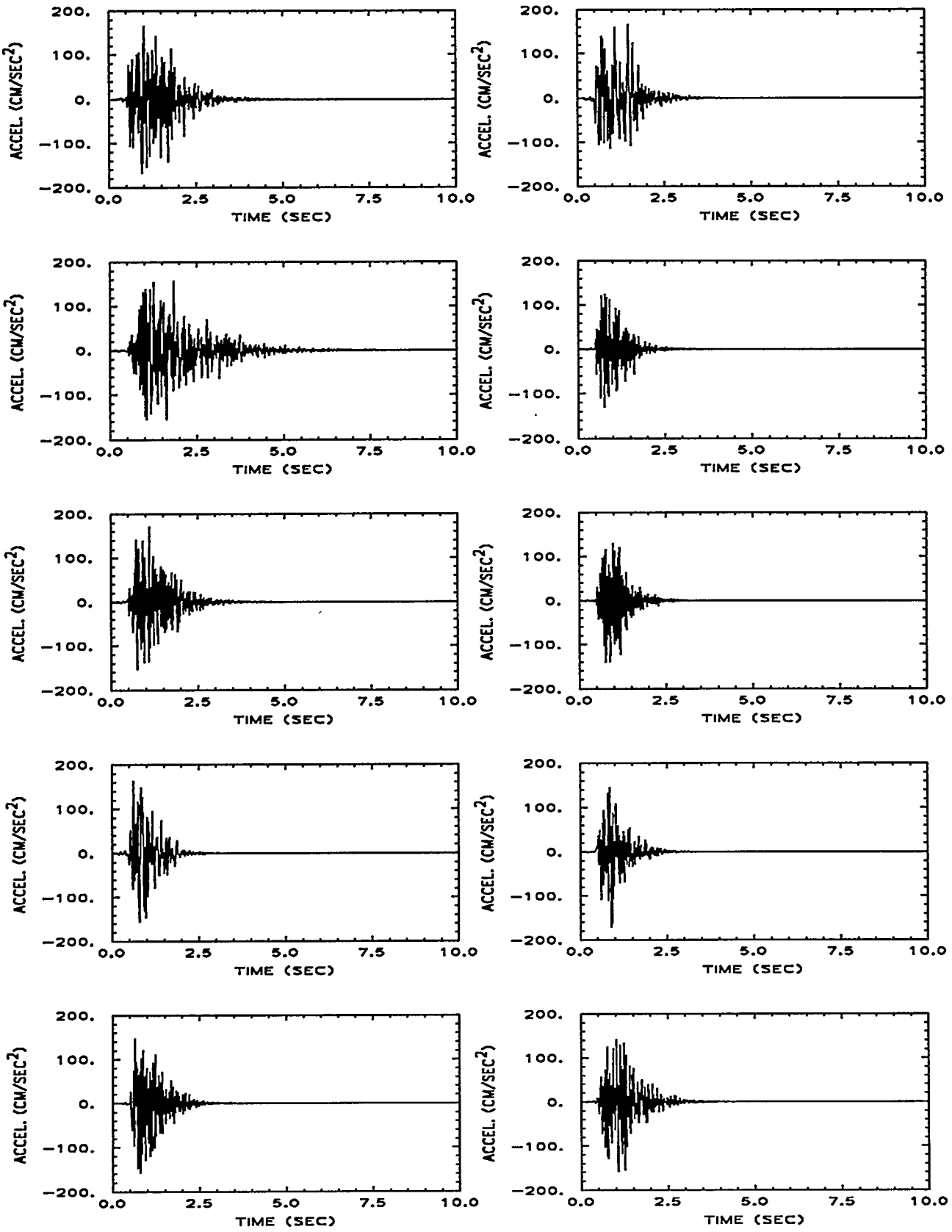

Figure 3-14. Time histories from 25 artificial ground motions generated for the magnitude-dependent seismic hazard analysis (m_b 4.5–5.0).

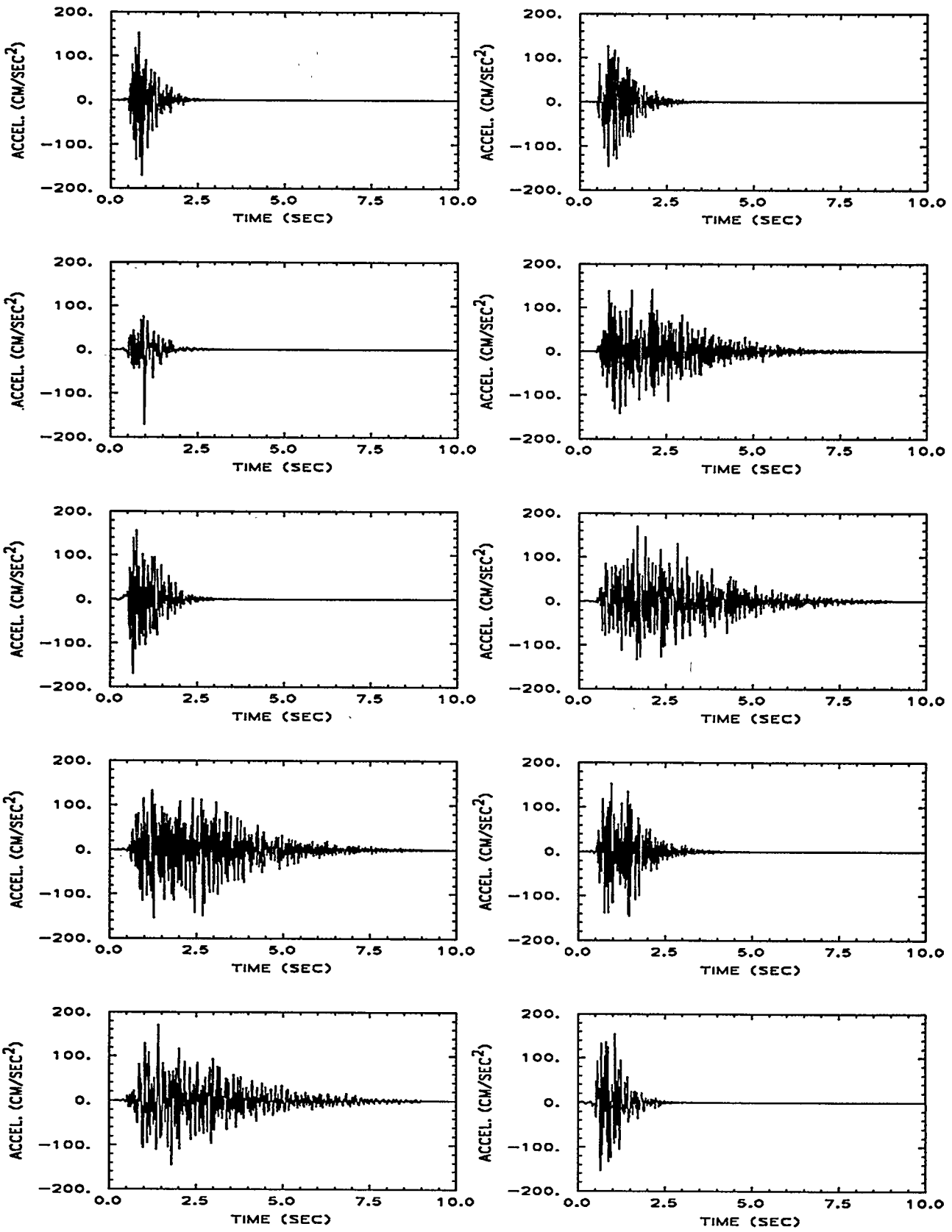

Figure 3-14 (continued)

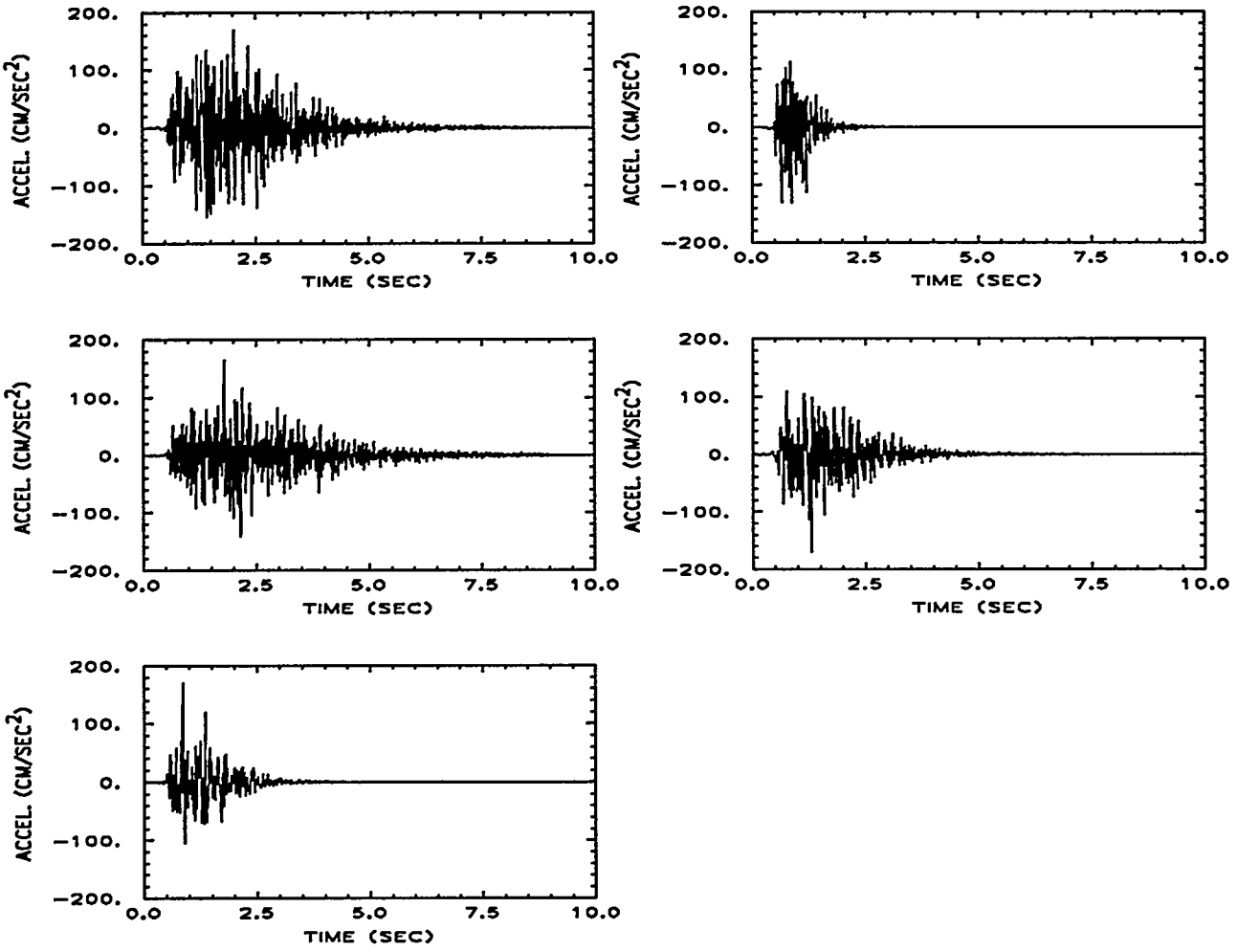

Figure 3-14 (continued)

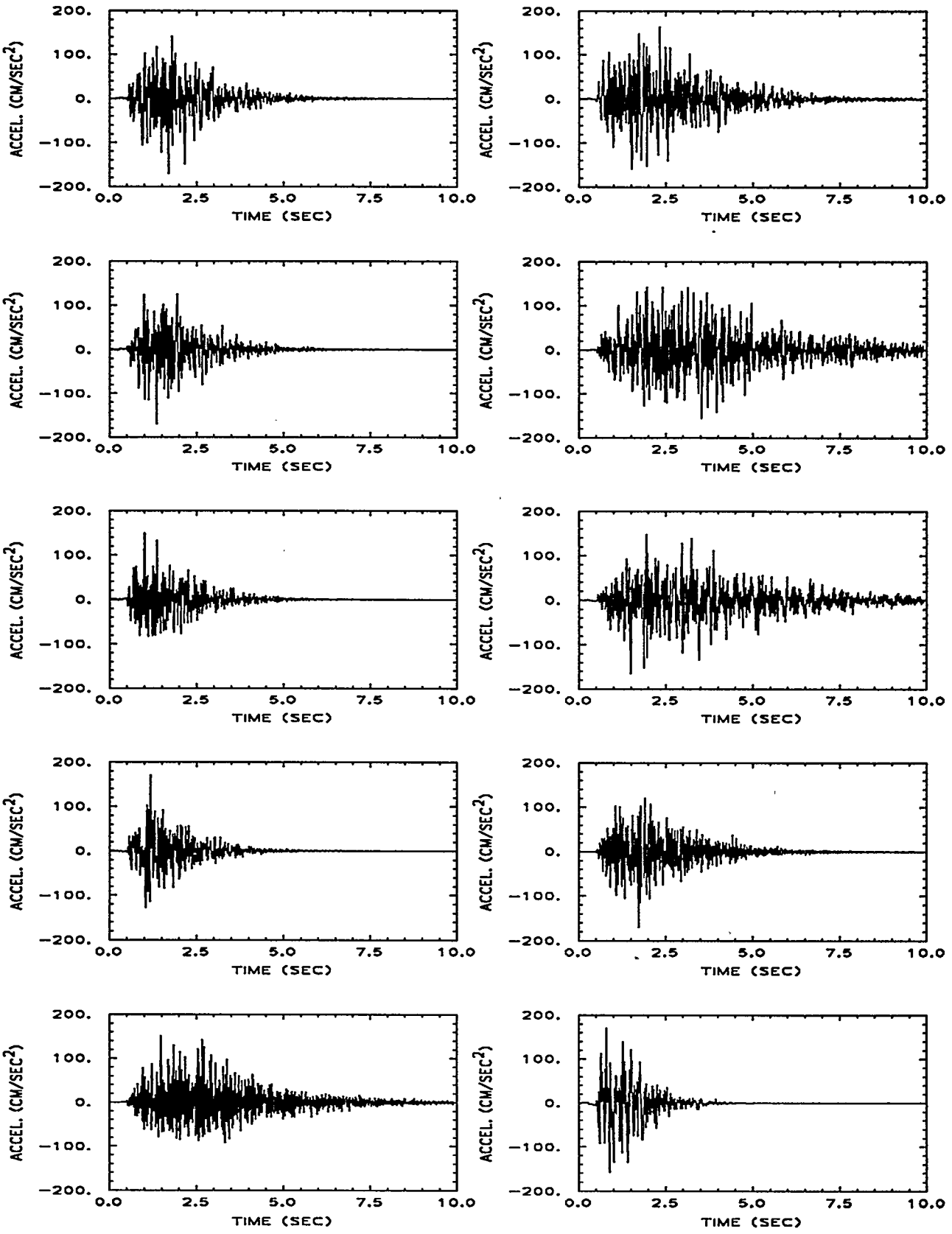

Figure 3-15. Time histories from 25 artificial ground motions generated for the magnitude-dependent seismic hazard analysis (m_b 5.0–5.5).

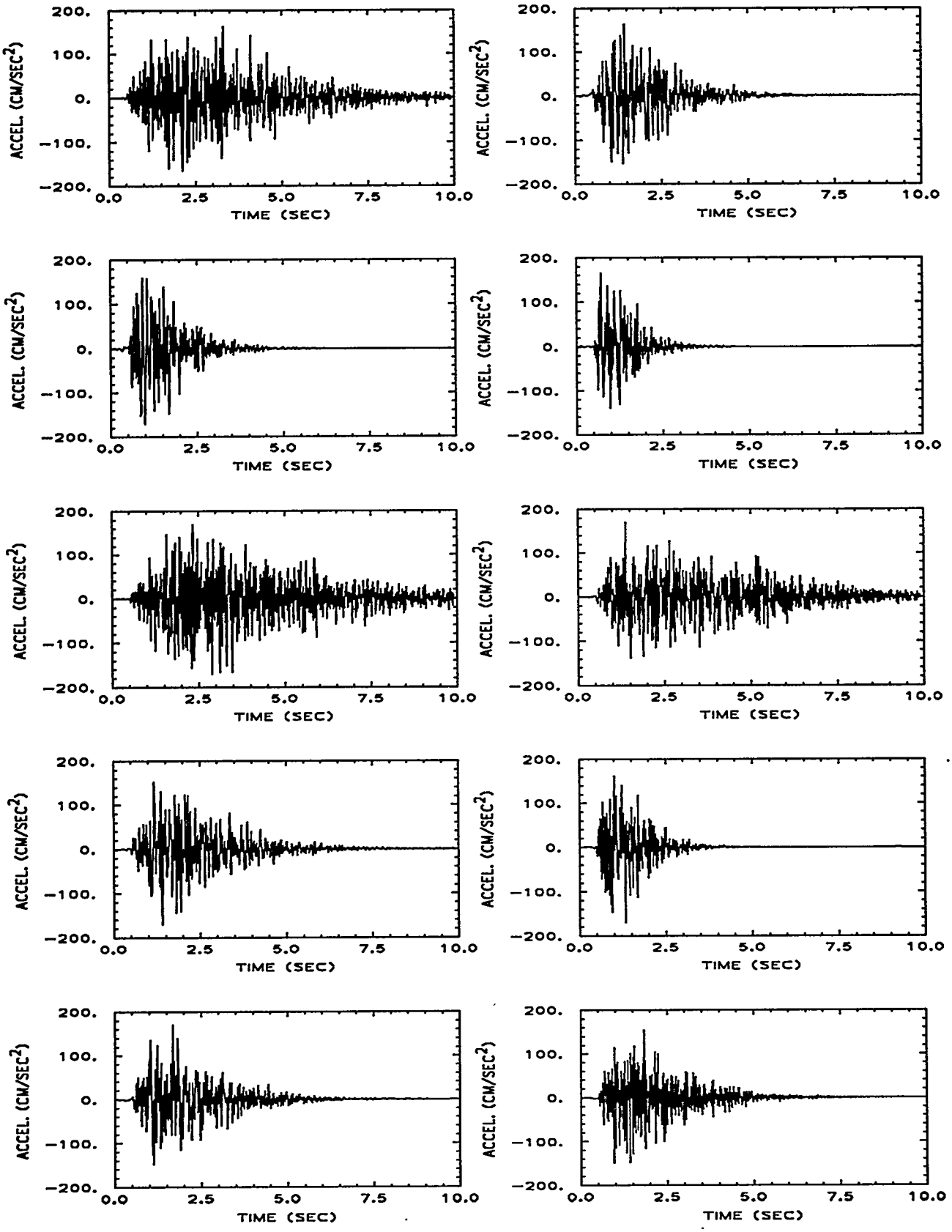

Figure 3-15 (continued)

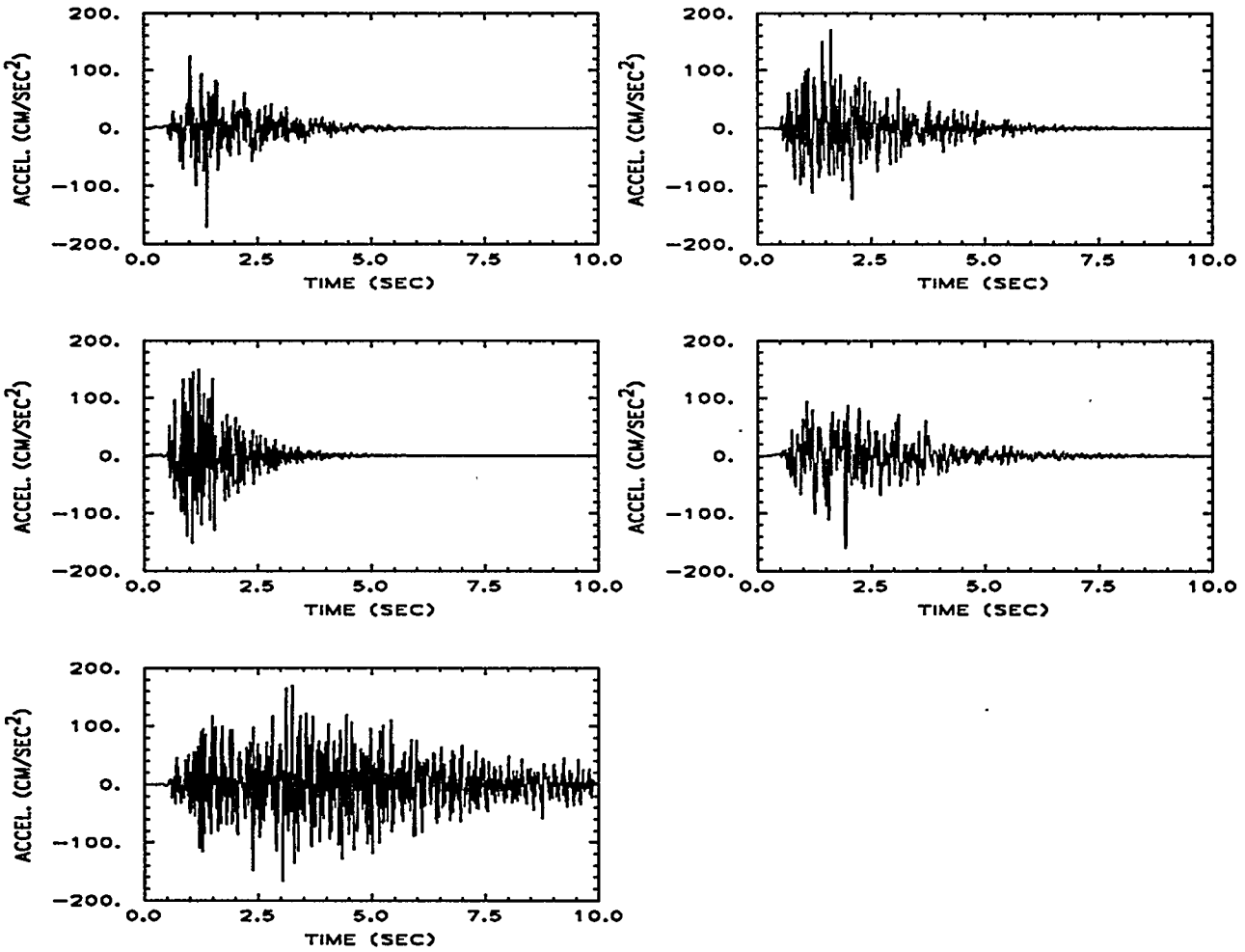

Figure 3-15 (continued)

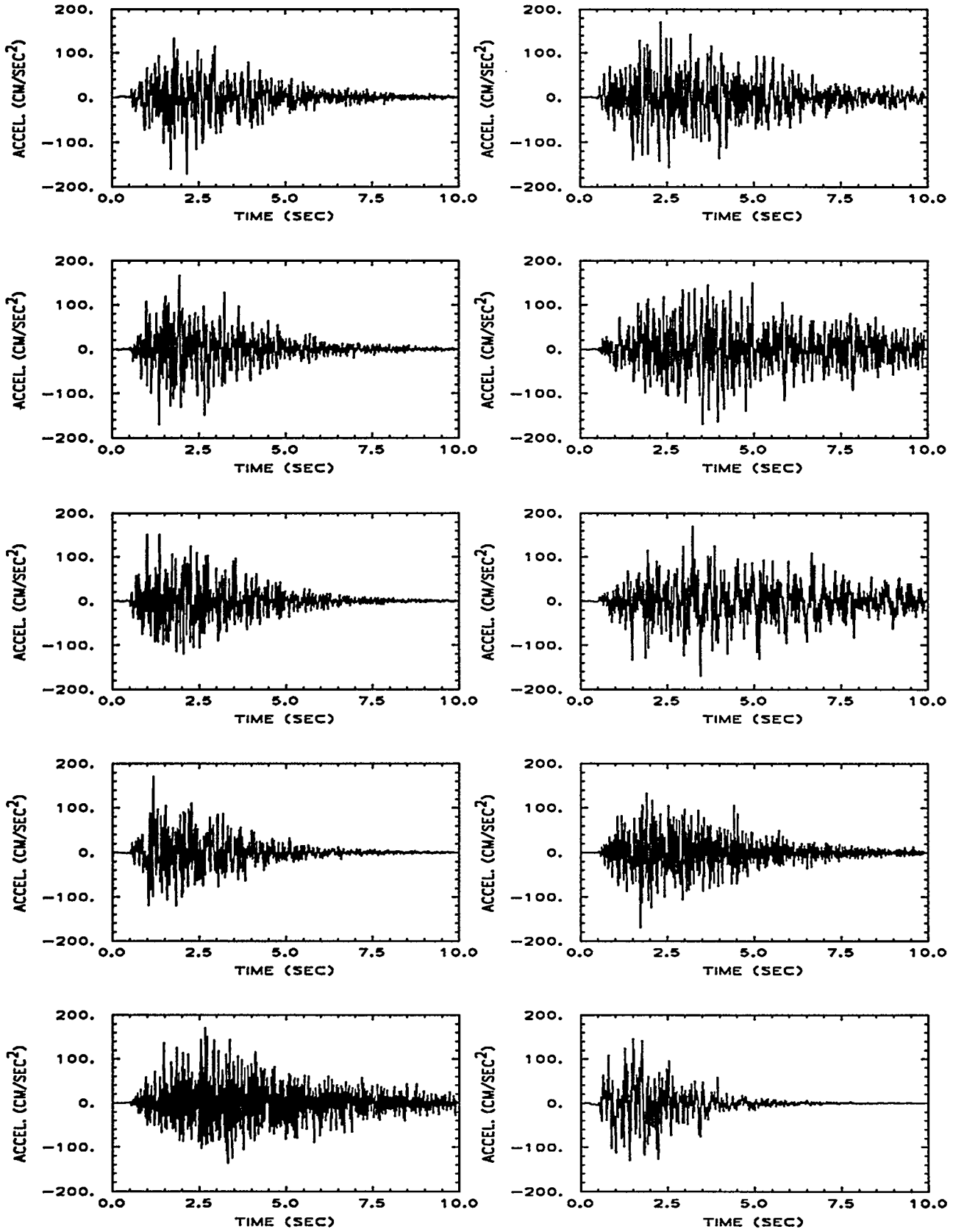

Figure 3-16. Time histories from 25 artificial ground motions generated for the magnitude-dependent seismic hazard analysis (m_b 5.5–6.0).

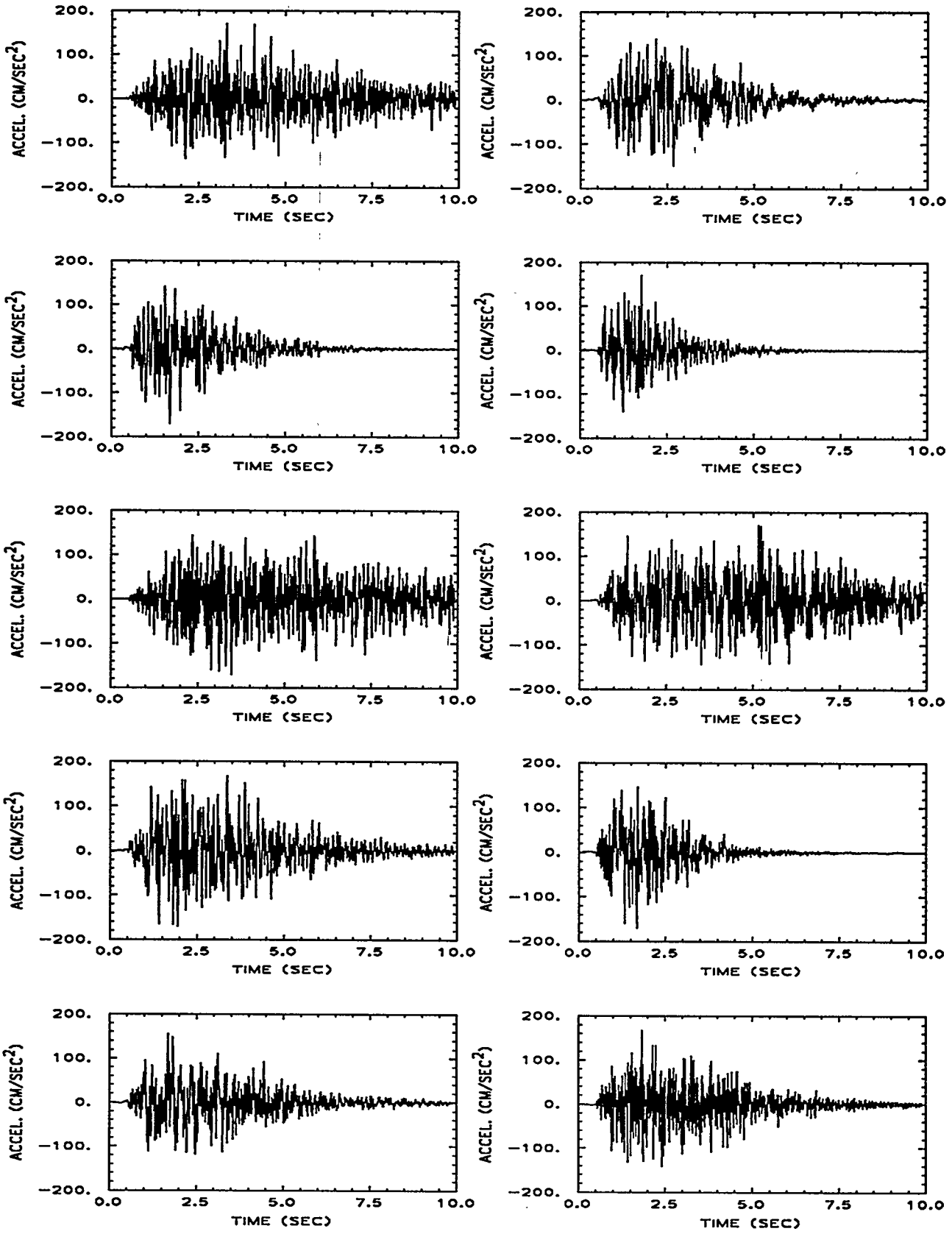

Figure 3-16 (continued)

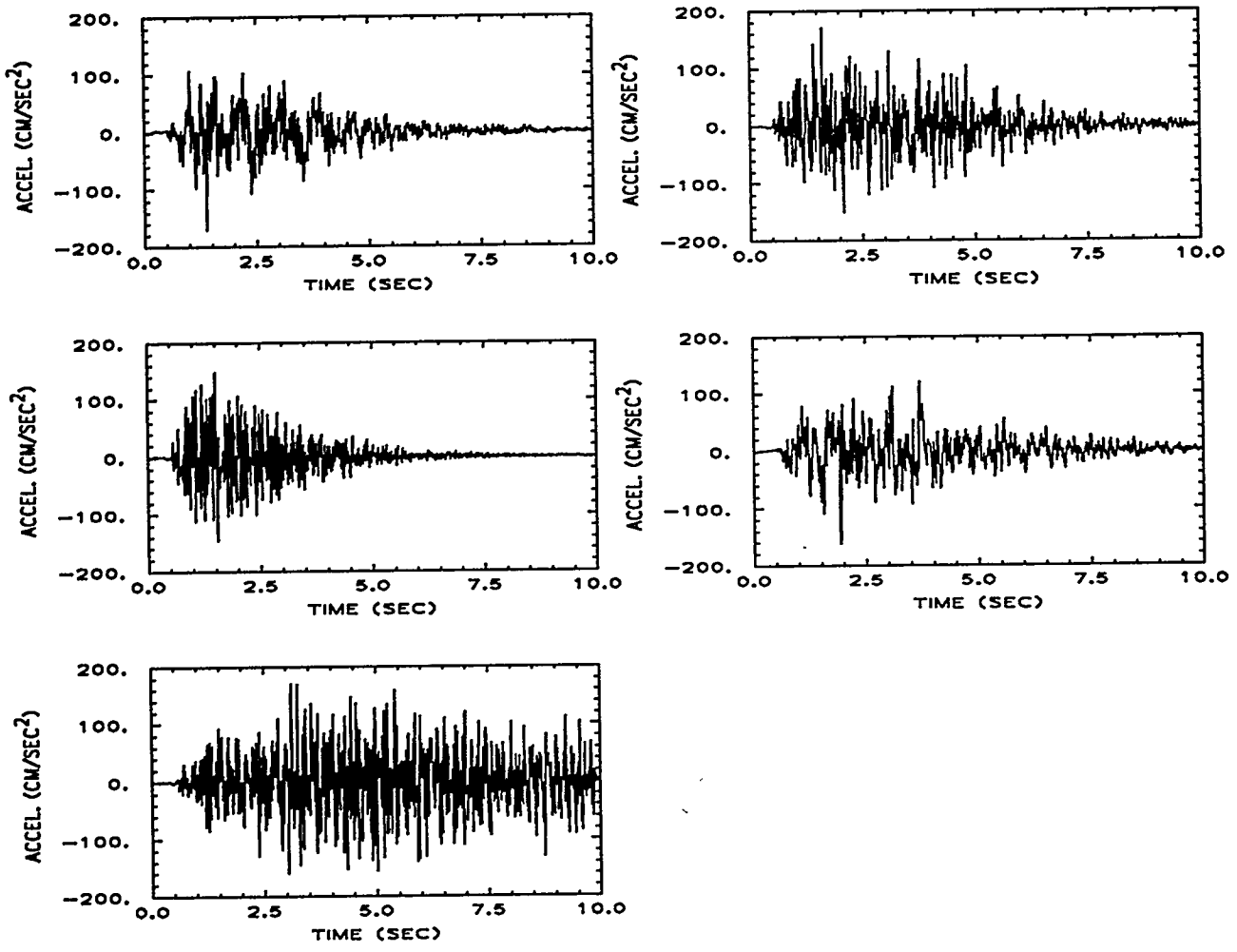

Figure 3-16 (continued)

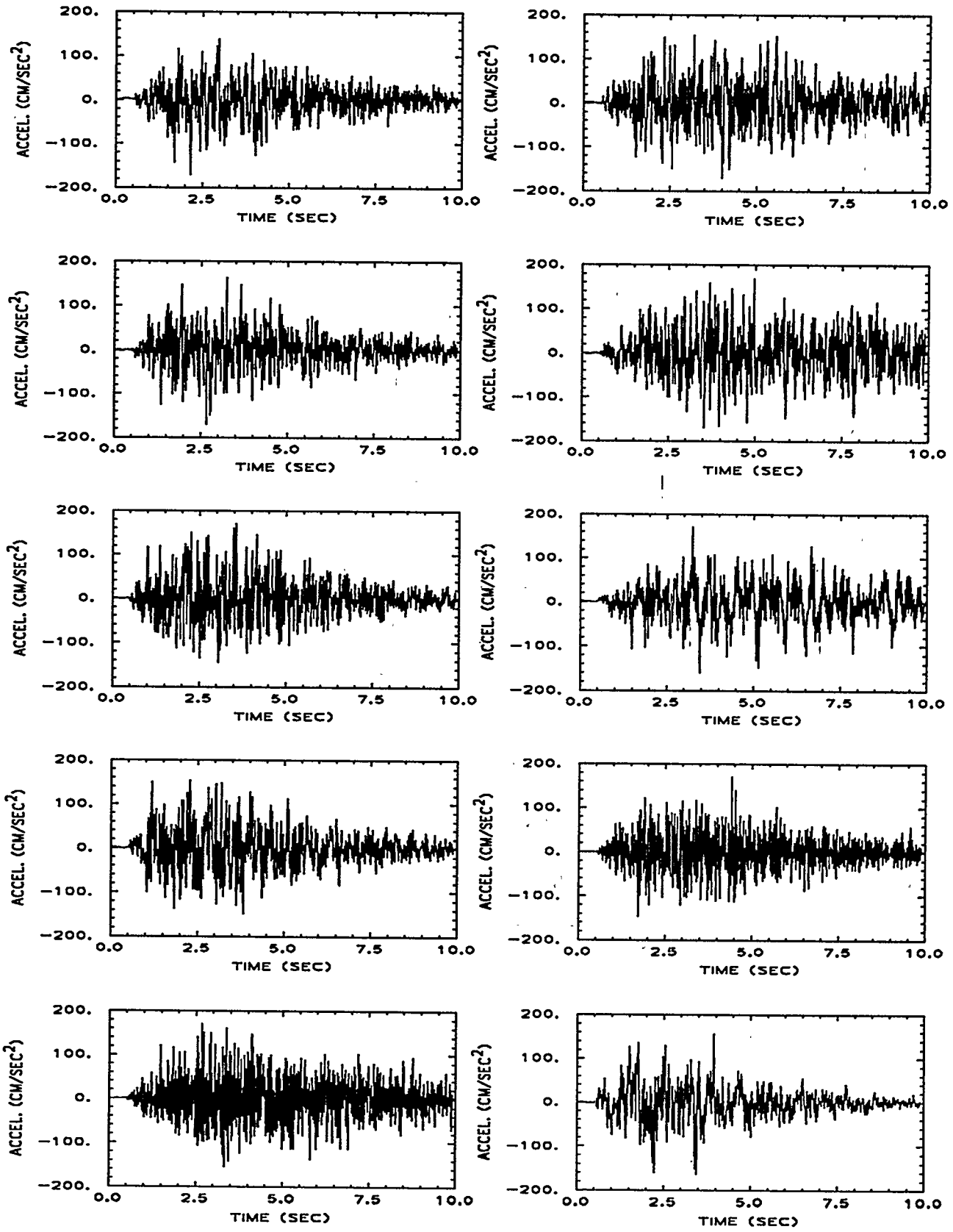

Figure 3-17. Time histories from 25 artificial ground motions generated for the magnitude-dependent seismic hazard analysis (m_b 6.0–6.5).

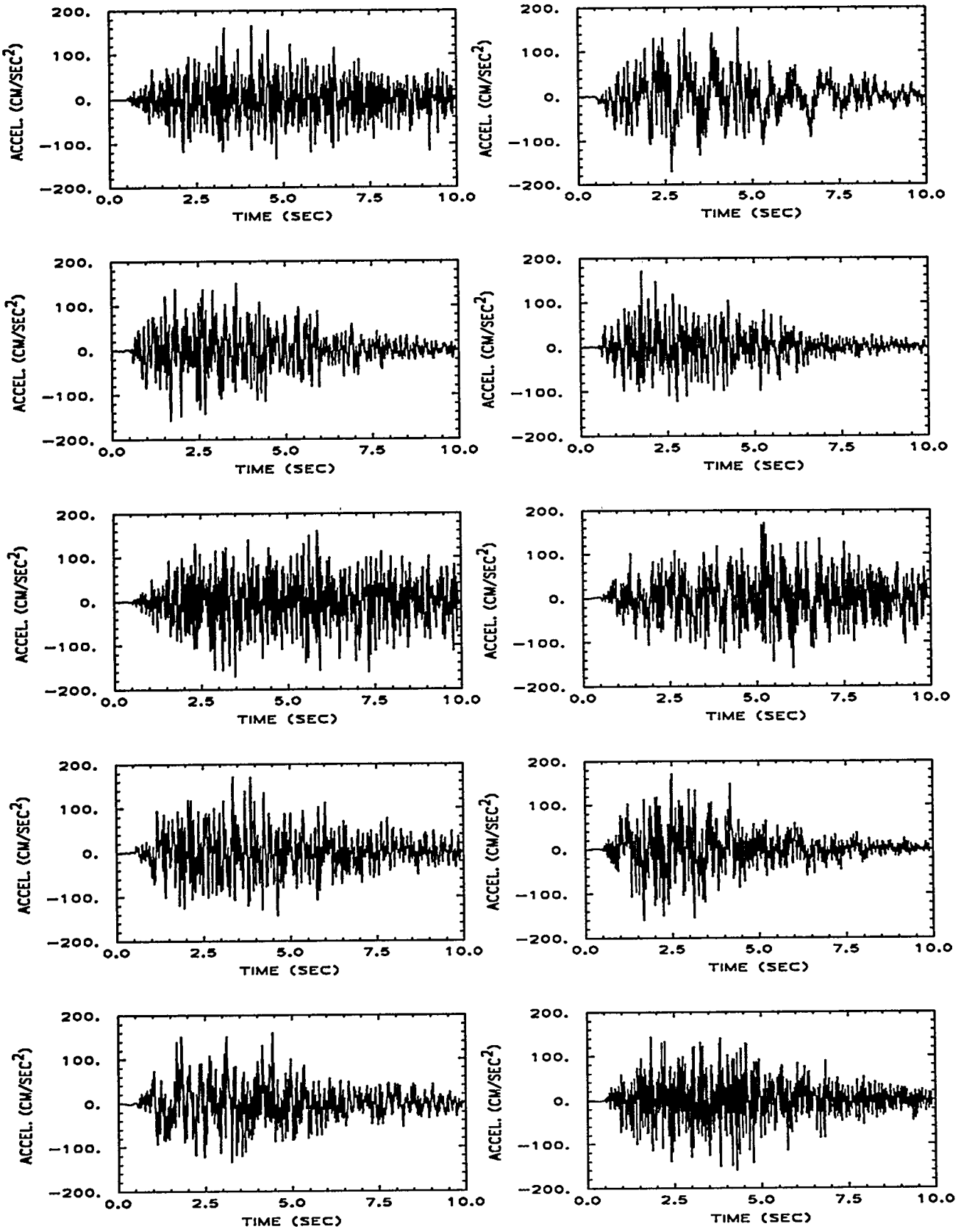

Figure 3-17 (continued)

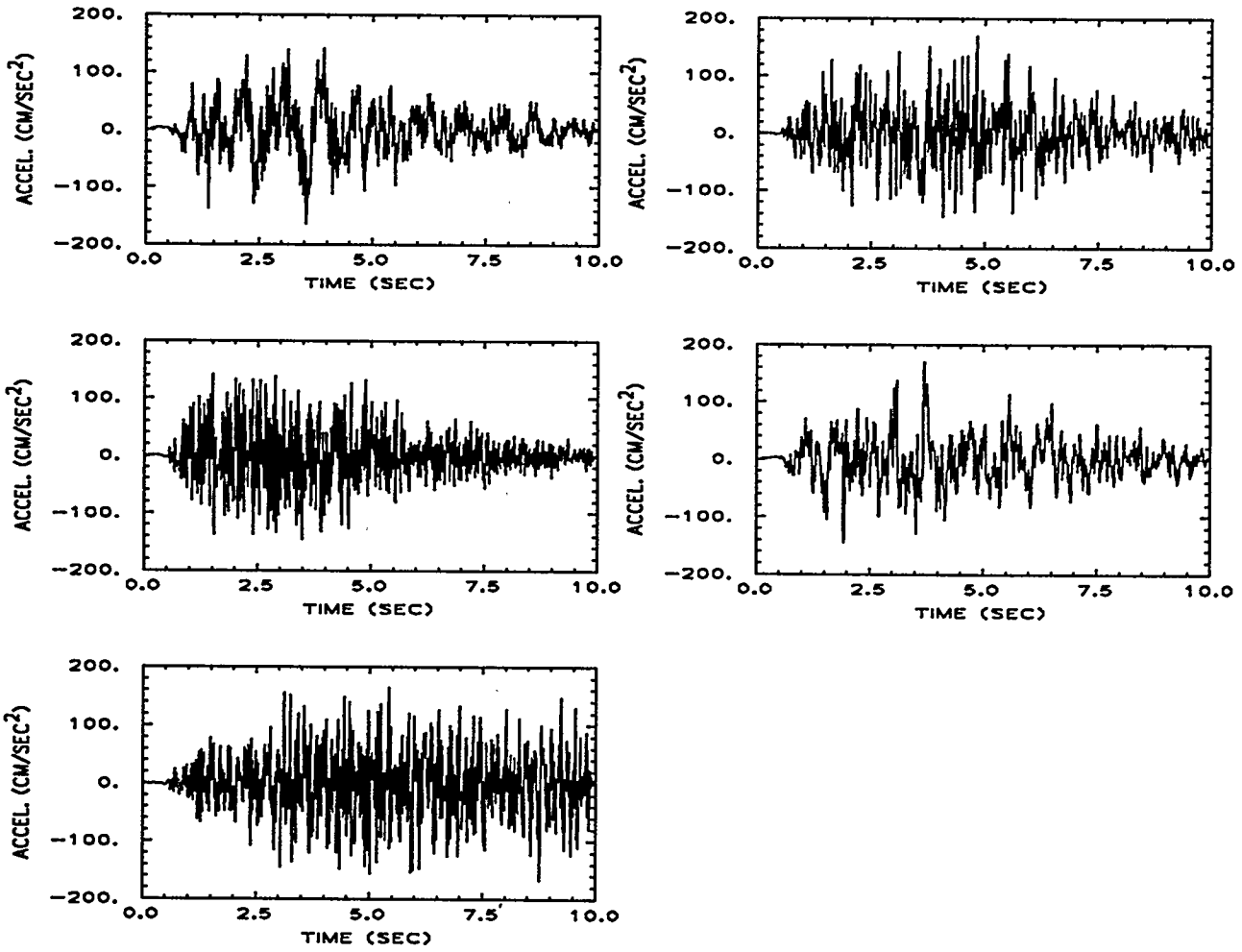

Figure 3-17 (continued)

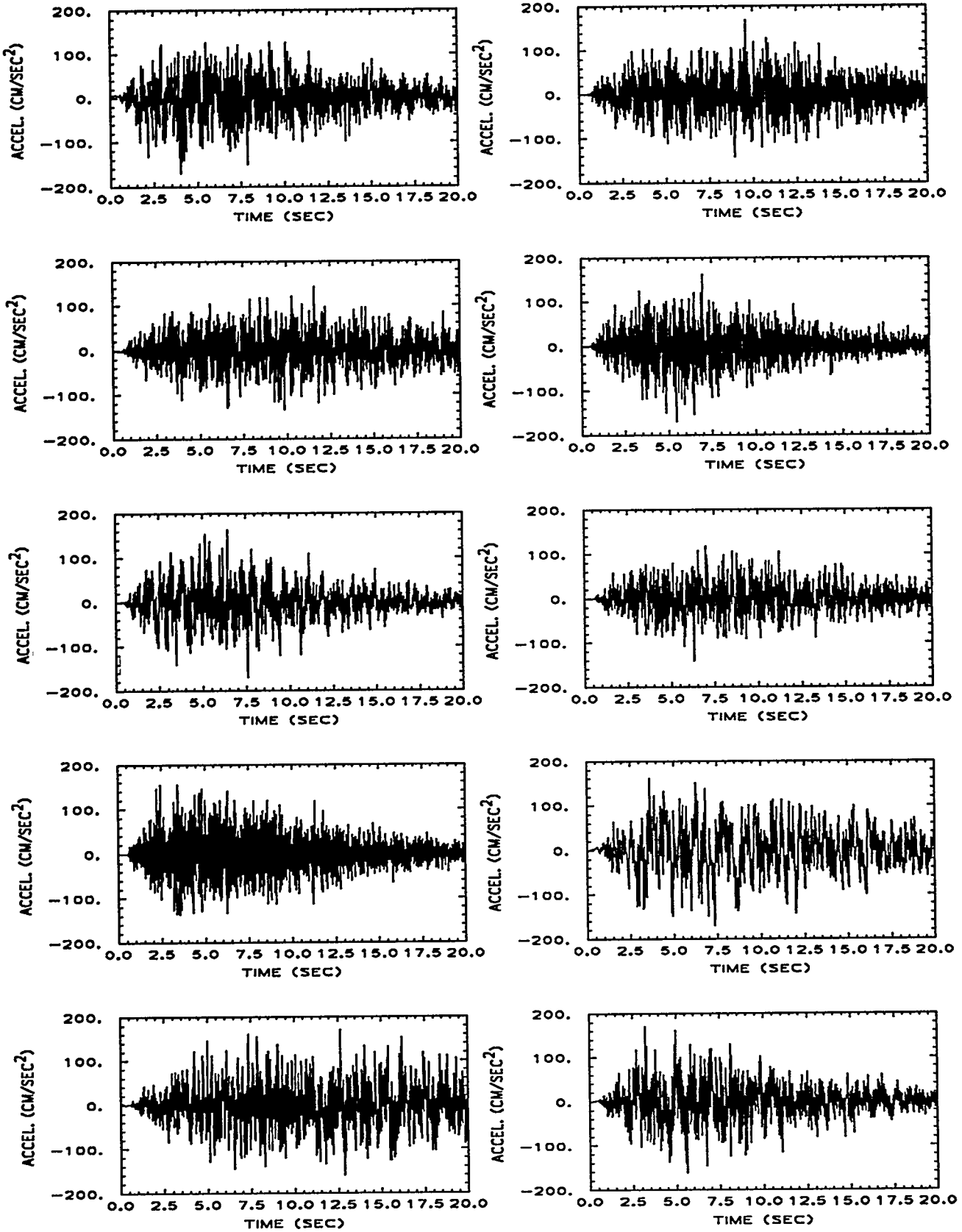

Figure 3-18. Time histories from 25 artificial ground motions generated for the magnitude-dependent seismic hazard analysis (m_b 6.5–7.0).

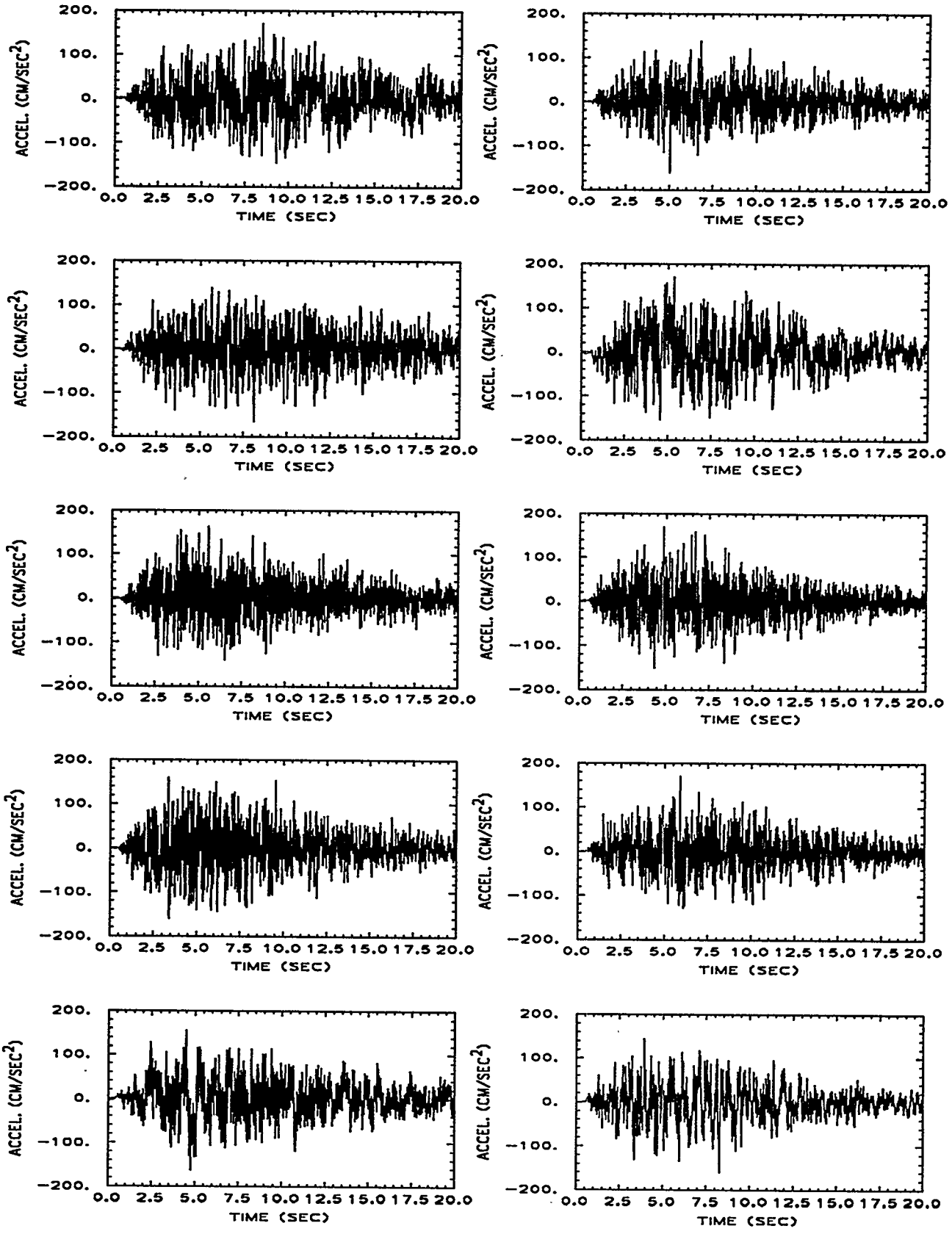

Figure 3-18 (continued)

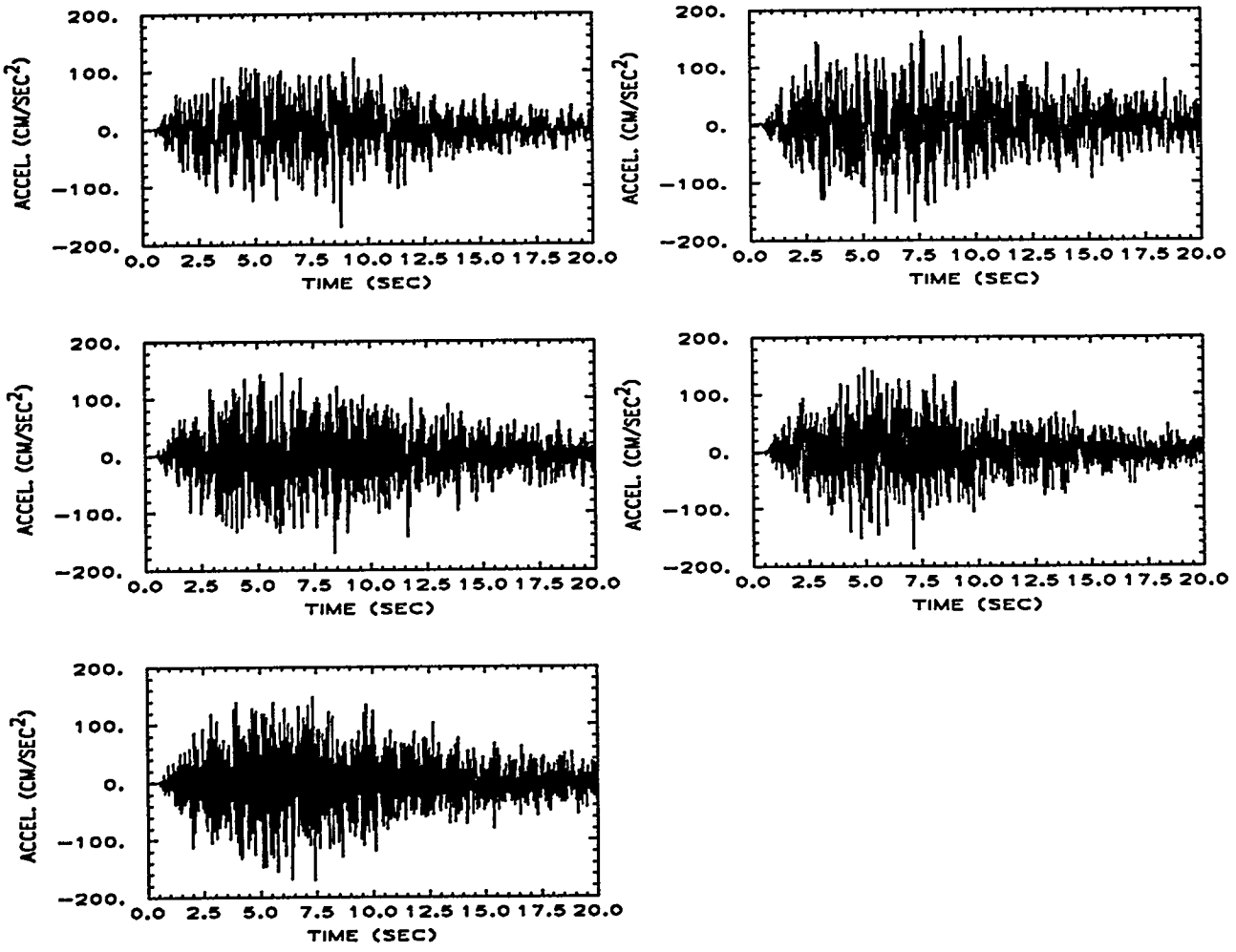

Figure 3-18 (continued)

Section 4
FRAGILITY ANALYSIS

This section describes the specific procedures used to develop seismic fragility curves in this study. As mentioned in Section 2, a shear-wall/diaphragm failure-mode category is selected for investigation due to the recurrence and importance of this type of failure mode in past SPRA studies.

The sets of motions generated in Section 3 are used as the ground motion input basis for fragility assessment. These motions are highly representative of eastern U.S. earthquakes, and exhibit realistic variability in motion characteristics, including event-to-event variabilities in frequency content, duration, and time-dependent behavior.

Using these sets of motions, fragility curves are developed in this section, for the following cases:

- A hypothetical, yet realistic replication of the SPRA Base Case analysis of floor-diaphragm (shear-wall type) failure in the control building, using motions consistent with the SPRA base-case spectrum.
- Diaphragm failure of the control building using (eastern U.S. type) site-specific motions obtained for all magnitudes (composite-magnitude/aggregate case).
- Diaphragm failure of the control building for site-specific motions obtained for five separate magnitude ranges (magnitude-dependent/disaggregated case).

For each of these cases, two sets of fragilities are obtained: the first set is obtained by anchoring all ground motion spectra to a common PGA; the second set is obtained by anchoring all ground motion spectra to a common measure of spectral acceleration averaged over the appropriate frequency range. In addition, for comparative purposes, composite-magnitude site-specific motion spectra are anchored to a common measure of inelastic spectral acceleration (at the proper frequency), and a composite seismic fragility is obtained for this case.

4.1 PROCEDURE

Section 2 described briefly the analytical methodology typically employed in seismic fragility assessment. This method starts with the design basis, and using linear-response results and general formulas for a variety of safety factors, generates a median capacity and estimates of randomness in capacity and uncertainty in median capacity. As previously mentioned, this method involves application of considerable engineering judgment, which may encourage the tendency to introduce compounding conservatisms.

The procedure implemented in this study is based on detailed, nonlinear time-history response analysis. With proper modeling, this approach inherently and directly captures the combined effects of all elemental safety factors typically considered in the standard fragility method. In other words, this approach eliminates the need for heuristics in several aspects of failure analysis.

The general methodology, including fundamental equations, values of variabilities in basic structural properties, and simulation technique, follows closely the procedures presented by Kennedy *et al.* (1). These procedures are considered as state-of-the-art in SPRA analysis for nuclear power plants, and are significantly more involved and advanced than standard procedures used in most SPRAs to date.

4.2 MODEL DESCRIPTION

Figure 4-1 presents a schematic of the dynamic model developed for the chosen diaphragm failure mode of the control building. This model is a realistic representation of a diaphragm failure. The model, however, must be considered as a hypothetical example, as it differs from the control building at the Millstone 3 plant in a number of significant ways. The most important difference is that the model considered here is symmetrical, whereas the Millstone 3 control building has unsymmetrical cut-outs and distribution of mass and stiffness at the top floor. Torsional loads that may develop during earthquake response are therefore not considered in our hypothetical model. Nevertheless, comparison of (linear) forces obtained in our analysis and the SPRA analysis imply that torsion is not a major factor in the Millstone 3 control building. As will be seen later in this section, results of our base-case analysis (under the constraint that all elements but the floor diaphragm remain elastic) and the SPRA analysis are quite similar, implying that the hypothetical model may in fact be closely representative of the actual Millstone 3 control building.

The SPRA found the control building response in each of the three directions $(x, y\ z)$ to be essentially uncoupled. Our study confirmed the SPRA finding that critical response occurs

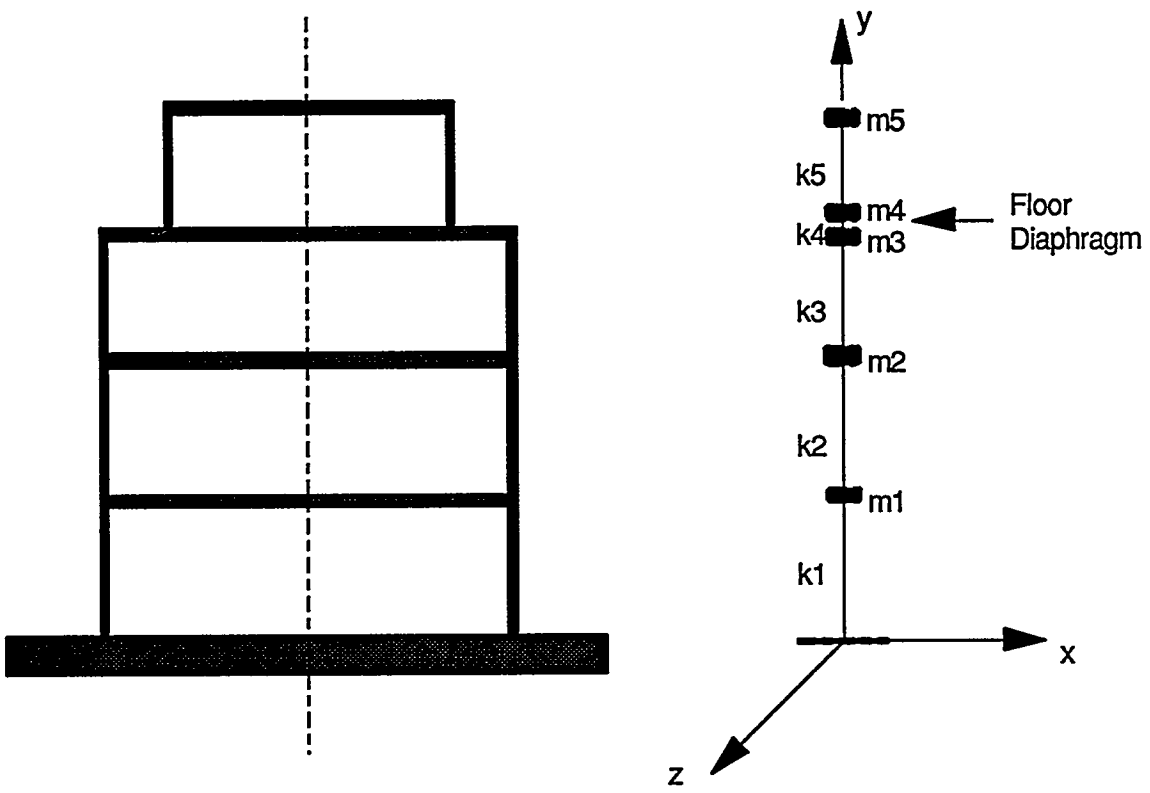

Figure 4-1. Dynamic model of control building, showing floor-diaphragm element.

in the x-direction, which is the direction considered in our fragility analyses. (Note that the x-direction is perpendicular to the plane of the paper in the block diagram of the control building in Figure 4-1).

The floor-diaphragm element (between masses 3 and 4) models flexibility (in shear) of the portion of the third floor between the shear walls above and below. A discontinuity in shear path above and below the third floor level requires this portion of the floor diaphragm to carry relatively large shear loads. This condition, combined with the fact that significant cut-outs exist in this portion of the floor diaphragm, leads to a low capacity/demand ratio in the floor-diaphragm element.

In Figure 4-1, to facilitate illustration of the floor diaphragm element, masses 3 and 4 are shown somewhat separated. It should be understood, however, that these masses actually both lay at the same y location. All deformations in this model occur in the x direction and all deformations occur exclusively in shear.

4.3 SHEAR STIFFNESS

Shear stiffness for the model elements are obtained from the following formula (1):

$$\check{k} = \check{F}_s \frac{A_v G}{h_w} \qquad (4-1)$$

where $\check{k}$ is the median shear stiffness of the element, $\check{F}_s$ is a median stiffness-knockdown factor, A_v is the wall shear area, G is the shear modulus, and h_w is the shear-wall height. From the SPRA analysis, the shear modulus was found to be $G = 1638$ ksi. The stiffness knockdown factor accounts for concrete cracking (and accompanying stiffness reduction) that occurs at loads significantly below the design basis. Representative values of $\check{F}_s$ vary from 0.5 to 1.0; a value of $\check{F}_s = 0.75$ was selected as representative and appropriate for this study.

Using Eq. 4-1, median shear stiffness were obtained for all model elements; these values, together with the nodal masses, are given in Table 4-1.

4.4 MEDIAN DYNAMIC PROPERTIES

4.4.1 Frequencies and Participation Factors

Using the median shear stiffnesses and masses shown in Table 4-1, a modal analysis was performed to obtain median structural frequencies, mode shapes, and participation factors. The results of this analysis are indicated in Table 4-2.

Table 4-1

Median Shear Stiffnesses and Masses of Control Building Model

Node No.	Element No.	Lumped Mass ($k - s^2/in$)	Shear Stiffness $\check{k}_i$ (k/in)
	1		209300
1		12.90	
	2		220800
2		12.63	
	3		283900
3		4.05	
	4		253900
4		12.58	
	5		195100
5		8.81	

Table 4-2

Median Structural Frequencies and Participation Factors

Mode No.	Participation Factor	Frequency (Hz)
1	6.70	7.01
2	-2.23	19.26
3	-0.88	31.18
4	-0.62	36.22
5	0.02	63.09

4.4.2 Damping

The median damping of the control building concrete structure was judged in the SPRA study to be 10% of critical. For our study, we assume Rayleigh damping with 10% of critical specified for the first two modes. Damping ratios that result for all modes are indicated in Table 4-3.

4.5 SHEAR STRENGTH

Median shear strengths $\check{v}_u$ for the control building model elements were obtained as the summation of concrete ($\check{v}_c$) and effective steel ($\check{v}_{se}$) contributions, using the following formula (1):

$$\check{v}_u = \underbrace{8.3\sqrt{\check{f}'_c} - 3.4\sqrt{\check{f}'_c}\left(\frac{h_{we}}{l_w} - 0.5\right) + \frac{N}{4l_w t_w}}_{\check{v}_c} + \underbrace{(A\rho_n + B\rho_h)\,\check{f}_y}_{\check{v}_{se}} \qquad (4-2)$$

where $\check{f}'_c$ is the median compressive strength of the concrete, $\check{f}_y$ is the median tensile strength of the reinforcing steel, h_{we} is the effective wall height obtained from the Moment/Shear ratio at the given section, l_w is the length of the shear wall, t_w is the thickness of the shear wall, N is the axial load acting on the shear wall, ρ_n is the reinforcement ratio for vertical reinforcing, and ρ_h is the reinforcement ratio for horizontal reinforcing.

Table 4-3

Median Modal Damping Ratios

Mode No.	Damping Ratio (% of critical)
1	0 100
2	0.100
3	0.135
4	0.152
5	0.248

The relative magnitudes of terms A and B in Eq. 4-2 govern the contribution of vertical and horizontal reinforcement to the effective shear strength derived from steel reinforcing. Values of A and B depend on the height-to-length ratio of shear walls, as expressed by the following relations (1):

$$A = \begin{cases} 1 & \text{for } \frac{h_{we}}{l_w} \leq 0.5 \\ 2\left(1 - \frac{h_{we}}{l_w}\right) & \text{for } 0.5 < \frac{h_{we}}{l_w} < 1.0 \\ 0 & \text{for } \frac{h_{we}}{l_w} \geq 1.0 \end{cases} \qquad (4-3)$$

and

$$B = 1 - A \qquad (4-4)$$

The values for median concrete compressive strength and steel tensile strength are obtained in the SPRA analysis as $\check{f}'_c = 4.5$ ksi and $\check{f}_y = 50$ ksi, respectively. The values of h_{we} were determined from shears and moments obtained from a linear modal analysis of the structure. Shear stresses from Eq. 4-2 are multiplied by 60% of the total effective length of the shear wall minus the total length of cut-outs, and by thickness, to obtain the median total ultimate shear load resistance $\check{V}_u$. The portions of total median shear resistance contributed by the concrete and steel are denoted, respectively, as $\check{V}_c$ and $\check{V}_{se}$. Values of $\check{V}_u$, $\check{V}_c$, and $\check{V}_{se}$, and values of capacity/demand ratio (using the modal-analysis forces for the base case), obtained for the control building are shown in Table 4-4.

Table 4-4

Median Element Shear Strengths

Element No.	$\check{V}_u$ (k)	$\check{V}_c$ (k)	$\check{V}_{se}$ (k)	Capacity/Demand Ratio
1	25930	10970	14960	4.79
2	43640	20270	23370	9.32
3	44840	21470	23370	12.81
4	9190	4650	4540	3.02
5	45010	21640	23370	33.72

We performed analyses of the structure permitting all elements to behave in a nonlinear fashion. The results of these analyses clearly showed that, although element 1 has a higher demand/capacity ratio than element 4, failure drifts will not be achieved in element 4. This result is obtained because once element 1 goes nonlinear it isolates the other elements from damaging motions. The SPRA fragility assessment for this failure mode, therefore, conservatively and implicitly assumed that only element 4 would experience nonlinearity. This assumption was introduced in the SPRA by taking simply the structural element with the smallest capacity-demand ratio as the critical failure member. In other words, a linear-response-based condition was incorrectly applied in making judgments of nonlinear response. We have already mentioned in Section 2 the potential of these types of assumptions to introduce substantial conservatisms in SPRA analyses. Such assumptions may, as well, lead occasionally to unconservatisms in SPRA analyses.

To maintain our comparison with the SPRA base case analysis of the diaphragm failure mode of the control building, we restricted our analysis to the same conditions; principally, these include constraining the bottom element to linear behavior. In the fragility analyses that follow, an infinite yield capacity was assumed for the bottom shear-wall element.

4.6 FORCE-DEFORMATION BEHAVIOR AND FAILURE THRESHOLD

The nonlinear behavior of a floor diaphragm is very similar to that of a vertical shear wall. In fact, a floor diaphragm can be modeled as a shear wall in a horizontal plane,

by ignoring the (usually negligible) effects of axial (i.e., in-plane) loads. In our selection of a force-deformation model of diaphragm response, we therefore used a hysteretic model representative of shear-wall behavior. The model we implement has been used extensively in characterizing the nonlinear response of both concrete shear-wall and steel braced-frame structures in nuclear power plants (1,2,3). Specific details of this model can be found in Kennedy *et al.* (1,2). The model is considered appropriate for simulating nonlinear behavior up to the point of the onset of significant structural damage, which is the damage threshold of interest in this, as well as most, engineering studies.

Definition of the nonlinear shear-wall model requires specification of the following four parameters: (1) yield resistance, (2) stiffness ratio, (3) unloading stiffness parameter, and (4) stiffness degradation parameter. The unloading stiffness and stiffness degradation parameters were chosen consistent with values previously found to produce realistic response; the unloading stiffness parameter was set at $\alpha = 0.35$, and the stiffness degradation parameter was set at $\gamma = 0.95$.

The determinations of yield resistance and stiffness ratio were made to best match the enveloping skeleton curve expected for real structural response (which typically displays a smooth force-deformation curve). The steps used to determine the yield strength and stiffness ratio are as follows:

- Set the element median yield resistance as $\check{V}_y = 1.10\check{V}_c$.
- Adjust the post yield stiffness so that the hysteretic energies absorbed for the model and the expected skeleton curve are equal at the failure deformation limit. The ultimate capacity reached by the model at the failure definition is termed V'_u, and should not exceed the actual ultimate shear resistance ($\check{V}_u$) of the skeleton curve by more than 20%.
- Determine the post-yield stiffness ratio s; this ratio should be in the range of 0.03 to 0.10.

In performing these steps, it is first necessary to define the failure-deformation limit. We use the same failure criterion as that used by Kennedy *et al.* (1), based on inter-element drift ratio. We assume that failure (expressed as severe structural distress) occurs at a drift ratio of 0.7% (of element height). Kennedy *et al.* (1) provides detailed discussion justifying the

selection of this drift limit; we have reviewed that discussion and accept it as a reasonable approach for our investigation of floor diaphragm failure.

Based on 0.7% median drift ratio as failure criterion, and implementing the steps described above, we assess values for element yield resistance and stiffness ratio; these values are presented in Table 4-5.

Table 4-5

Median Failure Drifts and Element Yield Resistances and Stiffness Ratios

Element No.	0.7% Drift Limit (in)	$\check{V}_y$ (k)	Stiffness Ratio, s	$V'_u/\check{V}_u$
1	1.68	(Infinite)	0.052	1.14
2	1.89	22300	0.070	1.14
3	1.47	23617	0.071	1.15
4	0.50	5120	0.046	1.17
5	2.16	23800	0.070	1.15

4.7 SECANT FREQUENCY AND FREQUENCY RANGE OF INTEREST

To compute seismic fragilities in terms of average elastic spectral acceleration, it is necessary to estimate a (median) secant frequency of the control building model at failure (of the third-story floor diaphragm). The nonlinear response of the control building will be largely influenced by the spectral ordinates between an effective frequency of the structure and the secant frequency at failure (2). Variability in secant frequency at failure must also be estimated, and is largely associated with variability in the failure drift. The secant frequency (at failure) and its variability are used as elements in determining the frequency range of interest over which spectral accelerations are averaged in deriving a ground-motion measure for anchoring fragilities.

A secant frequency, f_s, can be estimated from the following equation:

$$f_s = f\sqrt{\frac{1+s(\mu-1)}{\mu}} \qquad (4-5)$$

where f is the (fundamental) elastic frequency of the structure and μ is the system ductility at failure. The system ductility may be estimated from (1):

$$\mu = \frac{\sum \left[M_i \Delta_i^{\text{fail}}\right]}{\sum \left[M_i \Delta_i^{\text{el}}\right]} \qquad (4-6)$$

where M_i is the mass at node i, Δ_i^{fail} is the total drift (relative to the ground) at node i when failure is reached in the critical element [i.e., floor-diaphragm (element 4)], and Δ_i^{el} is the total drift (relative to the ground) at node i when incipient yield is reached in the critical element.

Values of Δ_i^{el} are obtained from the elastic deformed shape of the structure, scaled so that the (inter-story) yield drift is just reached in the critical failure element. Values of Δ_i^{fail} are obtained from an inelastic deformed shape of the structure. We estimate an inelastic deformed shape by determining the predominant-mode shape from an equivalent-linear analysis, where the (changing, inelastic) stiffness of element 4 is approximated by a (constant, linear) secant stiffness corresponding to the failure ductility. This equivalent-linear deformed shape is scaled so that the (inter-story) failure drift is just reached in the critical element.

Table 4-6 shows the incipient-yield deformed shape, and the approximate predominate inelastic deformed shapes (and frequencies) for element-4 failure (inter-story) drifts of 0.50 in. (median value), 0.94 in. ($+1.65\beta_C$ on failure drift) and 0.27 in. ($-1.65\beta_C$ on failure drift).[1] From these deformed shapes and from the nodal masses given in Table 4-1, using the above equation, three different values of system ductility (at failure) are found as $\mu = 3.8$, $\mu = 5.8$, and $\mu = 2.8$. These system ductilities imply secant frequencies of approximately $f_s = 3.8$ Hz (median), $f_s = 3.1$ Hz (lower-bound estimate), and $f_s = 4.5$ (upper-bound estimate), respectively.

The value $f_s = 3.1$ is a lower limit on the frequency range of interest, applicable to the response of a 7 Hz (median-frequency) structure. There is uncertainty, however, in estimation of the control building (initial) structural frequency; from the simulations developed later for conducting uncertainty analyses, this uncertainty is found to be characterized by a value of $\beta = 0.24$. We take a lower-bound estimate of the initial structure frequency at the -1.65β level, and obtain $f_{\text{el}}^{\text{l.b.}} = 7.0e^{-1.65(0.24)} = 4.7$. Assuming the same ratio of lower-limit secant frequency to initial frequency of $3.1/7.0 = 0.44$ as was implied by the analysis for the 7 Hz structure, a lower limit on the secant frequency of interest, considering uncertainty in elastic

[1] Values for β_C on failure drift are given in Table 4-7.

Table 4-6

Incipient-Yield and Approximate Inelastic Deformed Shapes at Failure

Node	Deformed Shape for: Incipient Yield	Failure when d_4† = 0.50 in.	Failure when $d_4 = 0.94$ in.	Failure when $d_4 = 0.27$ in.
	($f = 7.01$ Hz)	($f_s = 4.37$ Hz)	($f_s = 3.45$ Hz)	($f_s = 5.32$ Hz)
1	0.04198	0.06192	0.05898	0.06724
2	0.07703	0.11791	0.11326	0.12660
3	0.09757	0.15748	0.15312	0.16649
4	0.11757	0.65748	1.08912	0.43349
5	0.12892	0.68071	1.11263	0.45659

† d_4 denotes drift in element 4.

frequency, can be estimated as $f_s^{\text{l.b.}} = 0.44(4.7) = 2.1$. This lower-limit secant frequency is a lower-bound frequency of interest in fragility (and fragility uncertainty) analysis of the control building.

An upper-bound frequency of interest for the control building is found in a similar manner. Nonlinear response is primarily governed by the input strength at frequencies between the secant frequency and a higher, effective frequency, where the effective frequency can be approximated as: (2,1):

$$f_{\text{eff}} = (1-k)f + kf_s \qquad (4-7)$$

In this equation, f is the initial, linear frequency and k is a factor, between zero and one, that increases with ductility and with the number of significant inelastic cycles. For ductilities associated with failure of the control building, we judged $k = 0.75$ to be an appropriate value. To obtain an upper-bound estimate of the effective frequency of interest, we first take an upper-bound estimate of the initial structural frequency at the $+1.65\beta$ level, and obtain $f_{\text{el}}^{\text{u.b.}} = 7.0e^{+1.65(0.24)} = 10.4$. We also take an upper-bound estimate of the secant frequency, obtained as $f_s^{\text{u.b}} = (4.5/7.0)10.4 = 6.7$. An upper-bound on the effective frequency is thus found to be $f_{\text{eff}}^{\text{u.b.}} = (1-0.75)(10.4) + 0.75(6.7) = 7.6$. This upper-bound effective frequency is an upper-bound frequency of interest in fragility (and fragility uncertainty) analysis of the control building.

From this evaluation, the frequency range of interest for fragility assessment of the control building is about 2.1–7.6 Hz. (For later comparison, we note that the average frequency of interest is equal to $[(2.1+7.6)/2] = 4.9 \approx 5$ Hz.) It should be kept in mind, however, that determination of this frequency range is based on approximate analysis; use of alternative methods for assessing structural secant frequency can produce different results. For instance, if we had used the secant frequencies shown in Table 4-6, obtained from equivalent-linear analysis, we would have found a frequency range of about 2.3–8.5 Hz.

For our subsequent fragility analyses based on spectral acceleration, we use a frequency range of 2.5 Hz to 10 Hz over which to average spectral ordinates in obtaining a ground-motion measure. Thus, we use a slightly different frequency range than that found above. The reason for use of this different frequency range is that, in most SPRA analyses, a systems-level (i.e., plant-level) fragility curve (or its equivalent) must be derived based on fragilities of a number of components. In general, these components will consist of base-mounted equipment and floor-mounted equipment, in addition to civil structures. The frequency ranges of interest for base-mounted and floor-mounted equipment are likely to be significantly

higher and somewhat higher, respectively, than that for most civil structures. Consequently, the frequency range of 2.5 Hz to 10 Hz is considered more representative of that which would be found and used in a complete, systems-level SPRA analysis. The impact of using the 2.5 Hz to 10 Hz frequency range for analysis of the control building is a very slight, if not negligible (unavoidable) loss in precision in fragility and failure-rate assessment.

4.8 MEDIAN FRAGILITY ANALYSIS

Using the median stiffnesses, masses, modal damping, strengths, drift limits, and other model parameters presented previously, several median failure analyses of the hypothetical control building structure were conducted for the various ground motions sets generated in Section 3. The steps in evaluating median fragilities for any given set of motions are as follows:

- Scale all (25) ground motions to have identical levels of a common measure of some ground motion characterization (in this study, we use PGA, average spectral acceleration over 2.5 to 10 Hz, and inelastic spectral acceleration at 7 Hz).
- Using nonlinear time-history analysis, determine maximum drift responses d for each ground motion.
- For each evaluation of drift, determine a probability of severe structural distress based on the median drift limit, assuming randomness in the failure drift. The failure drift limit is assumed to be lognormally distributed with a logarithmic standard deviation of $\beta_R = 0.15$ (1). The probability of failure (severe structural distress) for any given motion is obtained as:

$$P[\text{Fail}] = \Phi\left[\frac{\ln\left(d/d_{0.7\%}\right)}{\beta_R}\right] \qquad (4-8)$$

  where Φ is the normal cumulative distribution function and $d_{0.7\%}$ is the median failure drift limit.
- Average the failure probabilities for all motions to obtain an estimate of the overall failure probability for the given ground motion intensity level.
- Repeat the above steps with a different intensity level of the chosen ground motion characterization. Find the levels of ground motion intensity corresponding to failure probabilities of 0.16, 0.50, and 0.84. Fit a lognormal distribution through these points (and other points, if calculated)[2] to parameterize the fragility curve by a median value and a logarithmic standard deviation β_R.

[2]The fitted distribution should best match the fragility points obtained over the failure probability range of 0.16 to 0.50 since this (lower-tail) range typically has a more dominant contribution to failure frequency than the upper tail.

4.9 UNCERTAINTY ANALYSIS

Assessment of uncertainty requires that various possible structural models be simulated as random realizations derived from the probability distributions of basic uncertain model variables (i.e., stiffness, mass, strength, damping, and failure threshold). Once the structure simulations are obtained, they may each be used separately to conduct individual fragility analyses, as described above, based on all motions. Such an analysis would produce a number of separate fragility curves that describe the uncertainty in capacity, and from which a value of β_U may be obtained. One strong point of this procedure is that it produces realistic variations in shape of individual structural fragility curves (e.g., the individual curves likely cross one another). The beneficial effect of these realistic variations is to reduce uncertainty in risk estimates. Unfortunately, however, performing the numerous individual analyses is extremely computer intensive. This weakness overshadows the benefits of reduced risk uncertainty, particularly when one considers the insignificance of this uncertainty reduction in face of the large uncertainty in seismic hazard.[3]

An alternative uncertainty analysis involves random combination of both structure and ground motion simulations together, and evaluation of a composite fragility curve using the median-type approach described in Section 4.8. From the composite fragility, a value of β_C is obtained in a manner identical to that described above for evaluation of β_R. The fragility uncertainty parameter is then back-calculated using the following equation:

$$\beta_C^2 = \beta_R^2 + \beta_U^2 \qquad (4-9)$$

or

$$\beta_U = \sqrt{\beta_C^2 - \beta_R^2} \qquad (4-10)$$

In this case, an accurate uncertainty analysis may be conducted that requires only about twice the computational effort of the median analysis (as opposed to about a ten- to twenty-fold increase in effort using the former approach).

For our uncertainty analyses, we simulated 50 structures, and randomly combined these structures with the 25 ground motions, using each motion exactly twice. We used Latin-Hypercube simulation (4) to sample from each basic-variable distribution and to randomly

[3]More specifically, a typical uncertainty, β_U, in hazard may be on the order of 1.2, whereas a representative β_U for fragility may be on the order of 0.5. Refinements in uncertainty assessment of fragilities may be anticipated to achieve only a moderate reduction in fragility uncertainty. In addition, the refinement of retaining and using individual simulation results is equally applicable to derivation of both hazard-curve and fragility-curve families.

combine the variable samples. From these 50 realizations, failure analyses were conducted using the median-type approach described above, composite fragility curves were determined, and values of β_C and β_U were obtained.

This approach for evaluating uncertainty in fragility curves is identical to that used by Kennedy *et al.* (1). We conducted a simple sensitivity analysis in the present study which verified that the use of 25 ground motions and 50 structure simulations (based on the Latin-Hypercube method) was adequate in capturing the fragility parameters $\breve{A}$, β_R, and β_U.

4.9.1 Uncertainty in Stiffness, Mass, Strength, Damping, and Failure Limit State

The distribution on uncertainty for simulation of each of the basic model variables is assumed to be lognormal. Each variable is expressed as a ratio to its median value. In any structure simulation, the simulated ratio of each variable was assumed to apply as a single multiplicative factor applicable for all structural-model elements. The values of β_U used to characterize the lack of knowledge of each basic variable are presented in Table 4-7 and are consistent with those used by Kennedy *et al.* (1).

Table 4-7

Distribution Parameters of Uncertain Variables

Variable	Median	β_R	β_U	β_C
Stiffness Ratio	1.00	0.00	0.50	0.50
Mass Ratio	1.00	0.00	0.10	0.10
Damping-Ratio Ratio	1.00	0.00	0.35	0.35
Strength Ratio	1.00	0.00	0.25	0.25
Drift-Limit Ratio	1.00	0.15	0.35	0.38

4.10 RESULTS

Median and uncertainty analyses of the seismic fragility for the control building diaphragm failure mode were conducted for each set of motions and for the three ground motion characterizations described previously. The results of each fragility assessment are presented and discussed below:

4.10.1 Base Case Analysis: PGA as Parameter

The base-case fragility result is obtained using the motions generated from the SPRA review spectrum. Motions are normalized to a common value of PGA in this assessment, to be consistent with the basis for analysis in the SPRA. Results of the analysis are shown in Table 4-8.

Observation of Table 4-8 shows that results for our study and the SPRA study are very similar. The slightly larger median capacity in our analysis may be due to neglecting torsional forces derived from asymmetries in the control building.

The values of β_R from the two analyses are also very similar; this observation helps to confirm that the event-to-event variability modeled in the generated ground motions (from Section 3) is representative.

The value of β_U derived from our analysis is significantly larger than that from the SPRA. This difference is likely due to two sources: (1) the simplified method used to obtain β_U in the SPRA analysis, and (2) larger variabilities selected in this study to model lack of knowledge of uncertain variables.

It is interesting to observe that the HCLPF (defined in Section 2) capacities for the SPRA and Base-Case results are in very close agreement, despite the differences in values of β_R and β_U for the two cases. This suggests that the combined variability in the SPRA analysis was properly determined, even though individual estimates of β_R and β_U differ from what a more detailed analysis shows. This observation is likely due to inconsistency in treatment of randomness and uncertainty in past SPRA practice; in particular, variability due to uncertainty may have, in some instances, been in fact treated as variability due to randomness. The HCLPF capacity by itself is considered to be a useful description of a component's seismic ruggedness, and serves as a basis for quantifying seismic margin.

4.10.2 Composite-Magnitude Analysis: PGA as Parameter

The composite-magnitude fragility assessment uses motions generated to match the site-specific composite spectrum modeled in Section 3. Figure 4-2 shows a plot of (10%-damped) pseudo spectral acceleration (PSA) for both the site-specific composite spectrum and the SPRA review spectrum. This figure indicates a factor of conservatism of about 2.0 in the SPRA spectrum vis-à-vis the site-specific spectrum, in the vicinity of an average frequency of interest of about 5 Hz. Also, the slope of the SPRA spectrum in the vicinity of the elastic

Table 4-8

Fragility Result for the Base Case Analysis: PGA as Parameter

Description	$\breve{A}$ (g)	β_R	β_U	β_C	HCLPF (g)
Base Case Result (This Study)	1.10	0.21	0.53	0.57	0.32
SPRA Result	1.00	0.24	0.43	0.49	0.33

frequency (7 Hz) is somewhat more severe that the slope of the site-specific spectrum; i.e., for a softening structure, which tends to respond to motions at a lower (than elastic structural) frequency, the SPRA review spectrum becomes relatively more severe than the site-specific spectrum.

The effect of these factors on seismic fragility is seen by comparing Table 4-9 with Table 4-8. Here it is noted that values of β_R and β_U for our base case analysis and our site-specific, composite analysis are very similar. There is a factor of 2.0 conservatism in the base-case result median capacity, which is due to the differences in spectra mentioned above. A plot of the two fragility curves is shown in Figure 4-3.

4.10.3 Magnitude-Dependent Analysis: PGA as Parameter

The magnitude-dependent fragility assessment uses motions generated to match the site-specific magnitude-dependent spectra modeled in Section 3.[4] Figure 4-4 shows a plot of (10%-damped) pseudo spectral acceleration (PSA) for site-specific magnitude-dependent spectra and for the site-specific composite spectrum. We observe that the composite spectrum

[4]Note that the magnitude-dependent target spectra of Section 3 are derived from uniform hazard spectra results, which are for 5% damping (see Figure 3-2). Response spectra of the resulting generated motions have been computed at 10% damping, corresponding to the median damping in the control building model. Unless specifically noted otherwise, the response spectra plotted in this section are for 10% damping.

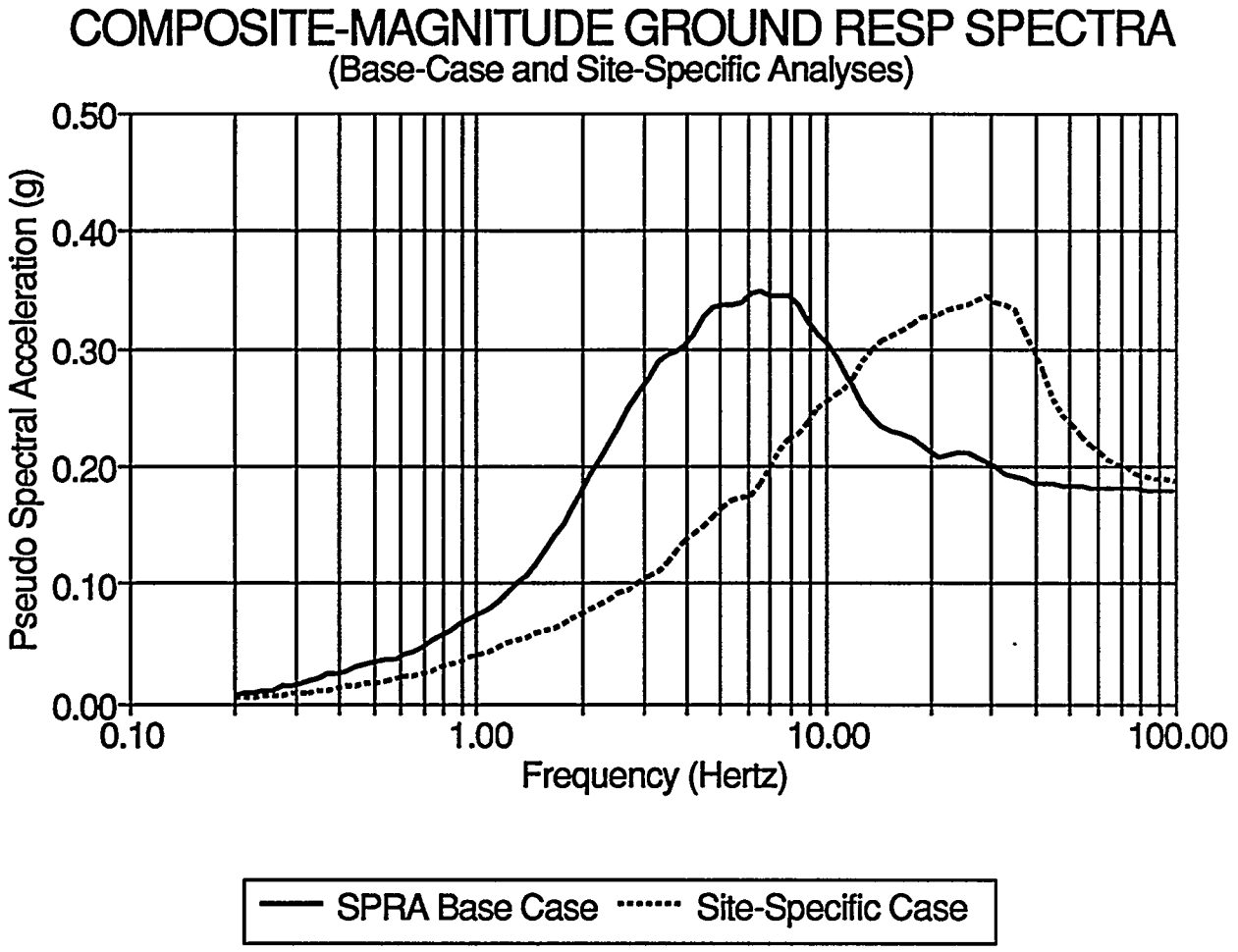

Figure 4-2. Response spectra (10%-damped) for the SPRA base-case and for the site specific composite-magnitude analyses.

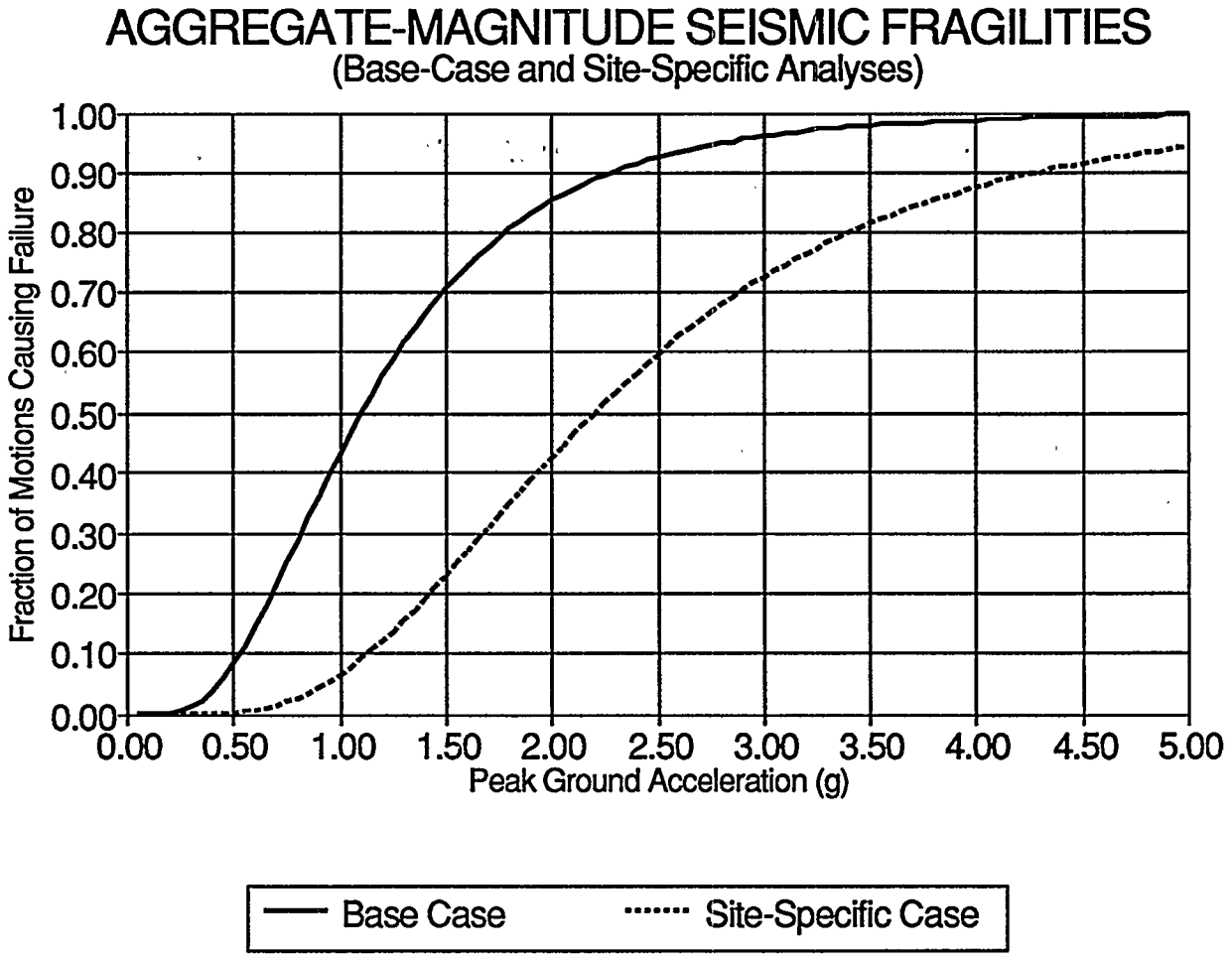

Figure 4-3. Seismic fragility results for the SPRA base-case and for the site specific composite-magnitude analyses, when PGA is used as the anchor-basis for review spectra.

Table 4-9

Fragility Result for the Site-Specific Composite-Magnitude Analysis: PGA as Parameter

Description	$\breve{A}$ (g)	β_R	β_U	β_C	HCLPF (g)
Site-Specific Composite-Magnitude	2.20	0.25	0.52	0.58	0.62

very closely matches the magnitude-dependent spectrum for the $m_b = 5.75$ review spectrum. Figure 4-4 shows that the average PSA ordinate, at a frequency of 5 Hz, is about 55% greater for the large magnitude (m_b 6.75, 6.25) motions than for the small magnitude (m_b 4.75) motions. It is therefore expected that the median capacity obtained for the $m_b = 4.75$ case will be at least 1.55 times the median capacity for the $m_b = 6.75$ case. Table 4-10 verifies this expectation. *This table also indicates a significant magnitude dependence of fragility parameters when PGA is used as the ground-motion parameter; the median capacity* $\breve{A}$, β_U, *and* β_C *all increase rather substantially with decreasing magnitude.*

Figure 4-5 plots the magnitude-dependent and composite seismic fragility curves for visual comparison. It is noted that the composite fragility corresponds closely with the fragility for $m_b = 5.75$.

It is interesting and important to note that the magnitude-dependence seen here for fragility curves based on PGA can be explained reasonably well by a simple examination of the differences in response spectra (and differences in slopes of response spectra) for the appropriate sets of motions.

The increase in β_U and β_C with decreasing magnitude is also interesting. This result implies that there is substantially greater variability in amplitudes of PSA in the vicinity of 5 Hz for small magnitude motions anchored to PGA than for larger magnitude motions anchored to the same PGA. This fact helps explains the surprising robust nature of the HCLPF capacity

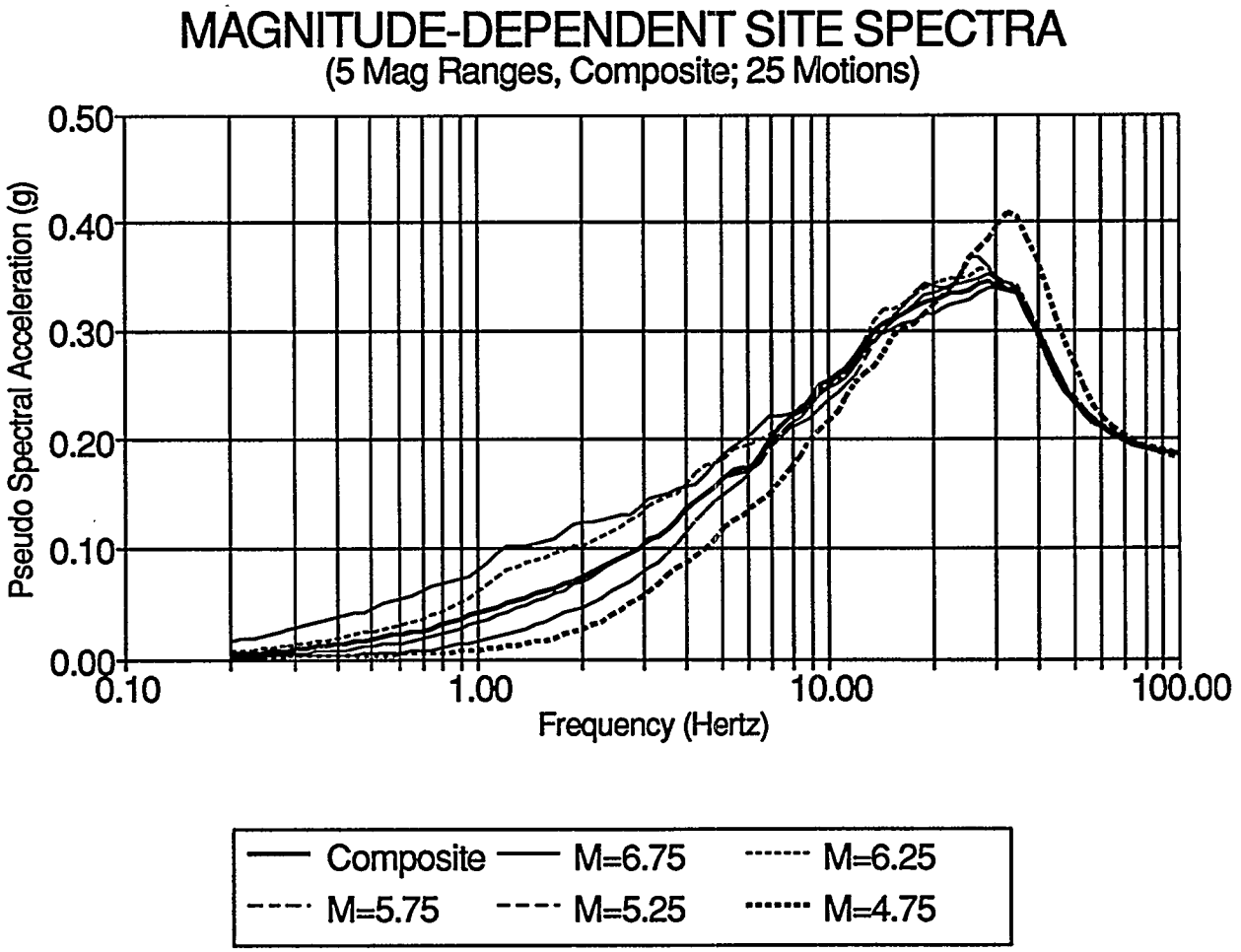

Figure 4-4. Response spectra (10%-damped), anchored to a common (SSE) PGA, for the site-specific magnitude-dependent and composite-magnitude analyses.

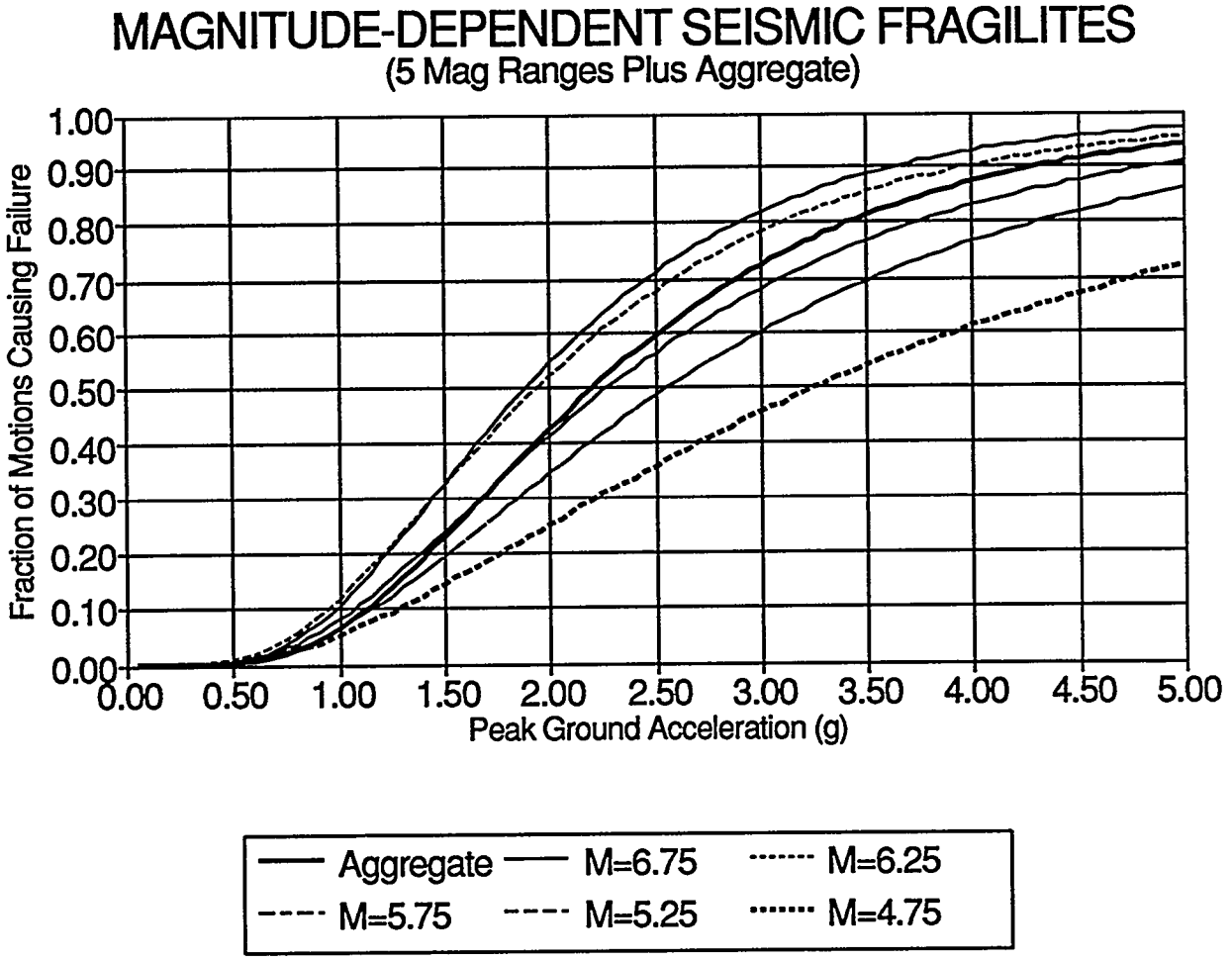

Figure 4-5. Seismic fragility results for the site-specific magnitude-dependent and composite-magnitude analyses, when PGA is used as the anchor-basis for review spectra.

Table 4-10

Fragility Results for the Magnitude-Dependent Analyses: PGA as Parameter

Description	$\breve{A}$ (g)	β_R	β_U	β_C	HCLPF (g)
$m_b = 6.75$	1.88	0.31	0.40	0.51	0.58
$m_b = 6.25$	1.93	0.27	0.49	0.56	0.55
$m_b = 5.75$	2.27	0.28	0.52	0.59	0.61
$m_b = 5.25$	2.55	0.31	0.54	0.62	0.63
$m_b = 4.75$	3.25	0.44	0.58	0.73	0.60

measure, even when the HCLPF is measured in terms of PGA. It is significant that (PGA-based) HCLPF capacities are observed to be largely invariant with magnitude. Apparently, the characteristic properties of ground-motion happen to encourage this stability of the HCLPF. In other words, the HCLPF was not explicitly (or implicitly) defined in such a way that small-magnitude motions would lead to the same result as large-magnitude motions. The magnitude-invariance of the HCLPF suggests that a composite-magnitude description of ground motion would serve adequately for conducting seismic margin assessments.

4.10.4 Composite-Magnitude Analysis: Elastic Spectral Acceleration as Parameter

Figure 4-6 shows PSA plots of both the site-specific composite spectrum and the SPRA review spectrum, now anchored to a common PSA measure. The common PSA measure is an arithmetic average of PSA amplitudes over the frequency range of 2.5 to 10.0 Hz [the PSA amplitudes are sampled at a constant interval of log(frequency)]. The justification for selection of this frequency range has been given previously (Section 4.7); this frequency range may serve as an appropriate PSA-measure basis in the seismic analysis of a number of different nuclear power plant systems.

Figure 4-6 shows that, when anchored to this common PSA measure, the site-specific spectrum contains significantly greater energy at high frequency, and somewhat lower energy

at low frequency than the base-case SPRA review spectrum The effect of this difference on seismic fragility is shown graphically in Figure 4-7, and in tabular form in Table 4-11.

The two fragility results are nearly identical. The difference between the two results is inconsequential, but may nevertheless again be explained by a simple consideration of the ground motion spectra. It is noted from Figure 4-6 that the SPRA spectrum is slightly (about 7%) greater in the vicinity of 5 Hz[5] that the site-specific spectrum. The median capacity of the site-specific fragility might thus be expected to be about 7% greater than that for the SPRA base case; in fact, however, it is only about 3.4% greater. The potential 7% effect is offset somewhat because of the much greater amplitudes of the site-specific spectrum at high frequency. Undoubtedly, the structure exhibits a greater level of second-mode response (near 20 Hz) under the site-specific set of motions than under the base-case set.

Table 4-11

Fragility Result for the Base Case Site-Specific Analyses: Average Elastic Spectral Acceleration (2.5–10 Hz) as Parameter

Description	$\breve{S}_a$ (g)	β_R	β_U	β_C	$\overline{S_a}$-HCLPF (g)
Base Case Result	2.61	0.17	0.45	0.48	0.94
Site-Specific Result	2.70	0.18	0.44	0.48	0.97

4.10.5 Magnitude-Dependent Analysis: Elastic Spectral Acceleration as Parameter

Figure 4-8 shows PSA plots of site-specific magnitude-dependent spectra and the composite spectrum, anchored to the common average (2.5–10 Hz) PSA measure. Variation in PSA values at 7 Hz for the magnitude-dependent spectra is about 20%, with the lower magnitudes

[5]Recall from Section 4.7 that 5 Hz is approximately the average frequency of interest for the control building model.

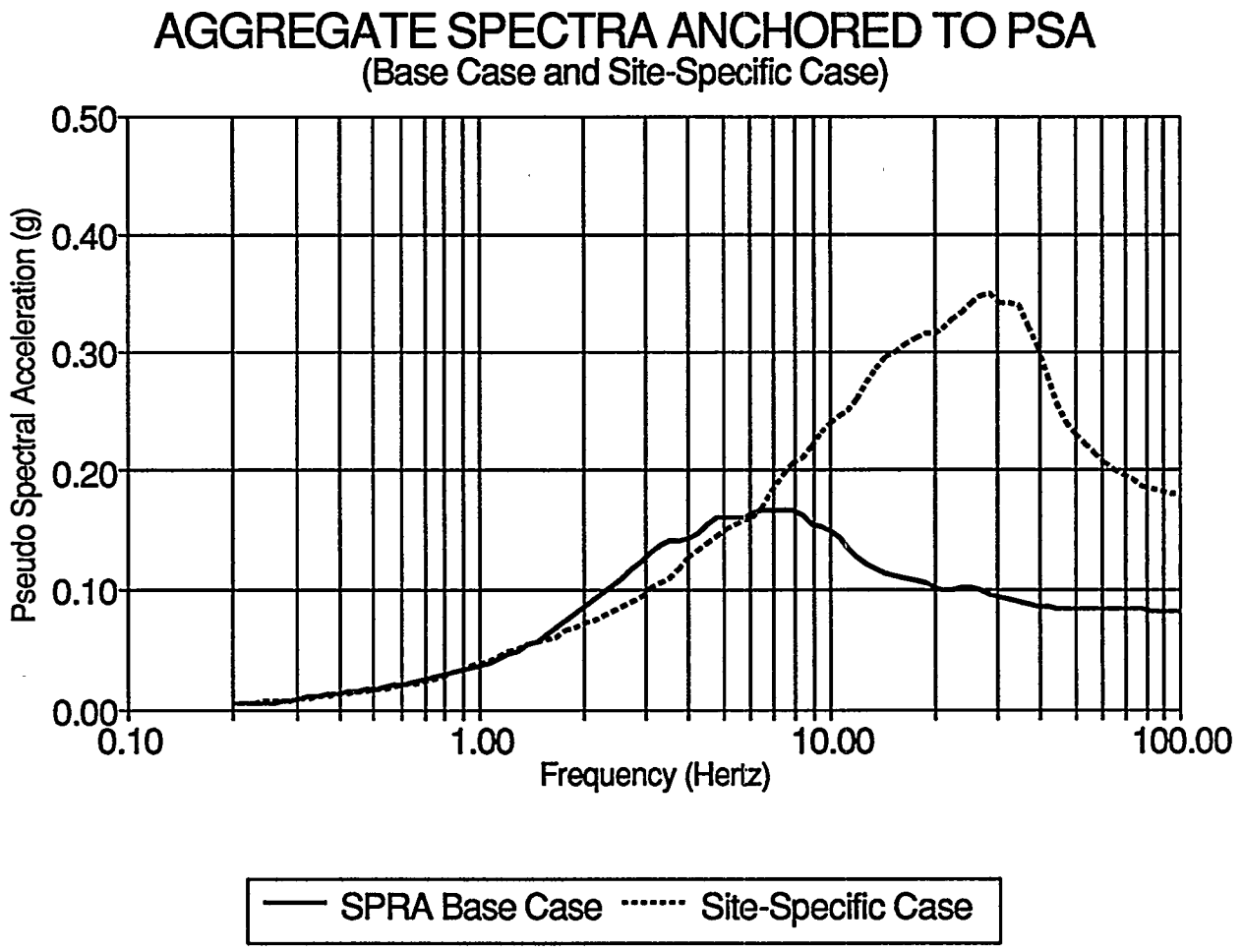

Figure 4-6. Response spectra (10%-damped) for the SPRA base-case and for the site specific composite-magnitude analyses, when average PSA (2.5–10 Hz) is used to anchor review spectra.

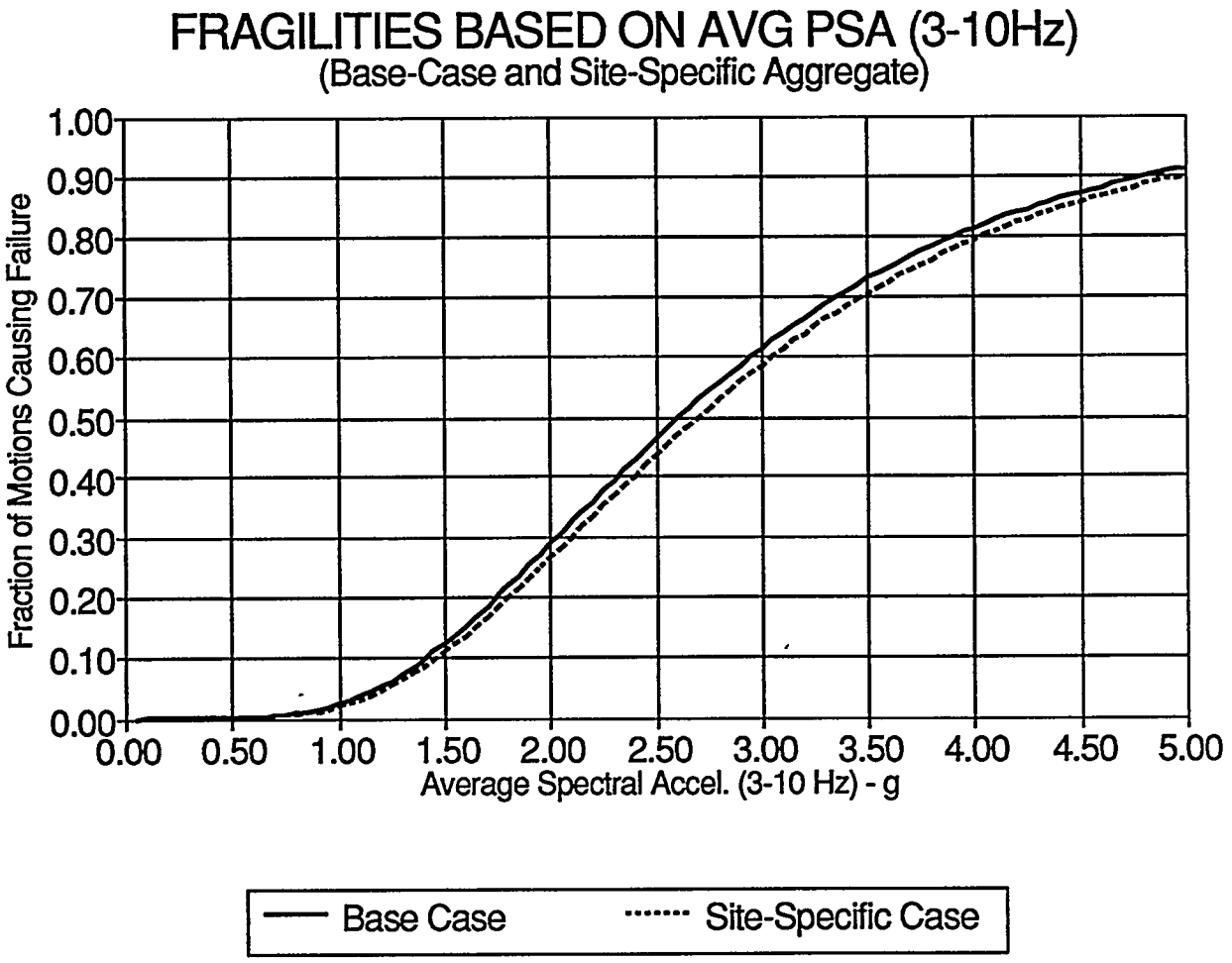

Figure 4-7. Seismic fragility results for the SPRA base-case and for the site specific composite-magnitude analyses, when average PSA (2.5–10 Hz) is used as the anchor-basis for review spectra.

exhibiting somewhat greater amplitudes that the larger magnitudes (all spectra appear to cross at about 5.0 Hz).

The implication of these small differences in PSA amplitudes on seismic fragility estimates is largely inconsequential; as can be seen by examination of Figure 4-9 and Table 4-12, the magnitude-dependent fragilities are nearly identical (i.e., the magnitude-dependent fragilities show no consistent magnitude dependence when PSA ordinates are averaged over the appropriate frequency range, to the soft (lower-frequency) side of the elastic frequency).

It is interesting to note from Table 4-12 that the $\overline{S_a}$-HCLPF values, although showing no clear systematic trend with magnitude, demonstrate greater magnitude-to-magnitude variability than do the median values. Hence, some robustness in HCLPF appears to be lost when average PSA is used as the ground-motion parameter.

Table 4-12

Fragility Results for the Magnitude-Dependent Analyses: Average Elastic Spectral Acceleration as Parameter

Description	$\breve{\overline{S_a}}$ (g)	β_R	β_U	β_C	$\overline{S_a}$-HCLPF (g)
$m_b = 6.75$	2.74	0.16	0.36	0.40	1.16
$m_b = 6.25$	2.68	0.17	0.44	0.47	0.98
$m_b = 5.75$	2.72	0.19	0.39	0.43	1.04
$m_b = 5.25$	2.74	0.21	0.42	0.47	0.97
$m_b = 4.75$	2.60	0.19	0.46	0.50	0.89

We draw the conclusion that differences in the control building seismic fragilities for different magnitudes are unimportant when an appropriate PSA measure is used to characterize ground motion and to anchor ground motion spectra. *Speaking more generally, in fragility analysis of nuclear power plant structures, an elastic PSA measure (taken over the proper frequency range) may often serve adequately to reveal this insensitivity to magnitude; in other*

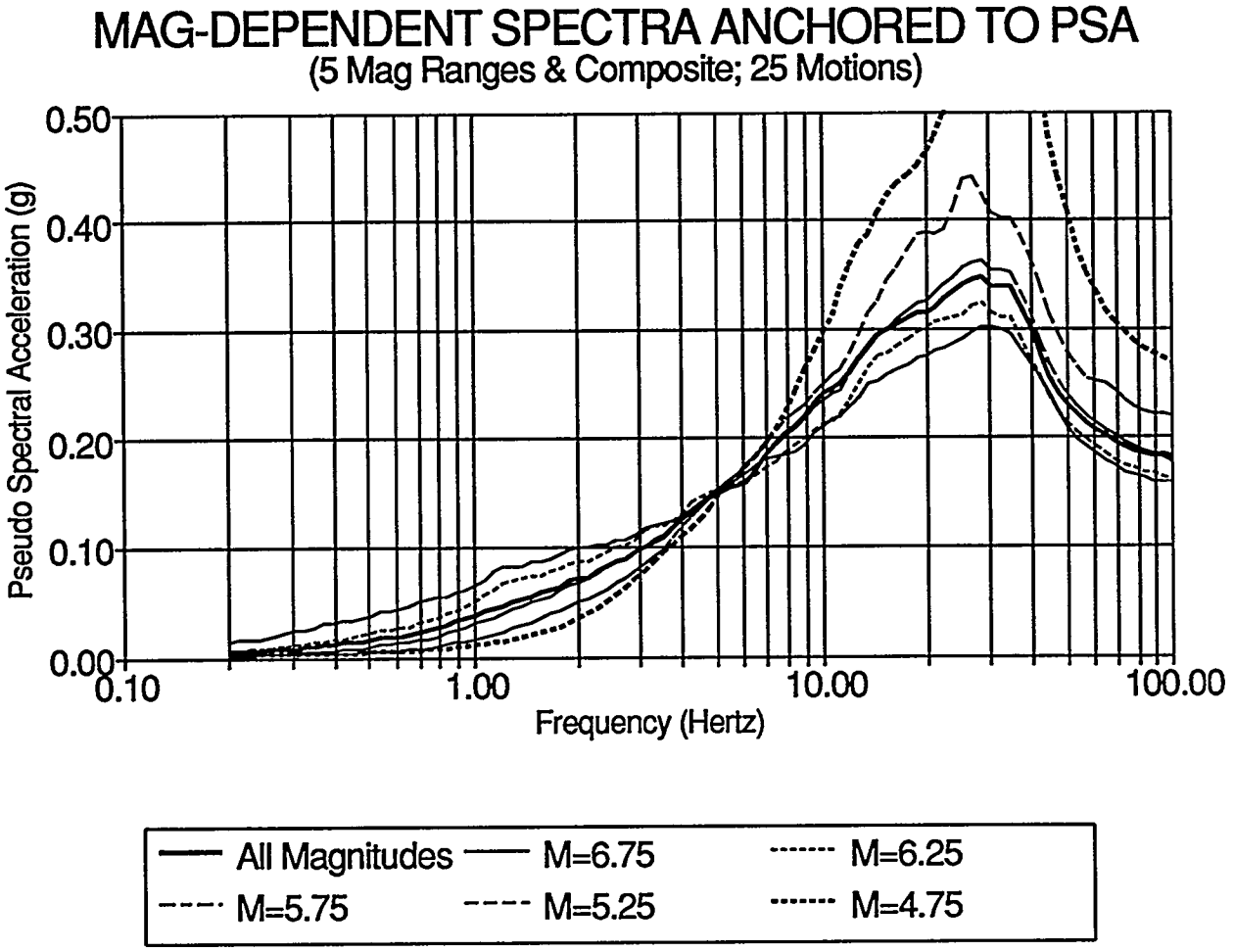

Figure 4-8. Response spectra (10%-damped) for the site-specific magnitude-dependent and composite-magnitude analyses, when average PSA (2.5–10 Hz) is used to anchor review spectra.

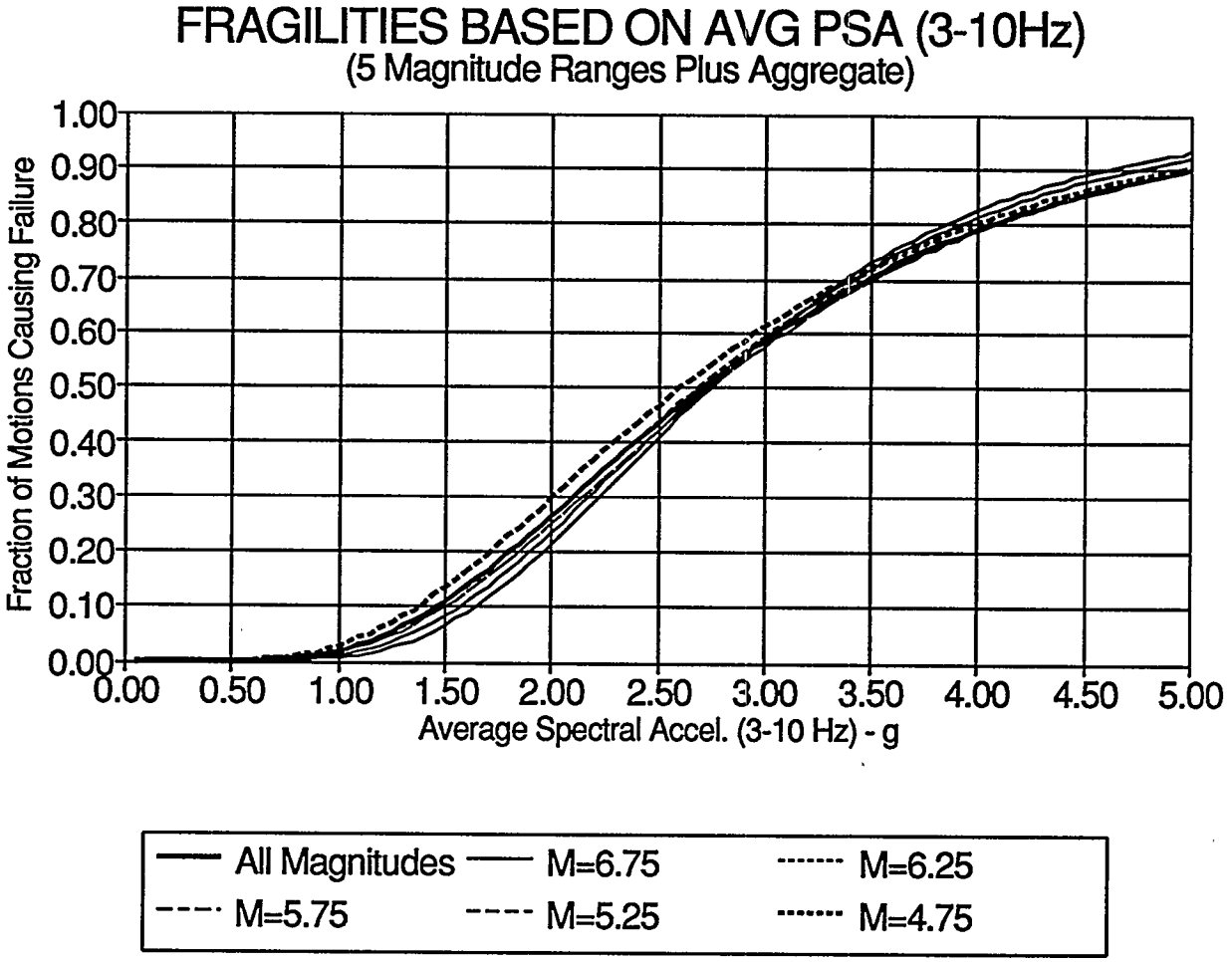

Figure 4-9. Seismic fragility results for the site-specific magnitude-dependent and composite-magnitude analyses, when average PSA (2.5–10 Hz) is used as the anchor-basis for review spectra.

cases (particularly those where the slope of the spectrum near the elastic frequency varies noticeably with magnitude), it is more appropriate to use an inelastic spectral acceleration measure.

These conclusions have been supported by earlier work by Kennedy *et al.* (1,2), and imply that spectral averaging often eliminates the need to look explicitly at particular characteristics of ground motion, such as duration, in predicting failure. The justifications for these conclusions, nevertheless, may not be immediately obvious to many engineers. In particular, many have looked to (independent and combined) scalar (frequency-independent) measures of motion intensity and motion duration as a way to characterize damageability. The above conclusions, therefore, undoubtedly have implications that may be non-intuitive (initially) to many. The insights obtained by understanding the above results are significant to anyone interested in describing and mitigating earthquake damageability.

Effect of Duration on Structure Capacity. What we observe in the above fragility results is that, *conditional upon an appropriate spectral measure*, both duration and magnitude have little (if any) systematic effect on structural damage. To better illustrate, consider Figure 4-10, which shows the effect of strong-motion duration T_d' (2) on median capacity (for fragilities anchored to average PSA in the range from 2.5 to 10.0 Hz). This figure indicates no dependence of the (median) structural fragility on strong-motion duration. Whether the earthquake record is one second or ten seconds long, coming from a magnitude 6.75 or 4.75 earthquake does not matter, as long as the spectral shape in the frequency range of interest is known. (By spectral shape, we mean not just a single amplitude at a given frequency, but spectral breadth, slope, etc. obtained from spectral amplitudes at several frequencies over the frequency range of interest.[6])

This result does not mean that duration and magnitude do not have important effects on structural damage; they do (if only implicitly through the response spectrum). The key point, rather, is that the elastic response spectrum (over the proper frequency range) or the

[6]For the present example, the slopes of all review spectra in the frequency range of interest are very similar. For this reason, the fragilities would be quite independent of magnitude even if a single elastic spectral amplitude were used as the fragility anchor basis. It should be stated that, even when given this single elastic PSA measure, variations in the damage potential of the individual ground motions exist. For some cases, the damage potential is severe, and for other cases, the damage potential is small. (Whether or not a given record is damaging depends on the slope of the spectrum at the initial, elastic frequency, in addition to the actual spectral amplitude). For the representative motions that we have studied, the combined effect (for any given magnitude range), reveals no consistent difference in damageability across magnitude, once the elastic spectral acceleration is known.

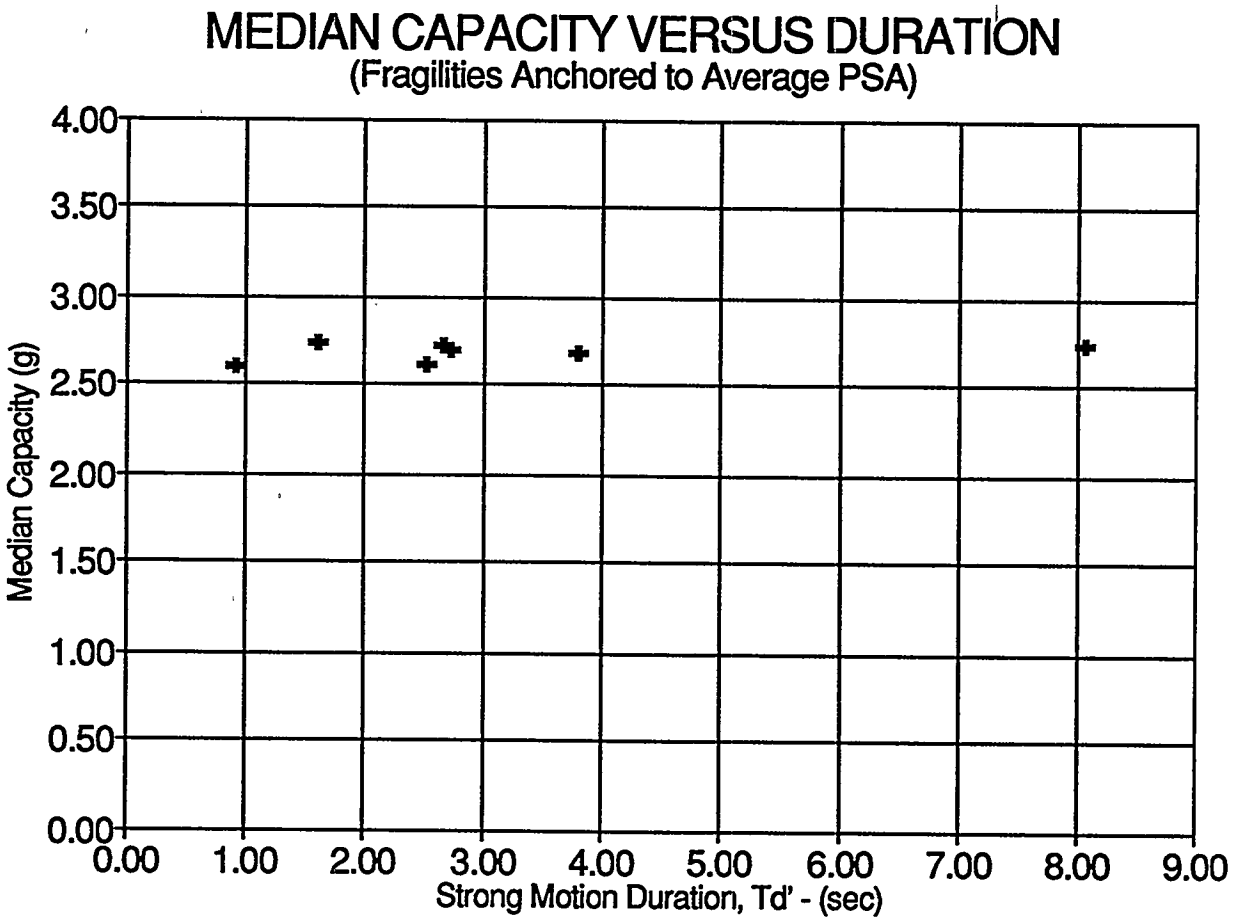

Figure 4-10. Median capacity $\check{A}$ of magnitude-dependent seismic fragility of the control building (floor-diaphragm failure mode) versus strong magnitude duration T'_d. [Median capacities are conditional on use of average PSA (2.5–10 Hz) as fragility parameter].

inelastic response spectrum (at the appropriate frequency) by itself is adequate to convey the damage-essence or importance of duration and magnitude for most structures and earthquakes of interest [i.e., for cases where the ground-motion duration is at least as great as the fundamental period of the structure, and for cases where the onset of significant structural damage (as opposed to structural collapse) is the limit state of interest]. The utility of knowing duration and magnitude for structural damage prediction, once the entire spectral shape and amplitude are known, appears to be negligible.

These statements require further explanation. First, we clarify that we are discussing failure definitions that pertain to the onset of significant structural damage, and not to actual structural collapse. There may likely be a correlation between duration and collapse, given a particular spectrum. In general, however, structural behavior at collapse is not well understood; this fact, combined with the fact that collapse is a situation to generally be avoided, suggests that the onset of significant structural damage is a more appropriate failure limit state.

In real earthquakes, structures that undergo significant damage, generally experience that damage well before the motion actually ends (i.e., during the strong-motion phase). Engineering intuition, however, is based largely on observation of, and concern with, collapsed or extensively damaged buildings after earthquakes or during aftershocks. This observation process leads to an experience base that may emphasize understanding of the effects of additional duration on damage to failed structures, rather than an understanding of how the onset of failure is influenced by duration, given the response spectrum. Consequently, from these observations, engineers do not say that additional duration would cause more damage and not simultaneously cause a change in the ground-motion spectrum. Most engineers likely appreciate that a change in the spectrum would be affected, but may not appreciate that that change in the spectrum conveys the importance (to damage) of the change in duration. In fact, by definition of the inelastic response spectrum (whose characteristics are strongly related to the elastic response spectrum), it would be difficult to conclude that additional strong motion duration would cause more (or wider-spread) damage, and simultaneously not cause a change in the response spectrum of the motion. For these reasons, engineers should not view this study's conclusions as counter-intuitive or counter to the experience base.

Situations may be conceived in which damage, under a given spectrum, depends on motion duration. Consider, for instance, a simple (steady-state) sinusoidal motion of given frequency; regardless of the motion duration, the elastic response spectrum remains constant. Assuredly, under this case, damage will depend on duration; the structure is more likely to

fail (given, of course, it has not already failed) as time passes, due (for instance) to low cycle fatigue effects. A key point, however, is that these types of (experimental) motions are not representative of real earthquakes. Real earthquakes release energy in a characteristic fashion: they build up to strong ground motion, exhibit a strong motion phase, and then decay. Changes in the length of strong motion duration of real earthquakes produce accompanying changes in the spectrum. Care is, therefore, required in interpreting the effects of duration on damage as obtained from experimental results; the laboratory investigation should be conducted in a manner to insure compatibility of duration (e.g., number of test cycles) with spectra from real earthquake motions.

Sewell (3) has shown (using nonlinear time-history analysis) that nonlinear damage potential of ground motion, conditional on spectral acceleration, is largely independent of magnitude (and implicitly, duration) for a combined set of real (western U.S.) earthquake motions. This observation was based on a wide variety of damage measures, that include ductility, hysteretic energy, combinations of ductility and hysteretic energy, and cumulative damage. The study employed the use of detailed nonlinear models capable of capturing duration effects on the onset of significant structural damage. The study was based on analyses of single-degree-of-freedom structures. The present fragility analysis, based on the response of a multiple-degree-of-freedom structure, produces results that are consistent with the observations and conclusions in the above study.

4.10.6 Composite-Magnitude Analysis: Inelastic Spectral Acceleration as Parameter

Figure 4-11 and Table 4-13 show fragility results for the control building, using site-specific magnitude-composite ground motions anchored to the same value of (10%-damped) inelastic spectral acceleration at a frequency of 7 Hz. A ductility-ratio damage measure of $\mu = 4.0$ was used as a basis for obtaining the inelastic spectral ordinates, and corresponds roughly to a system ductility associated with failure of the control building (see Section 4.7).

Comparing Tables 4-13 and Table 4-11, it is seen that the values of β_R and β_U are about the same for magnitude-composite fragilities. The lower median value seen in Table 4-13 is due simply to the normalization required to obtain inelastic spectral acceleration, with an average reduction, relative to the elastic spectral acceleration measure, of about $F_\mu = 3.6$. When integrated with appropriate seismic hazard curves, the differential effect on risk of using either the elastic-PSA-based or the inelastic-PSA-based fragilities would be negligible for the present case.

It is worth noting that indication of the worth or goodness of a ground motion characterization for fragility assessment can be found in the fragility parameters β_R and β_U. To

Table 4-13

Fragility Result for the Site-Specific Composite-Magnitude Analysis: Inelastic Spectral Acceleration as Parameter

Description	$\breve{S}_a^{\mu}$	β_R	β_U	β_C	S_a^{μ}-HCLPF
Site-Specific Composite-Magnitude	0.73	0.18	0.45	0.49	0.26

illustrate, for a ground motion characterization that is based on inelastic failure response of the structure of interest, by definition, the resulting fragility parameter β_R would approach a value of zero. The ability to reduce β_R is generally accompanied by an ability to reduce β_U, because sensitivity to modeling uncertainties typically lessens with increased ability to accurately predict failure.

By comparison of Table 4-12 and Table 4-10 (or Table 4-11 and Table 4-9), it is clear that average elastic PSA (2.5–10 Hz) is a better ground motion characterization for structural damage than PGA; i.e., values of both β_R and β_U are significantly lower when average PSA, as opposed to PGA, is used as the ground-motion parameter. Comparison of the values of β_R and β_U from Tables 4-13 and 4-10, indicate that the average PSA and the inelastic PSA measures are both about as good in characterizing the damage potential for the given set of motions. As suggested above, this result is due to the fact that all response spectra (regardless of magnitude) have about the same slope in the vicinity of 7 Hz. In general, however, inelastic spectral acceleration will serve as a better characterization of ground motion damage potential for fragility assessment.

Sewell and Cornell (3,5) note that inelastic spectral acceleration can be predicted with at least the same precision as elastic spectral acceleration in seismic hazard analysis, at no expense (in terms of increased analytical effort). As a result, use of seismic hazards and fragilities based on inelastic spectral acceleration may lead to more accurate estimates of seismic risk in some cases. In studies requiring higher accuracy in assessment of risk, we recommend that an inelastic spectral acceleration measure be used as the basis for hazard and fragility assessment.

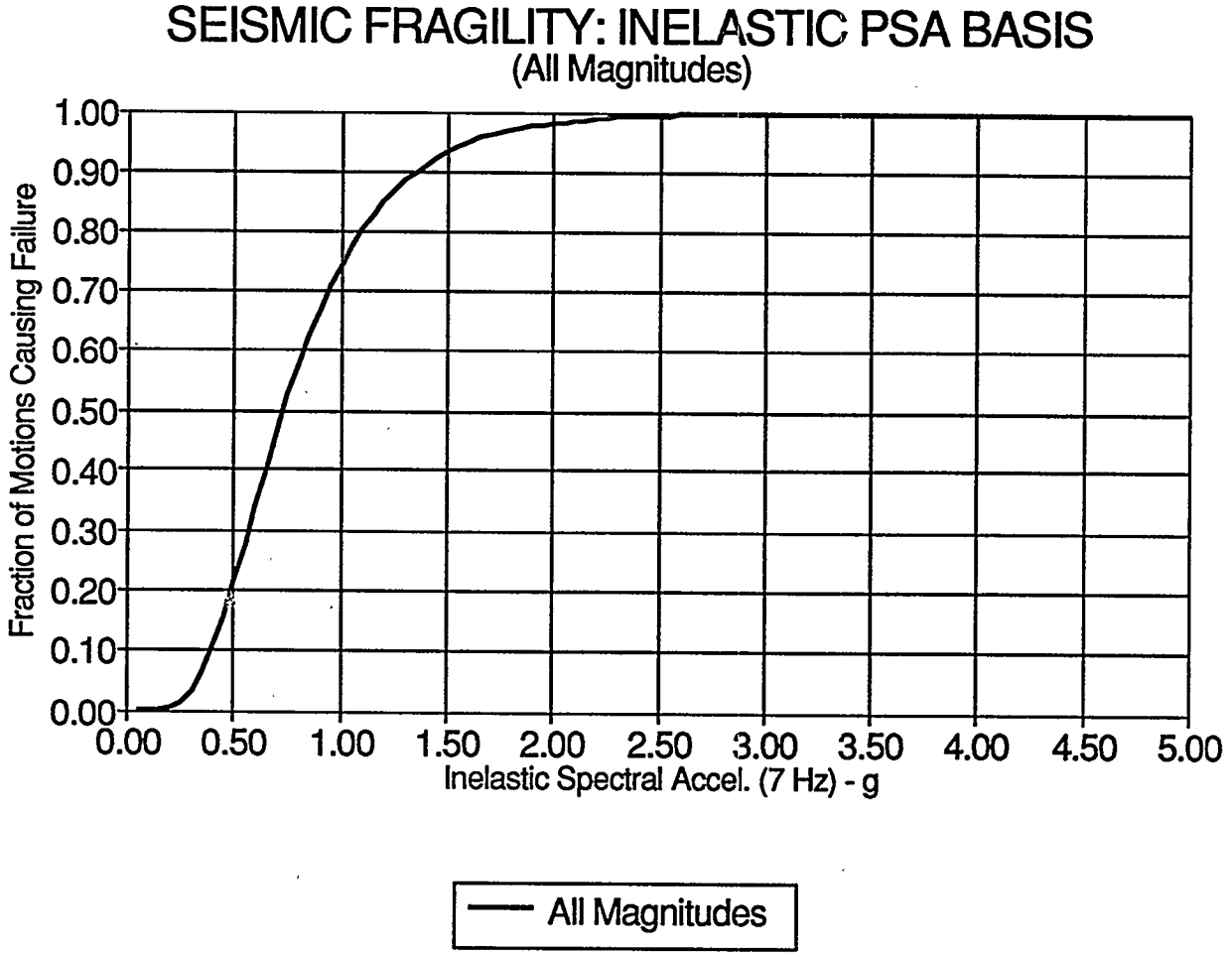

Figure 4-11. Seismic fragility result for the site-specific composite-magnitude analysis, when inelastic spectral acceleration (7 Hz) is used as the anchor-basis for review spectra.

4.11 REFERENCES

1. R. P. Kennedy, D. A. Wesley, and W. H. Tong. *Probabilistic Evaluation of the Diablo Canyon Turbine Building Seismic Capacity Using Nonlinear Time History Analysis.* Technical Report 1643.01, Pacific Gas and Electric, 1989.

2. R. P. Kennedy, S. A. Short, K. L. Merz, F. J. Tokarz, I. M. Idriss, M. S. Power, and K. Sadigh. *Engineering Characterization of Ground Motion – Task I: Effects of characteristics of free-field motion on structural response.* Technical Report NUREG/CR–3805, U.S. Nuclear Regulatory Commission, February 1984. Vol. 1.

3. R. T. Sewell. *Damage-Effectiveness of Earthquake Ground Motion: Characterizations based on the performance of structures and equipment.* Ph.D. Dissertation, Stanford University. Stanford, CA, 1989.

4. R. L. Iman and J. C. Helton. *A Comparison of Uncertainty and Sensitivity Analysis Techniques for Computer Models.* Technical Report NUREG/CR–3904, U.S. Nuclear Regulatory Commission, March 1985.

5. C. A. Cornell and R. T. Sewell. Non-linear-behavior intensity measures in seismic hazard analysis. In *Proceedings: International Conference on Seismic Zonation, Guangzhou, China*, 1987.

Section 5

SEISMIC HAZARD ANALYSES

5.1 INTRODUCTION

This section presents results from the evaluation of seismic hazard at the Millstone site, considering alternative characterizations of the hazard. These results will be used in Section 6 to compute failure probabilities under each of these alternative assumptions.

5.2 PRA SEISMIC HAZARD ANALYSIS

This analysis replicates the seismic hazard evaluation performed as part of the seismic PRA at the Millstone site (1). The SPRA analysis considered eleven alternative assumptions on seismic zonation, three possible values of Richter's b value, three possible maximum magnitudes, and four attenuation functions. Integration over magnitude was performed starting at m_b 4.5.

We replicated the SPRA hazard analyses by considering only a subset of the parameter combinations and by modeling only the dominant seismic source in each zonation. We used the same four attenuation functions as the SPRA analysis. We then performed minor adjustments to the maximum magnitudes and seismicity parameters in order to match the 0.15, 0.50, and 0.85th fractiles of the original hazard curves.

The calculated fractile hazard curves are shown in Figure 5-1. The sharp drops at accelerations of 0.6 to 1.0g are caused by the combined effect of truncation of the attenuation function and maximum magnitude.

5.3 COMPOSITE-MAGNITUDE SEISMIC HAZARD ANALYSIS

This seismic hazard analysis represents the current state of knowledge about zonation, maximum magnitudes, and ground-motion characteristics in the eastern United States, as exemplified in the recent EPRI (Electric Power Research Institute) and LLNL (Lawrence Livermore National Laboratories) seismic-hazard studies (2,3).

The EPRI and LLNL studies used multiple seismological interpretations, developed by independendent experts or teams of experts. Each expert or team specified multiple combinations

of active sources and multiple values of seismicity parameters and maximum magnitude for each source.

Both studies considered multiple attenuation functions. Attenuation functions based on ground-motion models of the type considered in Section 3.2.3 — with considerable energy at high frequencies and roughly the same magnitude scaling as attenuation functions for California — were given considerable weight, especially in the EPRI study.

We replicated the EPRI hazard results for Millstone (2), by using simple representations of the host source zones and typical assumptions about their seismicity parameters and maximum magnitudes. We then performed minor adjustments to the maximum magnitudes and seismicity parameters in order to match the results in the above reference. We used the same three attenuation functions as in the EPRI calculations (2), with minor modifications noted below.

Integration over magnitude was performed starting at magnitude m_b 4.5. Three types of hazard results were generated, as follows.

- Hazard curves for peak ground acceleration. For these calculations, the peak accelerations predicted by the EPRI attenuation functions were reduced by 20% to make them more consistent with the ground-motion model presented in Section 3.2.3. Results are shown in Figure 5-2.

- Hazard curves for spectral velocities at 1, 2.5, 5, 10, and 25 Hz. These results were used to construct a uniform-hazard spectrum, which was used in the generation of artificial ground motions associated with the composite hazard analysis (see Fig. 3-2).

- Hazard curves for the average spectral acceleration between frequencies of 2.5 and 10 Hz. As a first approximation, this quantity is assumed to have the same median attenuation function as the 5-Hz spectral acceleration. Variability about the median is characterized by standard deviation of 0.45. This standard deviation is lower than the value of 0.5 used for peak acceleration and spectral velocities, because the peak-to-valley variability is averaged out (i.e., we assume that the peak-to-valley variability has a standard deviation of 0.2). Results are shown in Figure 5-3.

5.4 MAGNITUDE-DEPENDENT HAZARD ANALYSES

For this analysis, the hazard contributed by the various magnitudes is not added together. Instead, the hazards contributed by earthquakes in the various magnitude ranges are stored separately. We store the hazard in five magnitude ranges, as follows: 4.5–5.0, 5.0–5.5, 5.5–6.0, 6.0–6.5, and 6.5–7.0. The result of this analysis is one set of hazard curves for each magnitude range.

For this analysis, we used the same seismological assumptions as in the composite hazard analysis. Results were produced for peak ground acceleration and for the average spectral acceleration between 2.5 to 10 Hz. These results are presented in Figures 5-4 through 5-13.

5.5 DISCUSSION

Comparing the hazard curves from the SPRA and composite hazard analysis, we observe that they roughly coincide for accelerations lower than 0.4g. At higher accelerations, the 0.15-fractile and median SPRA hazard curves drop sharply — due to the combined effect of truncation and maximum magnitude — whereas the mean SPRA hazard decreases somewhat faster than the mean hazard curve from the composite analysis.

The acceleration associated with the mean hazard curve and with an exceedance probability of 10^{-6} is 30% lower for the SPRA hazard analysis than for the composite analysis. If we consider the spectral shapes associated with each analysis (see Figures 3-1 and 3-2), we observe that the SPRA shape has higher amplification at the frequencies of engineering interest. This higher spectral shape more than offsets the lower hazard.

Observing the hazard curves from the disaggregated (magnitude-dependent) analyses, we note that the lower magnitude ranges (i.e., 4.5 to 5.0 and 5.0 to 5.5) contribute substantially to the hazard at low accelerations. The hazard curves for these magnitude ranges drop sharply and their contribution to the total hazard becomes negligible at higher accelerations.

In contrast, the moderate and high-magnitude ranges contribute little to the hazard at low accelerations. The hazard curves for these magnitude ranges become relatively flat and they dominate the hazard at higher accelerations.

For high values of peak acceleration, the 5.0–5.5, 5.5–6.0, and 6.0–6.5 magnitude ranges have roughly the same median hazard. The mean hazard, on the other hand, is much higher for the 6.0–6.5 magnitude range. Uncertainty is much larger when one considers large earthquakes, their chances of occurring near the site, and their effects.

The disaggregated hazard curves for average spectral acceleration between 2.5 and 10 Hz show more dominance of the higher magnitudes. This occurs because the spectral amplitudes in this frequency range have a stronger dependence on magnitude than peak acceleration. As an illustration of this effect, consider the increase in ground-motion amplitudes (at the same distance) between two earthquakes with magnitudes m_b 5.0 and 6.5: peak ground acceleration increases by a factor of 4.5, whereas 5-Hz spectral acceleration increases by a factor of 6.

5.6 REFERENCES

1. Dames and Moore. *Seismic Hazard and Design Spectra at Millstone Nuclear Power Plant, Unit 3.* Technical Report, Dames and Moore, Inc., 1984. Amendment 2.

2. R. K. McGuire, G. R. Toro, J. P. Jacobson, T. F. O'Hara, and W. J. Silva. *Probabilistic Seismic Hazard Evaluations in the Central and Eastern United States: Resolution of the Charleston Earthquake Issue.* Special Report NP-6395-D, Electric Power Research Institute, April 1989.

3. D. L. Bernreuter, J. B. Savy, R. W. Mensing, and J. C. Chen. *Seismic Hazard Characterization of 69 Plant Sites East of the Rocky Mountains.* Technical Report NUREG/CR5250, UCID-21517, U. S. Nuclear Regulatory Commission, 1988.

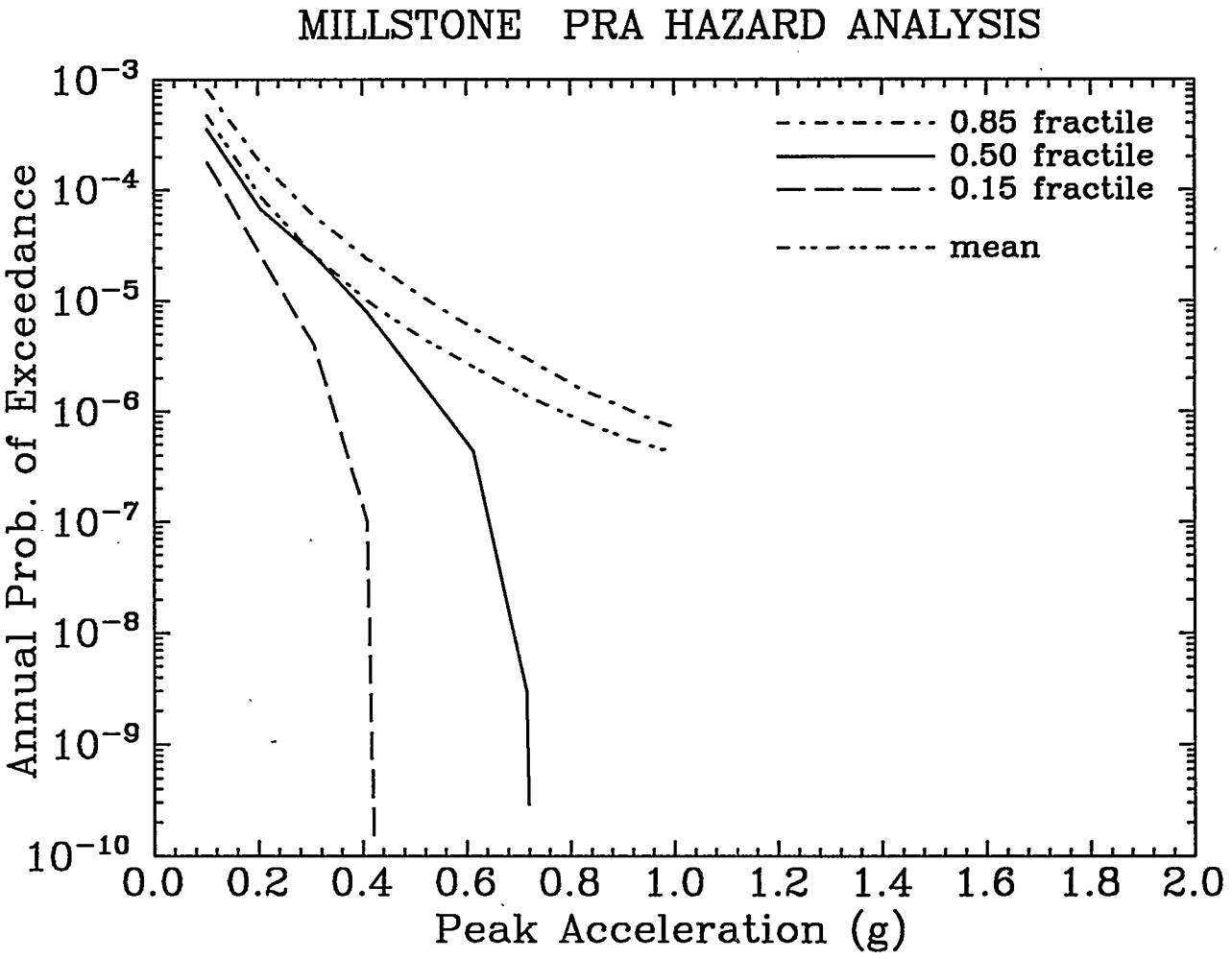

Figure 5-1. Summary hazard curves from the SPRA hazard analysis; peak ground acceleration.

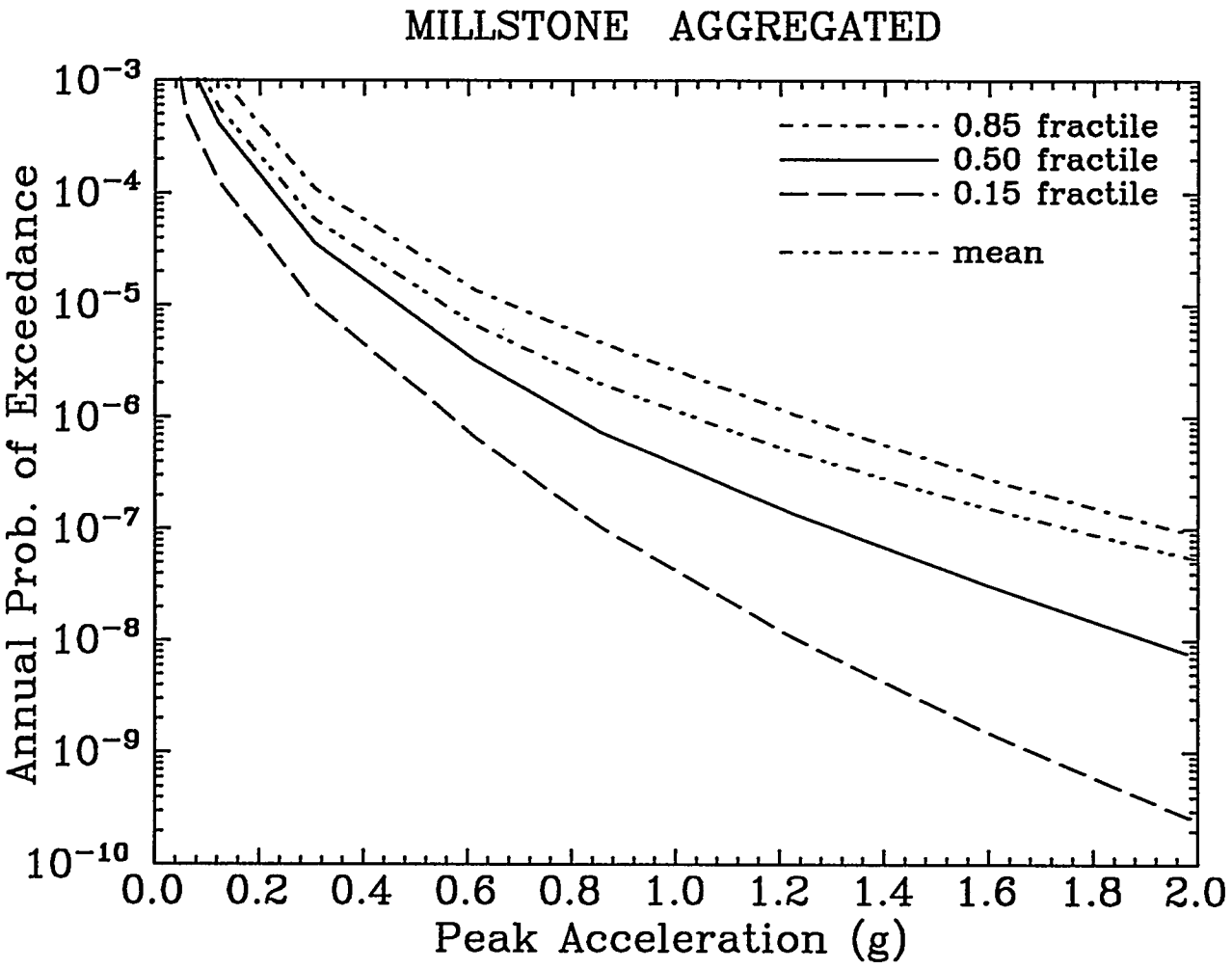

Figure 5-2. Summary hazard curves from the composite hazard analysis; peak ground acceleration.

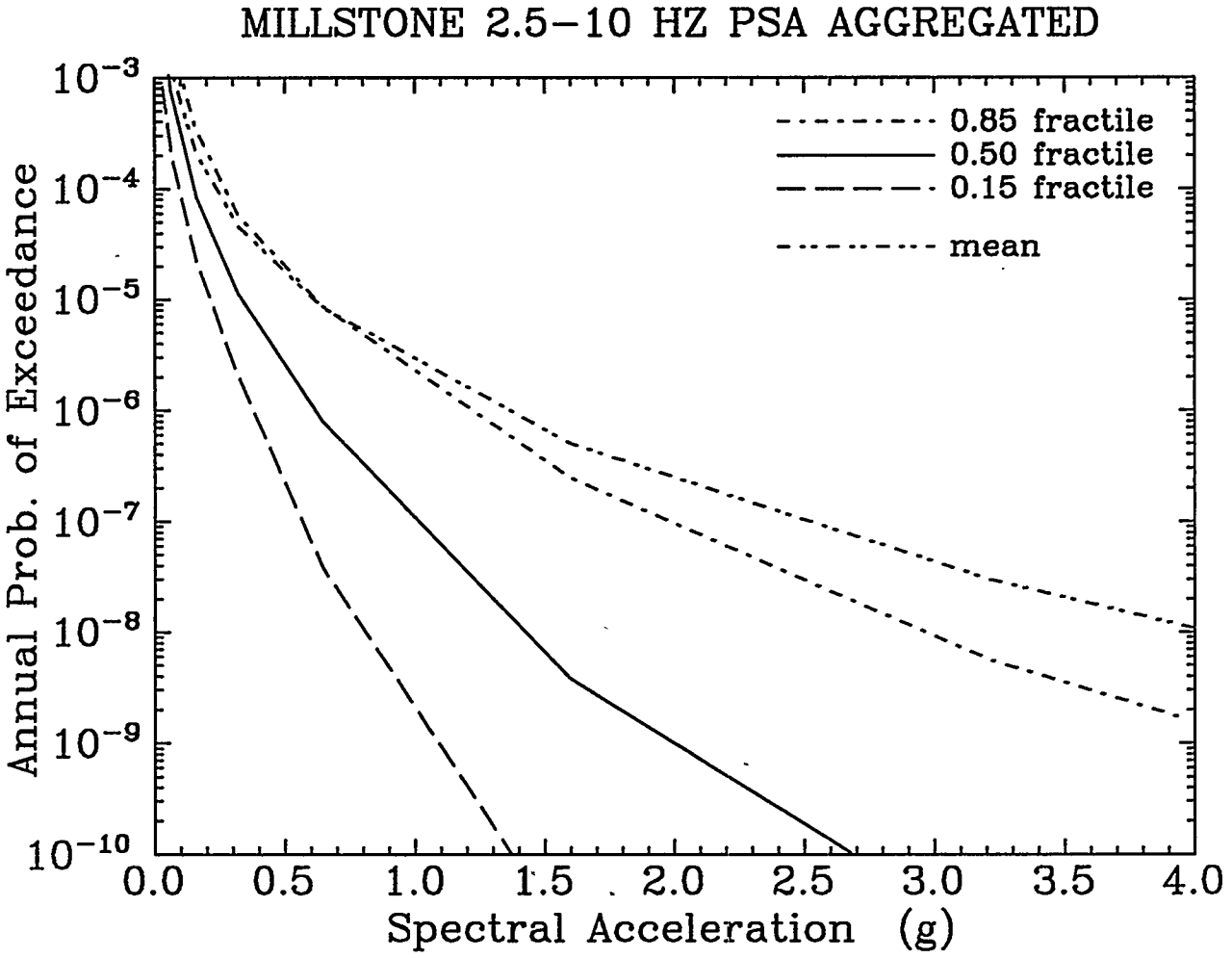

Figure 5-3. Summary hazard curves from the composite hazard analysis; average spectral acceleration between 2.5 and 10 Hz.

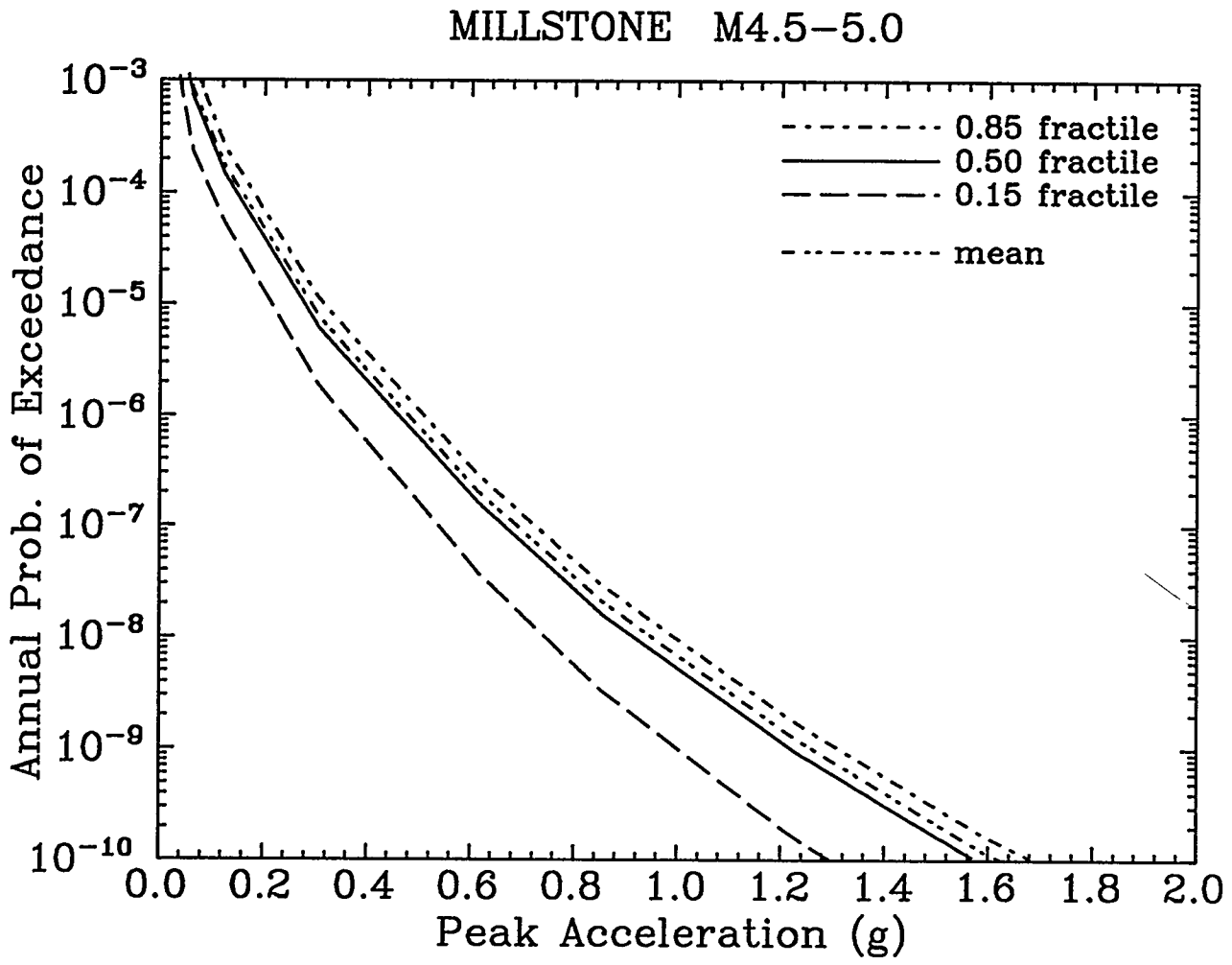

Figure 5-4. Summary hazard curves from the disaggregated hazard analysis (magnitudes 4.5–5.0); peak ground acceleration.

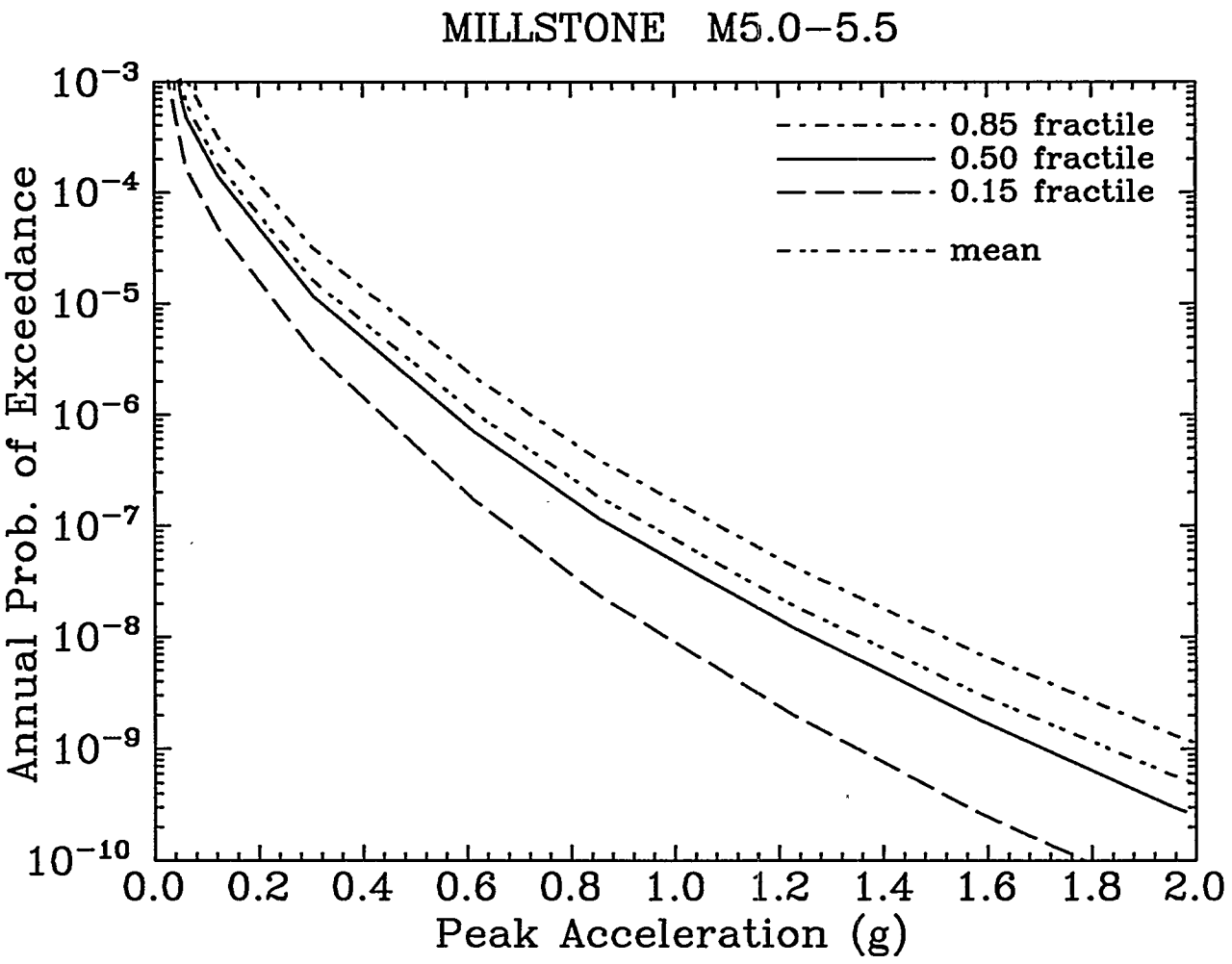

Figure 5-5. Summary hazard curves from the disaggregated hazard analysis (magnitudes 5.0–5.5); peak ground acceleration.

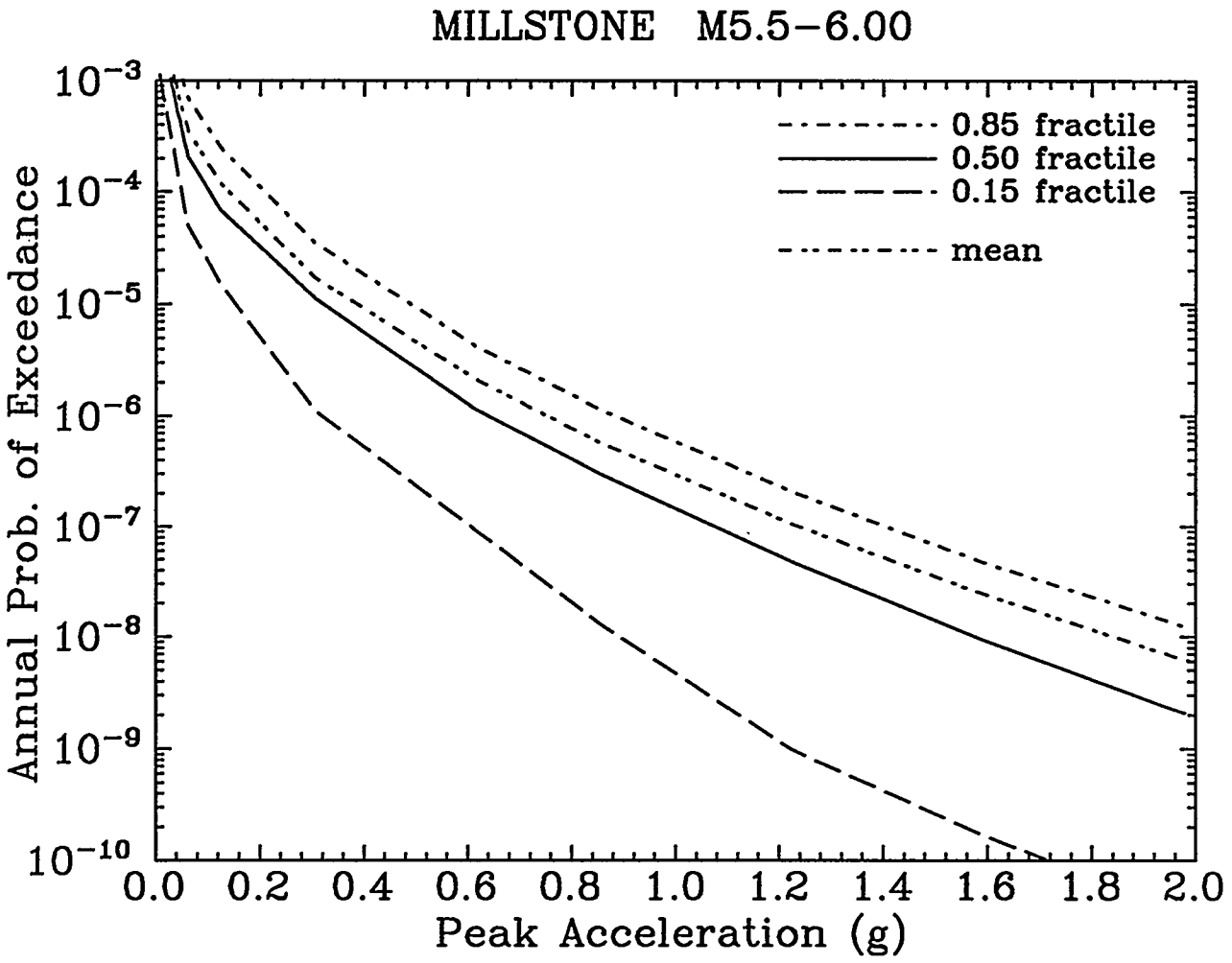

Figure 5-6. Summary hazard curves from the disaggregated hazard analysis (magnitudes 5.5–6.0); peak ground acceleration.

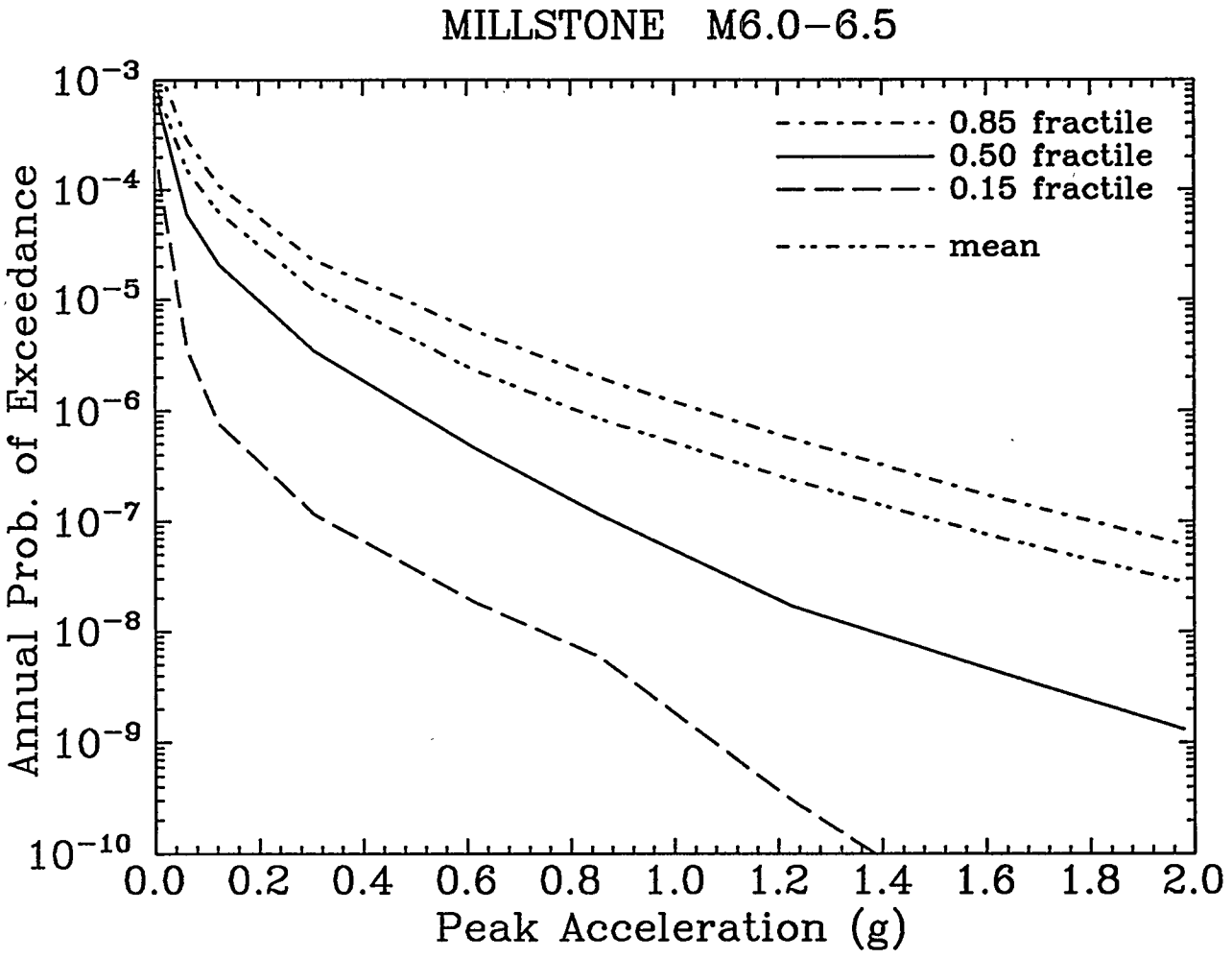

Figure 5-7. Summary hazard curves from the disaggregated hazard analysis (magnitudes 6.0–6.5); peak ground acceleration.

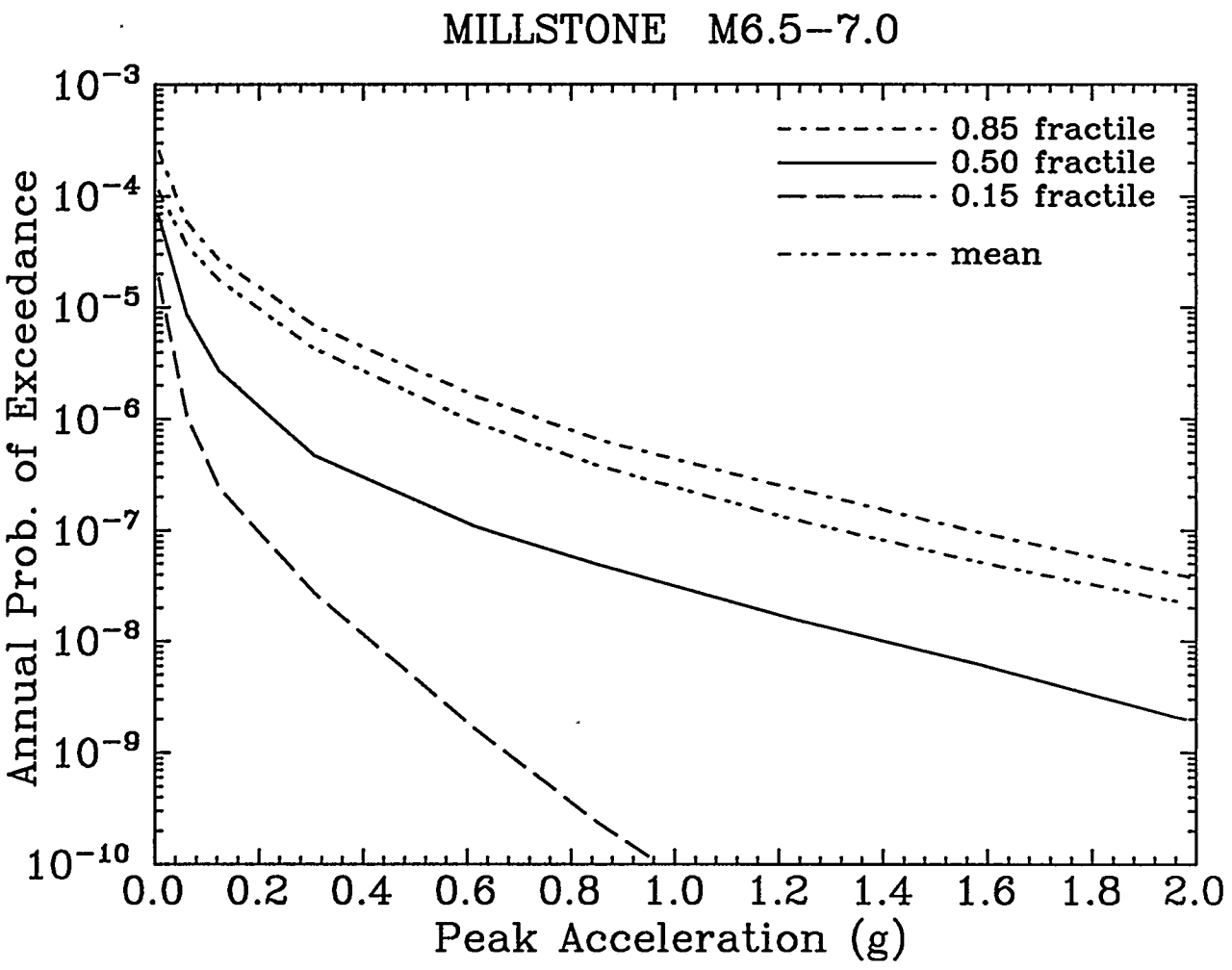

Figure 5-8. Summary hazard curves from the disaggregated hazard analysis (magnitudes 6.5–7.0); peak ground acceleration.

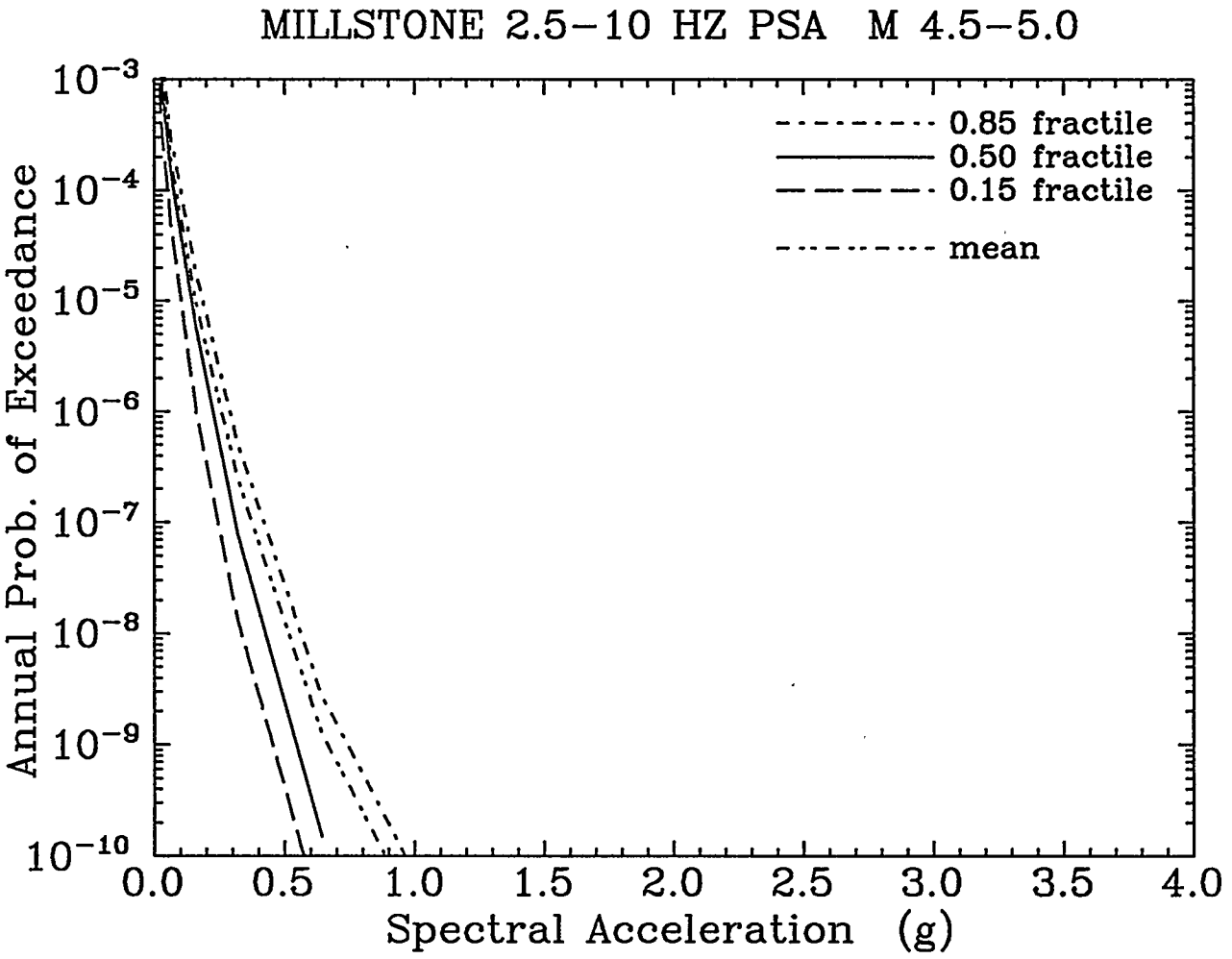

Figure 5-9. Summary hazard curves from the disaggregated hazard analysis (magnitudes 4.5–5.0); average spectral acceleration between 2.5 and 10 Hz.

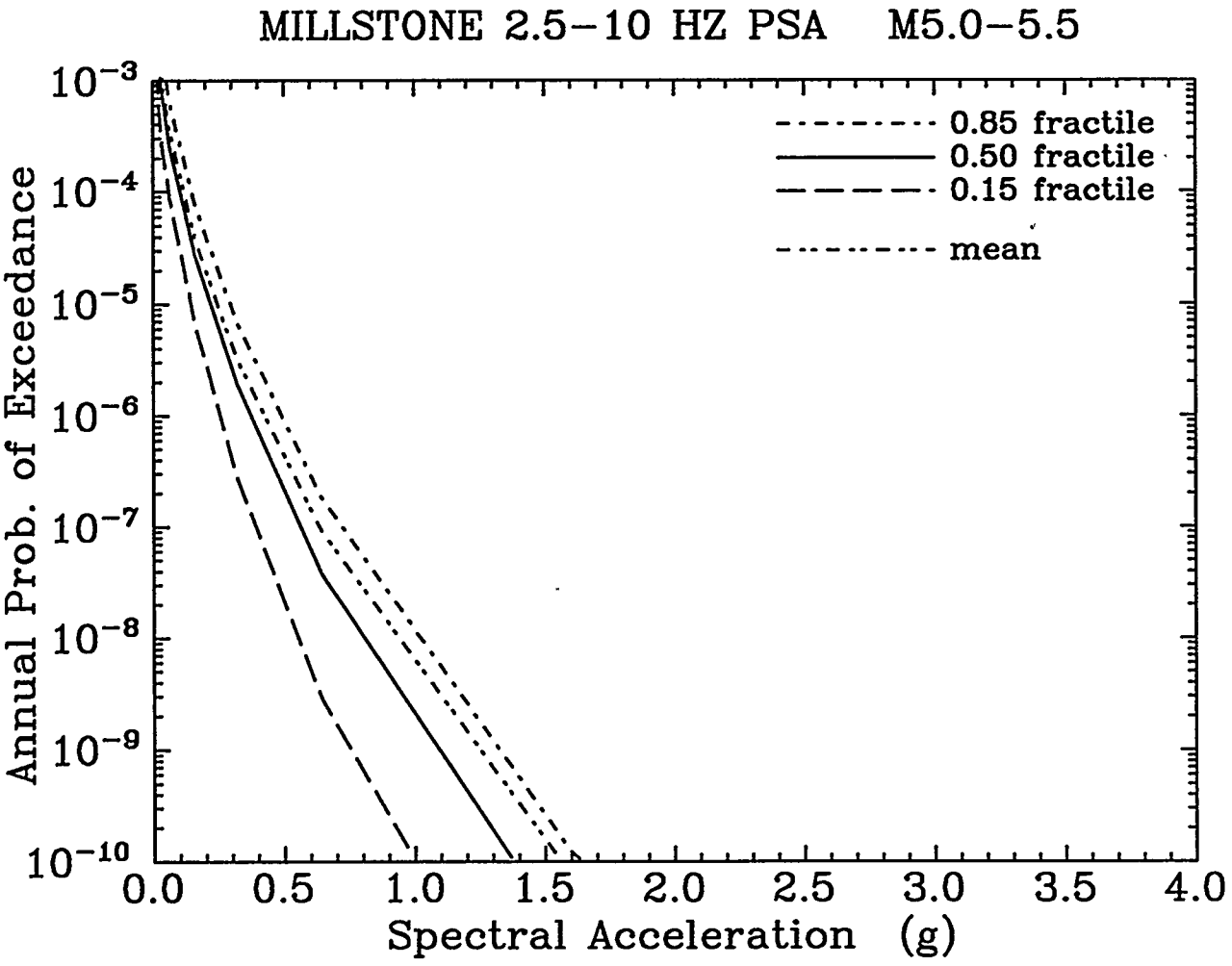

Figure 5-10. Summary hazard curves from the disaggregated hazard analysis (magnitudes 5.0–5.5); average spectral acceleration between 2.5 and 10 Hz.

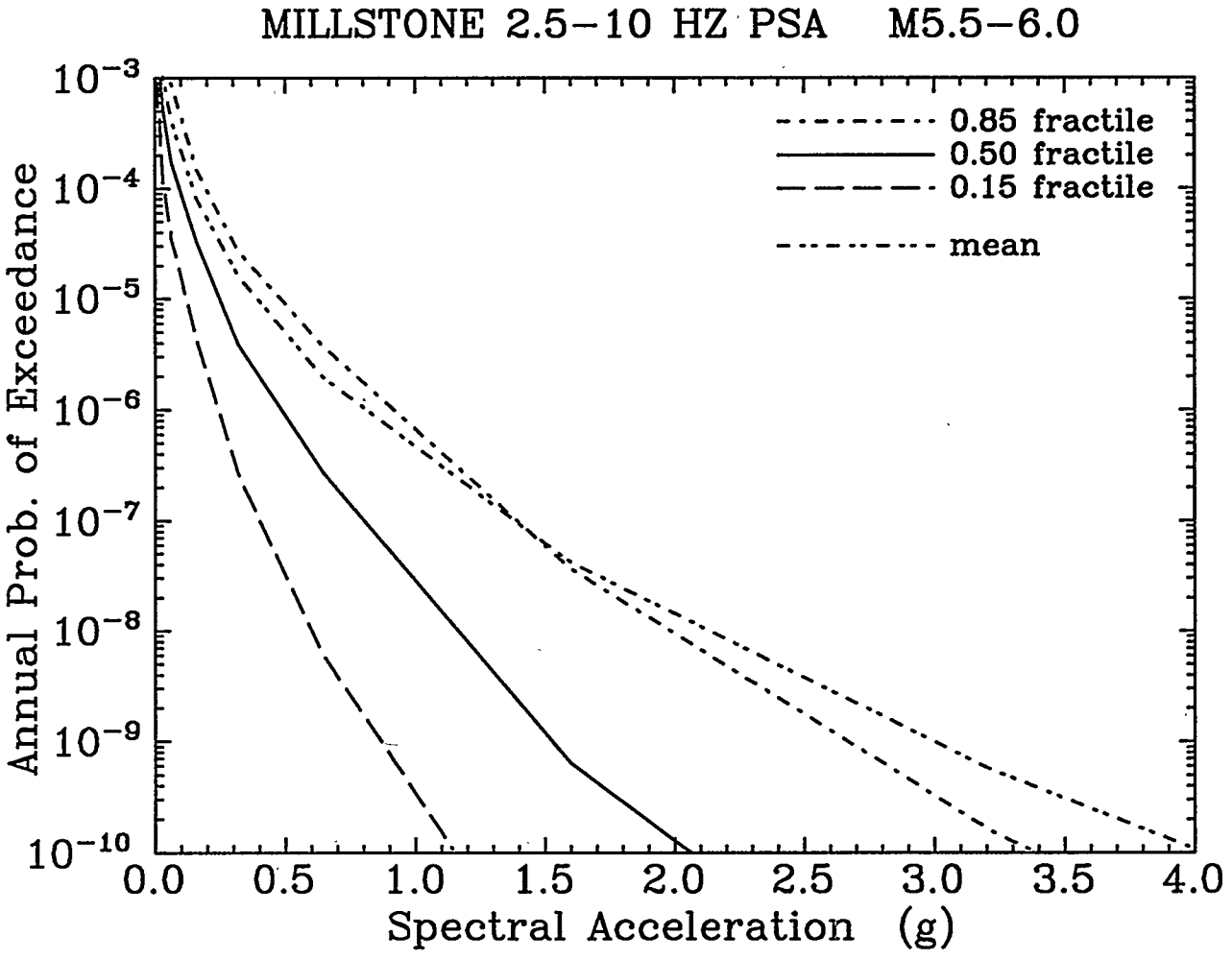

Figure 5-11. Summary hazard curves from the disaggregated hazard analysis (magnitudes 5.5–6.0); average spectral acceleration between 2.5 and 10 Hz.

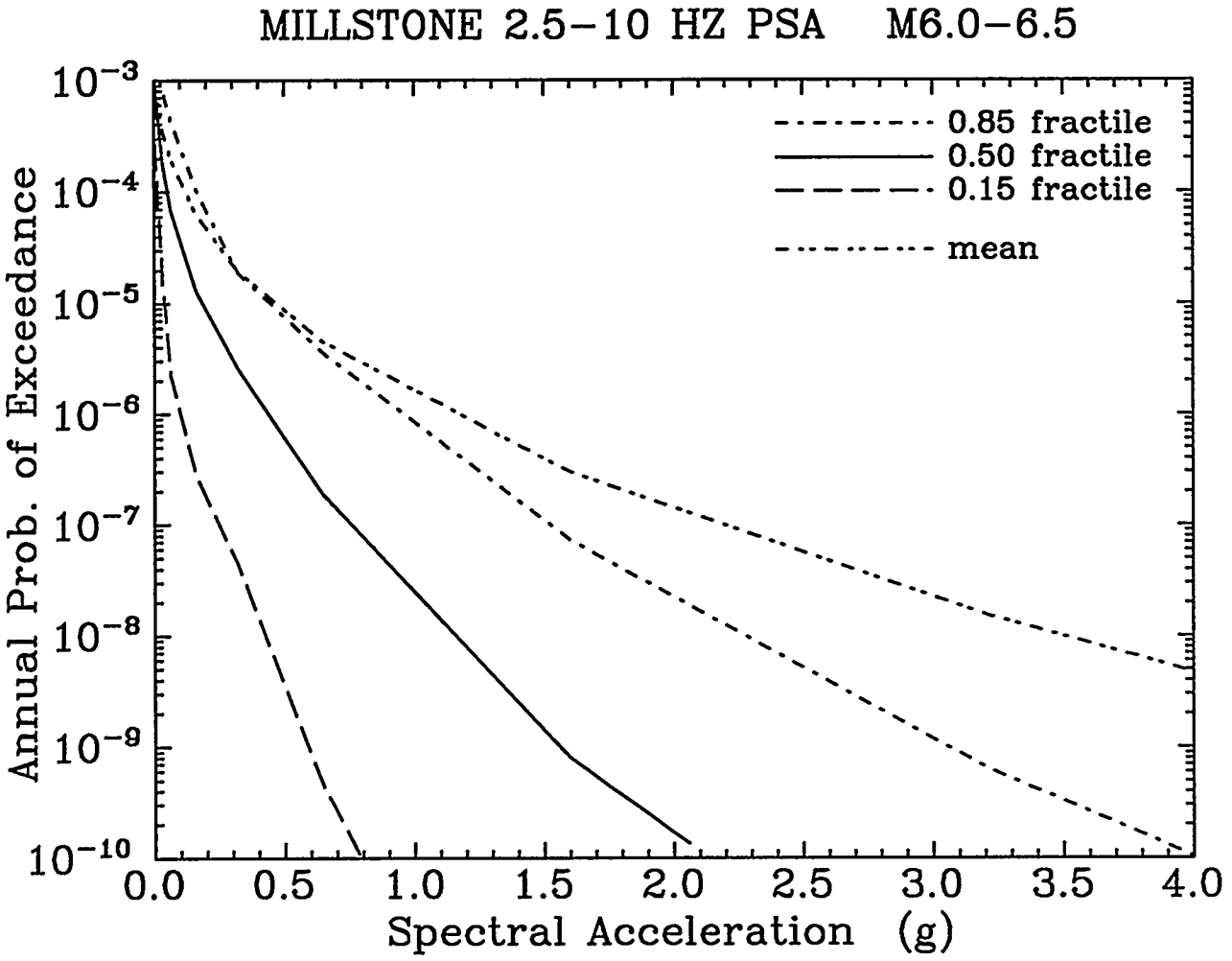

Figure 5-12. Summary hazard curves from the disaggregated hazard analysis (magnitudes 6.0–6.5); average spectral acceleration between 2.5 and 10 Hz.

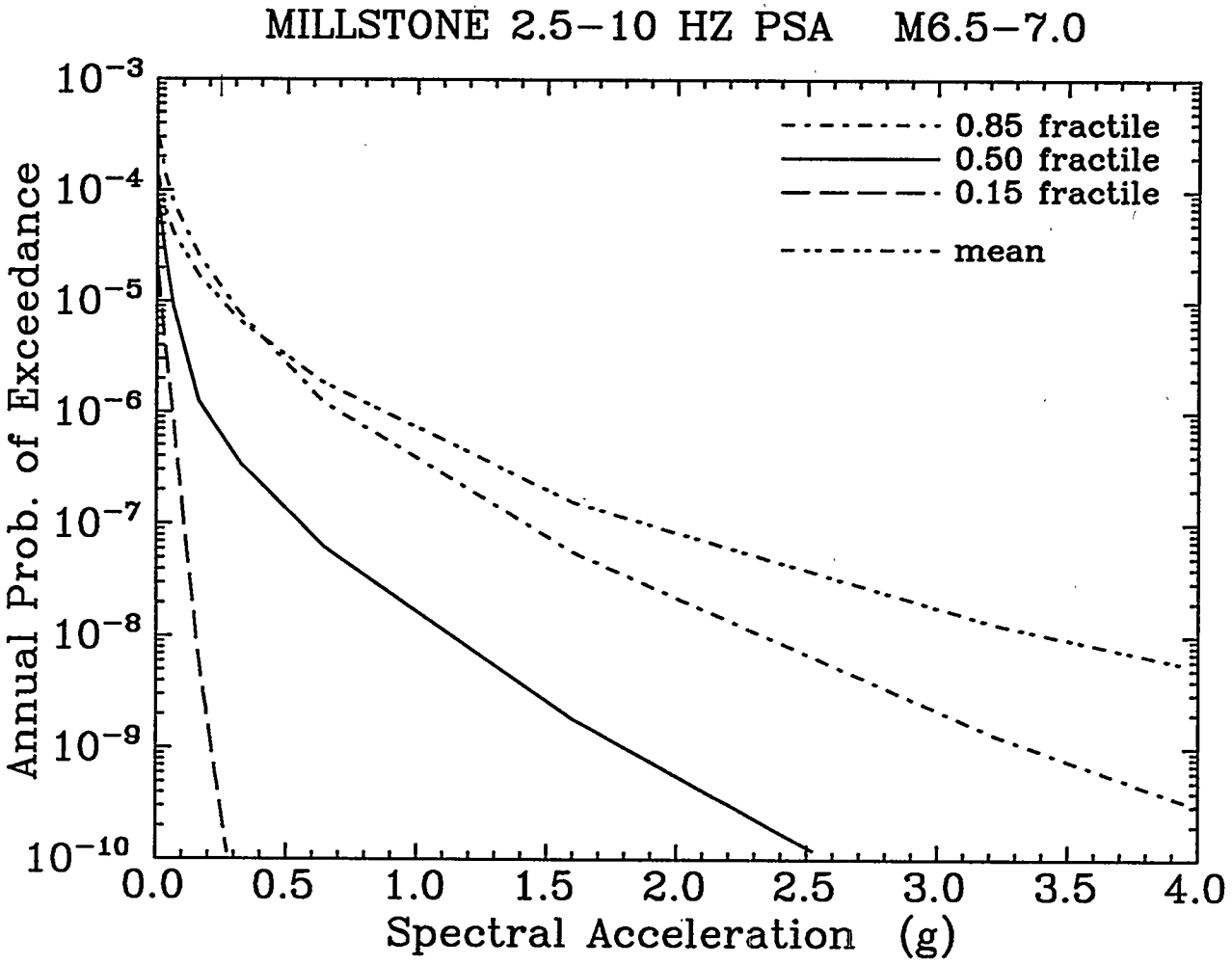

Figure 5-13. Summary hazard curves from the disaggregated hazard analysis (magnitudes 6.5–7.0); average spectral acceleration between 2.5 and 10 Hz.

Section 6
PLANT-DAMAGE RISK ANALYSIS

This section presents and discusses the impact on seismic annual failure rate (risk) estimates of magnitude disaggregation and ground motion characterization procedures in seismic hazard and fragility assessments. Comparisons of both mean risk and risk uncertainty are made for the following cases:

1. Base-case SPRA results versus site-specific results when PGA is used as the basis for ground motion characterization.
2. Magnitude-composite results versus magnitude-dependent results when PGA is used as parameter for seismic fragility and hazard curves.
3. Magnitude-composite results versus magnitude-dependent results when spectral acceleration measures are used as parameters for seismic fragility and hazard curves.

For each case, the standard, well-documented procedure (1) for integration of hazard and fragility curves in deriving individual failure rates was employed. For each risk assessment, several (on the order of 200) individual hazard/fragility integrations were performed to obtain a probability distribution of risk, considering the weights of all hazard/fragility combinations.

Although the evaluations presented here are based on detailed numerical integrations, insight into risk and risk-uncertainty results can be obtained by consideration of the following simple analytical formulas [which are strictly valid only for lognormal fragilities, for hazard curves with a constant (local) slope in log-log space, and for a lognormal distribution of uncertainty in seismic hazard]:

$$\overline{R} = \overline{H}(\breve{A}) \exp\left[0.5 K_H^2 (\beta_R^2 + \beta_U^2)\right] \qquad (6-1)$$

and

$$\mathrm{Var}[R] = \overline{R}^2 \left[\exp\left(\beta_H^2 + (K_H \beta_U)^2\right) - 1\right] \qquad (6-2)$$

where $\overline{R}$ denotes mean risk, $\overline{H}(\breve{A})$ is the mean hazard at the median acceleration capacity, Var[R] denotes variance of risk, K_H is the local slope[1] of the hazard curve, β_H is the logarithmic standard deviation (uncertainty parameter) of hazard, and β_R, β_U are randomness, uncertainty variabilities in fragility (as defined in Section 2). These equations are presented here for the reader's information; we shall make use of these formulas in subsequent discussion to facilitate understanding of the effects and importance of key hazard and fragility parameters pertaining to risk and risk uncertainty.

6.1 MAGNITUDE COMPOSITE RESULTS: COMPARISON OF BASE AND SITE-SPECIFIC CASES

Results of risk and risk-uncertainty quantification for the magnitude-composite SPRA and site-specific analyses are presented in Table 6-1. These results indicate a factor of conservatism of nearly 4.5 in the PRA Base Case analysis. This conservatism is significant and is due mostly to the higher mean base-case PGA hazard at the median base-case capacity of 1.10g than the site-specific PGA hazard at the site-specific-based (composite) median capacity of 2.20g. This difference is a direct consequence of using a conservative spectral shape (based on western U.S. motions) anchored to peak ground acceleration.

Table 6-1 indicates a larger standard deviation, but a somewhat lower coefficient of variation, in risk for the PRA base case as opposed to the site-specific case. The uncertainties in the latter analysis, however, are considered to be more realistic and representative of modern understanding of ground motion hazard.

We conclude from this comparison that spectra representative of western U.S. (albeit small-magnitude) motions are not appropriate for general application to risk analyses of sites in the eastern U.S., and such application has likely led to significant over-estimation of seismic risk in past SPRAs.

6.2 MAGNITUDE-DEPENDENT RESULTS FOR PGA-BASED CHARACTERIZATION

Table 6-2 compares risk results for the magnitude-dependent and magnitude-composite site-specific results when PGA is used as the basis for anchoring the fragility review spectra. The small difference in mean risk (on the order of 20%) and the negligible difference in coefficient

[1]The evaluations of $\overline{R}$ and Var[R] are sensitive to the particular value chosen for K_H. Typically, the mean failure rate will be dominated by the hazard for accelerations between the HCLPF and median capacities. In general, therefore, K_H should be taken as the average slope of the mean seismic hazard curve (on log-log scale) between the HCLPF acceleration and $\breve{A}$.

Table 6-1

Comparison of Base-Case and Site-Specific-Case Risk Results.

Analysis	Mean Failure Rate (per year)	Coefficient of Variation of Failure Rate	Standard Deviation of Failure Rate
SPRA Base Case	1.73×10^{-6}	3.29	5.69×10^{-6}
Site Specific (Composite) Case	3.86×10^{-7}	4.04	1.56×10^{-6}

of variation between the magnitude-composite and magnitude-dependent (overall) results are considered to be unimportant and within the limits of accuracy of the numerical methods used in risk quantification.

These results suggest that, although the seismic fragilities based on PGA are very much influenced by magnitude, variations in seismic hazard with magnitude produce both a compensating effect and a tendency for a particular magnitude range to dominate the (hazard and) risk results. This observation implies that a single, well-chosen aggregate spectrum, representative of site conditions and hazard dominance, is appropriate, valid, and generally sufficient for characterizing ground motions for seismic fragility assessment when PGA is used as ground motion parameter. Examination of Table 6-2, nevertheless, reveals important information about which magnitude ranges are the dominant contributors to seismic risk. This information would be lost if a magnitude-disaggregated analysis were not performed. In general, the value of seismic risk results is not just in having an estimate of the "bottom-line" risk number, but also (and perhaps more importantly) in the "anatomy" of the risk. Hence, we encourage the practice of magnitude disaggregation as a means to obtain useful insights into seismic risk.

6.3 MAGNTIUDE-DEPENDENT RESULTS FOR SPECTRAL CHARACTERIZATION

Table 6-3 compares risk results for the magnitude-dependent and magnitude-composite site-specific results when elastic spectral acceleration (averaged over frequencies ranging from 2.5

Table 6-2

Comparison of Magnitude Dependent and Composite Results for PGA-Based Characterization.

Analysis	Mean Failure Rate	Coefficient of Variation of Failure Rate
All Magnitudes	3.86×10^{-7}	4.04
$m_b = 6.75$	8.55×10^{-8}	4.42
$m_b = 6.25$	2.14×10^{-7}	3.87
$m_b = 5.75$	1.09×10^{-7}	4.23
$m_b = 5.25$	3.85×10^{-8}	4.58
$m_b = 4.75$	1.25×10^{-8}	4.81
Overall	4.60×10^{-7}	4.14

to 10 Hz) is used as the basis for anchoring the fragility review spectra. Again, the small difference in mean risk (on the order of 20%) and the relatively small difference in coefficient of variation between the magnitude-composite and magnitude-dependent (overall) results are considered to be unimportant.

Section 4 indicates that, *conditional on elastic spectral acceleration (averaged over the appropriate frequency range) or inelastic spectral acceleration (taken at the proper frequency)*, structural capacity shows no noticeable sensitivity to magnitude and earthquake duration. Consequently, the seismic fragilities based on spectral acceleration show no important magnitude dependence. The similarities observed in the magnitude-composite and magnitude-dependent results of Table 6-3 are, therefore, not surprising.

This observation further confirms that a single, well-chosen aggregate spectrum, representative of site conditions and hazard dominance, is generally accurate in characterizing ground motions for seismic fragility assessment. Again, however, information on the magnitude range that dominates contribution to risk, and how this magnitude range differs for PGA-anchored versus $\overline{S_a}$-anchored fragilities, is lost when conducting magnitude-composite analyses. The magnitude-disaggregated analysis, therefore, conveys additional information that seismic risk experts may find valuable in developing improved assumptions and in formulating better mitigative seismic safety solutions.

6.4 COMPARISON OF PGA-BASED AND SPECTRAL-ACCELERATION-BASED RISK RESULTS

For final comparison, we consider the difference in PGA-based (Table 6-2) and spectral-acceleration-based (Table 6-3) risk results. This comparison indicates a factor of conservatism of about 1.8–2.8 in the overall mean risk results obtained for PGA. Although clearly within the noise of risk uncertainty, this noticeable factor of conservatism is considered to be significant, and the explanation for its cause is important. This source of conservatism in risk estimation is associated with the fact (noted in Section 4) that fragilities based on spectral acceleration have dramatically lower values of β_R and β_U than fragilities anchored to PGA. To explain this effect in analytical terms (as opposed to simply comparing numerical results), we make use of Eq. 6-1. This equation shows that mean risk increases with increase in β_R or β_U, and with increase in slope K_H. We compare risk results obtained from Eq. 6-1 using values based on PGA versus values based on average spectral acceleration. For the present comparison, as obtained from Tables 4-9 and 4-11, β_R increases from about 0.18 to 0.25 (between spectral-acceleration-based and PGA-based fragilities) and β_U correspondingly increases from about 0.44 to 0.52. The slope, K_H, of the mean seismic hazard curve

Table 6-3

Comparison of Risks for Magnitude Dependent and Composite Spectra Anchored to Average Spectral-Acceleration (2.5–10 Hz).

Analysis	Mean Failure Rate	Coefficient of Variation of Failure Rate
All Magnitudes	2.09×10^{-7}	5.77
$m_b = 6.75$	3.41×10^{-8}	7.13
$m_b = 6.25$	1.15×10^{-7}	6.01
$m_b = 5.75$	1.70×10^{-8}	6.69
$m_b = 5.25$	2.08×10^{-10}	6.67
$m_b = 4.75$	3.47×10^{-12}	7.46
Overall	1.67×10^{-7}	6.31

between the HCLPF and $\check{A}$ accelerations is 4.05 for PGA and 3.58 for $\overline{S_a}$. [2] Substituting these values into Eq. 6-1, a factor of conservatism of about 3.6 is roughly implied. We note however, that the value of $\overline{H}(\check{\overline{S_a}})$ [i.e., 6.02×10^{-8}] is about 1.8 times the value of $\overline{H}(\check{A})$ [i.e., 3.29×10^{-8}].[3] Accounting for this difference, an overall factor of conservatism of 2.0 is estimated; this factor is consistent with the observation above based on numerical results.

Using Eq. 6-1, substituting the appropriate values for $\overline{H}$, K_H, β_R and β_U, we obtain results of $\overline{R}_{\text{PGA}} = 5.0 \times 10^{-7}$ and $\overline{R}_{S_a} = 2.6 \times 10^{-7}$. These values are within about 10% to 50% of the (more-computationally involved) numerical results of Tables 6-2 and 6-3.

As a further observation, comparison of the magnitude-dependent (disaggregated) results indicates that there is a sharper magnitude dominance for spectral-acceleration-based versus PGA-based results of risk and its uncertainty. This sharper magnitude dominance is largely related to the functional form of magnitude-dependence used in the attenuation law that dominates mean risk for average spectral acceleration.

It is also of interest to note from Table 6-3 that the uncertainty (coefficient of variation) in risk is significantly larger when spectral acceleration, as opposed to PGA, is used as the hazard and fragility parameter. This observation is tied to the fact that hazard predictions for PGA are somewhat more certain than for spectral acceleration (resulting in a lower value of β_H for predictions of PGA). Still, the standard deviation in risk for the case of spectral acceleration is lower than that for the PGA case. In any event, the reduction in mean risk achieved through use of spectral acceleration is considered to be sufficient motivation

[2] Given the same uncertainties in hazard for PGA and $\overline{S_a}$, one would expect the value of K_H to be slightly greater for $\overline{S_a}$ hazard than for PGA hazard. (This expectation is due to the fact that, as mentioned in Section 5.3, a slightly lower variability, σ, was used in the hazard assessment of $\overline{S_a}$ than that of PGA.) The hazard uncertainty, β_H, for $\overline{S_a}$, however, is significantly larger than that for PGA (compare, for instance, Figures 5-2 and 5-3). This increased uncertainty produces a corresponding decrease in K_H for $\overline{S_A}$ mean hazard (especially at large accelerations). The final effect is the somewhat lower value of K_H in mean hazard noted here for $\overline{S_a}$ compared to PGA. [If we consider the slopes of the median hazard curves (compare Figures 5-2 and 5-3), which are untainted by uncertainty, then we indeed find that the slope K_H for $\overline{S_a}$ is slightly higher than that for PGA, as expected].

[3] Values of $\overline{H}$ and K_H are very much interrelated, and both are effected by hazard uncertainty. The difference seen here in values of $\overline{H}$ is again due to the fact that the uncertainty in $\overline{S_a}$ hazard is notably larger than the uncertainty in PGA hazard. [Note from Figures 5-2 and 5-3, however, that the median hazards $\check{H}(\check{\overline{S_a}})$ and $\check{H}(\check{A})$ are quite similar, as expected for consistent fragility assessments]. This larger uncertainty causes the mean hazard curve for $\overline{S_a}$ to flatten (most noticeably at large accelerations) significantly more than the mean PGA hazard curve. The end effect is the larger value of $\overline{H}(\check{\overline{S_a}})$, seen here, as compared to $\overline{H}(\check{A})$.

for basing fragility and hazard assessments on spectral characterizations (whether elastic or inelastic) of ground motion.

The reader is encouraged to use Eq. 6-1 and the hazard curves of Figures 5-2 to 5-13 to better understand the magnitude-dependent results presented in Tables 6-2 and 6-3. The observations and conclusions in this section apply to estimates of hazard and risk at very high ground motion levels. For low-to-intermediate ground motion levels, the slope of the mean hazard curve and uncertainty in hazard are dominated by different factors; thus risk results for lower-capacity components (or series-type systems of components) may show different trends in magnitude dependence, and perhaps different effects of ground-motion characterization. Recommendations given in Section 7 outline aspects of Phase II research that address the significance of these issues.

6.5 REFERENCES

1. American Nuclear Society and Institute of Electrical and Electronic Engineers. *PRA Procedures Guide.* Technical Report NUREG/CR–2300, U.S. Nuclear Regulatory Commission, January 1983.

Section 7
SUMMARY, CONCLUSIONS AND RECOMMENDATIONS

This study lends greater insight into the problem of potential seismically-induced effects to nuclear plant structures, particularly for sites in the eastern U.S. Several implicit assumptions regarding the calculation of plant risk, and the interface between seismic hazards and seismic fragilities, have been examined in depth to determine their effects on accuracy in representing mean risk and risk uncertainty.

As a result of the Phase 1 scope of work for this study, the following conclusions and recommendations are summarized:

- The past SPRA practice of using a spectral shape derived from western U.S. motions to evaluate seismic fragility curves for eastern U.S. nuclear power plants is generally acknowledged to be substantially conservative, as this study confirms. Specifically, eastern U.S. ground motions are known to produce high amplitudes at high frequencies, by comparison with West Coast earthquakes. Stated another way, for a given spectral acceleration at 5 Hz, an eastern U.S. earthquake will have a higher peak acceleration than an earthquake recorded in California. Proper representation of the spectral characteristics of earthquakes in the eastern U.S. is fundamental to an accurate analysis of seismic effects on nuclear plants. To eliminate bias in the decision process, therefore, motions better representative of the particular eastern U.S. site should be used.

- Accurate application of the standard fragility approach, based on median safety factors, requires the use of substantial engineering judgment. In past SPRAs, such judgment (by chance and by design) has sometimes introduced a source of conservatism in modeling of fragilities. Such judgment may also sometimes lead to unconservative results. Because structural failure is a complicated problem that involves determination of nonlinear response, and because risk estimates should be as free of bias as possible for proper decisionmaking, it is recommended that nonlinear time-history methods be implemented for fragility analysis of important structures and equipment.

- The common procedure in seismic PRAs of characterizing (and anchoring) the earthquake ground motion with a single variable (for instance, without explicit consideration of earthquake duration) has been confirmed in this study to be generally valid and accurate, but should be based on an averaged measure of (elastic or inelastic) spectral acceleration over the frequency range of interest. This procedure has been used in a recent PRA conducted for a western U.S. plant, and this spectral-based characterization of ground motion should be applied in modern EUS applications as well.

- The common SPRA practice of using a composite spectral shape to describe ground motions from different magnitudes is generally valid for obtaining accurate seismic risk results. Risk analysis and decision experts generally agree, however, that one should not rely solely on risk numbers. Rather, an important value of PRA is to demonstrate what dominates contribution to risk. By taking a composite-magnitude spectral shape, one loses the ability to demonstrate what magnitude range dominates seismic risk and its uncertainty. It is therefore recommended that magnitude-disaggregation be implemented in routine PRA practice to enhance understanding and communication of seismic risk results. Phase 2 research will produce magnitude-disaggregated results for a variety of nuclear plant systems, and will develop efficient techniques for performing a magnitude-dependent seismic hazard analysis.

- As has been described in this report, sophisticated models have been used here to account for the nonlinear, strength- and stiffness-degrading behavior of structures shaken by earthquakes. For these models, it is apparent that, *for realistic earthquake motions and for limit states associated with the onset of significant structural damage (i.e., short of collapse)*, the elastic ground-motion spectrum (for spectral ordinates averaged over the proper frequency range) or the inelastic spectrum (at the appropriate frequency) carries sufficient information regarding damageability that the magnitude of the earthquake and the duration of shaking, *conditional on the spectral amplitudes*, are of secondary importance. The conclusions from this study confirm analytical results obtained elsewhere, but (strictly speaking) apply for a specific type of (multiple-degree-of-freedom) structure, shaken by ground motions with at least 1 second duration. Conclusions may be different for more flexible structures with periods of one second or longer.

- Given the important nature of these results, and the fact that many engineers may be unfamiliar with their justification, it will be important to produce simple summaries and comparisons to illustrate why they hold. The conclusions reached here

apply to realistic earthquake motions and failure limits that do not imply structural collapse. They may not apply to laboratory studies that (typically) apply quasi-static (or pseudo-dynamic) loads to structures with a simple sinusoidal motion, although results of this type of testing have played a significant role in the development of engineering intuition. Communication of the insights derived from this study would assist engineers to improve modeling and testing procedures targeted at predicting a variety of thresholds of structural damage for realistic motions.

- This study aims at developing improved methods that reduce bias and uncertainty in seismic risk assessment. Although this study does not specifically address decision-making, the authors recognize that conservatism and uncertainty in risk estimates are significant elements to be considered in decision context. In using risk results as a basis for decisionmaking, there may be a tendency to either ignore uncertainties or use uncertainties improperly to mask possible effective safety solutions. Clearly, the use of mean risk alone as a decision criterion may lead one to exclude several potentially effective decision alternatives that derive from a variety of interpretations. Ignoring important aspects of risk uncertainty in this manner encourages vulnerable and unstable decisionmaking; that is, decisions based on the mean are driven mostly by a few interpretations that lie at the upper tail of all possible interpretations. Because these few interpretations are extreme, they actually are candidate outliers; decisions based solely on such candidate outliers are tenuous. In other words, decisions based on the mean alone put heavy confidence in extreme (whether legitimate or questionable) viewpoints, which is exactly what, intuitively, should be avoiding in a rational decision process. For these reasons, decisionmaking based on the mean alone may actually be a very poor decision strategy. We recommend exploration of the feasibility of developing (and assessing the impact of) fundamental, rational decision approaches based on consideration of all categories of interpretation that encompass risk uncertainty. At the same time, research that reduces uncertainty in seismic hazard and fragility estimates should continue, in order for the decision process to improve and become well focused.

Appendix A

DETAILS OF THE GROUND MOTION SIMULATION PROCEDURE

A.1 GENERATION OF THE RESPONSE SPECTRUM RESIDUALS

As stated in Section 3, the assumptions that the response-spectrum residuals $\varepsilon(f)$ have the correlation structure of Equation 3-7 [which depends only on $\ln(f_1) - \ln(f_2)$] and a standard deviation that does not depend on frequency, imply that $\varepsilon(f)$ may be treated as a stationary random process with parameter $\theta = \ln(f)$. The autocovariance function of $\varepsilon(\theta)$ is triangular and given by the expression

$$\mathrm{Cov}[\varepsilon(\theta_1), \varepsilon(\theta_2)] \approx \begin{cases} \sigma_\varepsilon^2 \left(1 - \frac{1}{\tau_0}|\theta_1 - \theta_2|\right); & |\theta_1 - \theta_2| \le \tau_0 \\ 0; & |\theta_1 - \theta_2| > \tau_0 \end{cases} \qquad (A-1)$$

with $\tau_0 = 3$.

To generate realizations of $\varepsilon(\theta)$ in the Fourier domain,[1] we need the power spectral-density function of $\varepsilon(t)$, which is

$$\begin{aligned} S_\varepsilon(\lambda) &= \frac{1}{2\pi}\int_{-\infty}^{\infty} e^{-i\lambda\tau}\mathrm{Cov}\left[\varepsilon(\theta)\varepsilon(\theta+\tau)\right] d\tau \\ &= \frac{\sigma_\varepsilon^2}{\tau_0 \lambda^2 \pi}(1 - \cos\lambda\tau_0) \end{aligned}$$

Samples of $\varepsilon(t)$ are generated in the Fourier domain as

$$\tilde{\varepsilon}(\lambda_j) = \sqrt{S_\varepsilon(\lambda_j)\Delta\lambda}\ \ e^{i\phi_j}; \quad j = 1, (n/2+1) \qquad (A-2)$$

where $\lambda_j = (j-1)\Delta\lambda$ and ϕ_j is a random phase angle (uniformly distributed between 0 and 2π). Transformation to the θ-domain [i.e., transformation of $\tilde{\varepsilon}(\lambda)$ into $\varepsilon(\theta)$] is performed using the FFT algorithm.

This approach generates realizations of ε at equally spaced values of $\ln(f)$. We use linear interpolation to obtain the values of ε at equally spaced frequencies, as required for the calculation of the spectral density function of ground acceleration.

[1] We use the term Fourier domain, instead of frequency domain, because f itself is a frequency.

A.2 CALCULATION OF POWER SPECTRAL DENSITY FUNCTION OF GROUND ACCELERATION

Generation of the artificial ground motions is performed in the frequency domain and requires knowledge of the power spectral density function (PSDF) of ground acceleration. In our application, as is often the case, the ground motions are specified by their response spectrum.

The procedure presented here uses simple concepts of stationary and transient random vibrations. We start with the response spectrum $PSV(f) \cdot \varepsilon(f)$ [2] and the duration T, and we want to obtain the spectral-density function $S_a(\omega)$, where $\omega = 2\pi f$. Using random-vibration theory [(1), for example], we may write the spectral velocity as the product of three terms, as follows:

$$PSV(f) \cdot \varepsilon(f) \approx u_{\text{rms}}(f) \cdot N_f(f,T) \cdot P_f(f,T) \qquad (A-3)$$

where

$u_{\text{rms}}(f)$ is the stationary root-mean-square displacement response (multiplied by $2\pi f$) of an oscillator of frequency f to ground acceleration with spectral-density function $S_a(\omega)$.

$N_f(f,T)$ is a nonstationarity factor that corrects the above RMS for the effect of finite duration of the ground motion. Following reference (1), this factor is approximated as

$$N_f(f,T) = \sqrt{1 - \exp[-2\xi(2\pi f)T]} \qquad (A-4)$$

where ξ is the damping ratio

$P_f(f,T)$ is the peak factor (i.e., peak value divided by RMS). We use an expression for peak factor which corrects for the effect of bandwidth [modified from DerKiureghian (2)]

$$P_f \approx \sqrt{2\ln(N_e)} + \frac{0.577}{\sqrt{2\ln(N_e)}} \qquad (A-5)$$

where N_e is the equivalent number of cycles, i.e.,

$$N_e = \max\left\{2fT(1.63\delta^{0.45} - 0.38), 1.33\right\} \qquad (A-6)$$

and δ is Vanmarcke's (1) bandwidth parameter [$\delta \approx \sqrt{\frac{4\xi}{\pi}}$; for a damping ratio of 5%, $\delta \approx 1/4$ and $(1.63\delta^{0.45} - 0.38) \approx 1/2$].

[2] $\varepsilon(f)$ is a particular realization of the response-spectrum residuals; $PSV(f)$ is the pseudo-velocity response spectrum associated with a certain damping ratio ξ.

Referring again to Equation A-1, we note that N_f and T_f are known, so we may obtain $u_{\text{rms}}(f)$ from $PSV(f) \cdot \varepsilon(f)$. The relationship between u_{rms} and $S_a(\omega)$ is more complicated; we approximate this relationship by the following equation, which is based on (1):

$$u_{\text{rms}}^2(\omega_n) \approx \frac{S_a(\omega_n)}{\omega_n}\left(\frac{\pi}{2\xi} - 2\right) + \frac{2}{\omega_n^2}\int_0^{\omega_n} S_a(\omega)d\omega \qquad (A-7)$$

The first term in the above equation represents the dynamic (or amplified) response; this term is dominant at frequencies where the ground motion contains significant energy. The second term represents static response; this term is dominant at high frequencies.

We can approximate the integral in the above equation as a summation, obtaining

$$u_{\text{rms}}^2(\omega_n) = \frac{S_a(\omega_n)}{\omega_n}\left\{\frac{\pi}{2\xi} - 2\right\} + \frac{2}{\omega_n^2}\sum_{j=1}^{n} S_a(\omega_j)\Delta\omega; \quad \omega_n = n\Delta\omega \qquad (A-8)$$

Note that $S_a(\omega_{n+1})$, $S_a(\omega_{n+2}), \ldots$ do not enter this expression. Thus, we may solve sequentially for $S_a(\omega_1)$, $S_a(\omega_2), \ldots$ by means of expression:

$$S_a(\omega_n) = \frac{\omega_n}{\frac{\pi}{2\xi} - 2 + \frac{2\Delta\omega}{\omega_n}} \max\left\{0, \left[u_{\text{rms}}^2(\omega_n) - \frac{2\Delta\omega}{\omega_n^2}\sum_{j=1}^{n-1} S_a(\omega_j)\Delta\omega\right]\right\} \qquad (A-9)$$

We introduce the max { } operator in the above equation because the term in brackets may not converge to zero, due to mis-specification of the response spectrum or to the many approximations introduced in this derivation. When the term in brackets becomes zero, it means that we have reached the frequency where the ground motion has no power; the spectral velocity at this frequency is controlled by the ground motions at lower frequencies.

$S_a(\omega_n)$ is obtained for each frequency used in the generation of the artificial time history. We generate one spectral density function and one artificial time history for each realization of the response-spectrum residuals $\varepsilon(f)$.

A.3 GENERATION OF ARTIFICIAL GROUND MOTIONS

Safak and Boore (3) have shown that the straightforward simulation procedure of generating the artificial ground motions in the frequency domain, transformation into the time domain, and windowing with the desired time envelope introduces spurious low-frequency energy in the spectrum.

This phenomenon occurs because windowing of a non-white signal changes the frequency content of the signal.[3]

Therefore, we use the procedure suggested by Safak and Boore, which is as follows:

1. Generate discrete-time, Gaussian white noise with unit power (i.e., with a variance of $\frac{2\pi}{\Delta T}$, where ΔT is the time step) in the time domain.
2. Multiply the white noise by the time envelope in Figure 3-3. (Because the signal is white, its frequency content is not changed by this windowing.)
3. Transform the enveloped white noise to the frequency domain using the FFT algorithm.
4. Multiply the quantity obtained in step 3 by $\sqrt{S_a(\omega)}$, where $S_a(\omega)$ is the power spectral density function of ground acceleration. This step introduces the desired amplitude and frequency content in the signal.[4]
5. Transform the signal back to the time domain using the FFT algorithm.

A.4 CALIBRATION

Because we are modifying the target spectrum, and because of the approximations involved in obtaining a spectral density function from a response spectrum, the geometric-average of response spectra from multiple ground motions does not exactly match the target spectrum. This mis-match is large enough at low frequencies (0.5 and 1 Hz) to require an empirical correction which is introduced as a factor in the left-hand side of Equation A-5. This factor was selected separately for each type of ground motions considered.

[3]Multiplying a signal by a time envelope is equivalent to convolving the Fourier transforms of the signal and the envelope. Unless the signal is white, the effect of this convolution is to "leak" energy from frequencies where the amplitude is high into frequencies where the amplitude is low.

[4]A phase shift should be introduced at this step, in order to maintain causality. This would improve the appearance of the initial portion of the simulated motions.

A.5 REFERENCES

1. E. Vanmarcke. "Structural Response to Earthquakes". In C. Lomnitz and E. Rosenblueth, editors, *Seismic Risk and Engineering Decisions*, chapter 8, Elsevier, 1976.

2. A. Der Kiureghian. *On the Response of Structures to Stationary Excitation.* Report UCB/EERC 79-32, Earthquake Engineering Research Center University of California, Berkeley, 1979.

3. E. Safak and D. Boore. "On Low-Frequency Errors of Uniformly Modulated Filter White- Noise Models for Ground Motions". *Earthquake Engineering and Structural Dynamics*, 16:237–240, 1988.

NRC FORM 335 (2-89) NRCM 1102, 3201, 3202

U.S. NUCLEAR REGULATORY COMMISSION

BIBLIOGRAPHIC DATA SHEET

(See instructions on the reverse)

1. REPORT NUMBER (Assigned by NRC. Add Vol., Supp., Rev., and Addendum Numbers, If any.)
NUREG/CR-6467

2. TITLE AND SUBTITLE
Impact of Ground Motion Characterization on Conservatism and Variability in Seismic Risk Estimates

3. DATE REPORT PUBLISHED
MONTH: July
YEAR: 1996

4. FIN OR GRANT NUMBER
L1279

5. AUTHOR(S)
R. T. Sewell, G. R. Toro, R. K. McGuire

6. TYPE OF REPORT
Technical

7. PERIOD COVERED *(Inclusive Dates)*

8. PERFORMING ORGANIZATION – NAME AND ADDRESS *(If NRC, provide Division, Office or Region, U.S. Nuclear Regulatory Commission, and mailing address; if contractor, provide name and mailing address.)*
Risk Engineering, Inc.
4155 Darley Avenue, Suite A
Boulder, CO 80303

9. SPONSORING ORGANIZATION – NAME AND ADDRESS *(If NRC, type "Same as above"; if contractor, provide NRC Division, Office or Region, U.S. Nuclear Regulatory Commission, and mailing address.)*
Division of Engineering Technology
Office of Nuclear Regulatory Research
U.S. Nuclear Regulatory Commission
Washington, DC 20555-0001

10. SUPPLEMENTARY NOTES
N. Chokshi, NRC Project Manager

11. ABSTRACT *(200 words or less)*

This study evaluates the impact of alternative methods in treatment and characterization of earthquake ground motions on estimates of seismic risk and its uncertainty. The objective is to formulate specific procedures and characterizations that may lead to less biased and more precise estimates of risk. This report focuses on sources of conservatism and uncertainty in risk that may be introduced by simplifications that are made at the interface of seismic hazard and fragility assessments, particularly the use of a fixed spectral shape for all magnitudes and the anchoring of this shape to PGA. Results indicate significant conservatism in the use of standard review spectra at eastern U.S. Nuclear plant sites and a strong dependence of seismic fragility on earthquake magnitude when PGA is used as the ground-motion characterization. This study concludes that a single, composite-magnitude spectrum of the appropriate shape can generally be used to characterize ground motion for fragility assessment without introducing significant bias or uncertainty in seismic risk estimates. Results also show that the inelastic or elastic spectral acceleration are superior to PGA as spectral anchors, but they bring only a modest benefit in uncertainty reduction because uncertainty in the risk is dominated by the large uncertainty in the hazard.

12. KEY WORDS/DESCRIPTORS *(List words or phrases that will assist researchers in locating the report.)*
earthquake, ground motion, artificial time history, simulation, seismic risk, seismic hazard, uncertainty, conservatism, fragility, response spectra, spectral shape, nuclear plant

13. AVAILABILITY STATEMENT
Unlimited

14. SECURITY CLASSIFICATION
(This Page)
Unclassified
(This Report)
Unclassified

15. NUMBER OF PAGES

16. PRICE

NRC FORM 335 (2-89)